

**Mathematisch-Naturwissenschaftliche Fakultät
der Universität Augsburg**

**Organic Field-Effect Transistors for Application in
Radiation Biophysics**

Dissertation

**zur Erlangung des akademische Grades
eines Doktors der Naturwissenschaften
(Dr. rer. nat.)**

von

Anna-Lena Idzko

2011

1. Korrektor PD Dr. Stefan Thalhammer

2. Korrektor PD Dr. Giuseppe Scarpa

Tag der mündlichen Prüfung: 24.01.2012

Abstract

The average public exposure to ionising radiation in Germany is about 4.1mSv per year. About half of it, 2mSv, is generated by natural background radiation, the other part is man-made. Medical applications are making the major contribution to this artificial generated radiation. Here, the local radiation doses range from about 1mSv in the dental field up to 30mSv for a cranial computer tomography. Up to now, the effects of low doses of ionising radiation smaller than 100mSv on the organism or single cells are unknown. Thus, it is of common interest to determine the particular biological effect of radiation exposure in this regime for risk prognosis. The existing concept of a linear dose-effect relation, which is valid for medium to high doses, does not hold for the low dose regime. With so far used retrospective analysis no distinct results could be gained for the dose-effect relation since especially there, effects like adaptive response, cell abnormality, bystander effects and genomic instability influence the dose-effect relation. As most of the effects occur on the cellular level a sensor, which is capable for time-resolved measurements, based on the organic polymer poly(3-hexylthiophene) (P3HT), was developed. It was shown that the sensors meet the special demands for the application in radiation biophysics, like biocompatibility, stable performance in tissue culture medium, stability under ionising irradiation as well as sensitivity to pH and changes in the concentrations of ions. In this work, organic materials were chosen for device fabrication due to their known advantages over inorganic materials. The sensors were extensively characterised in terms of the above-mentioned demands. Furthermore, the sensor performance was evaluated with respect to the polymeric thin-film morphology.

The biocompatibility of the used organic materials could be proved in this work. It was found that cells grow very well on the chemically or physically functionalised organic surfaces and that the transistor material itself does not influence the living cells in any way. With the usage of different polymer and solvent compositions for device fabrication it was possible to create tuneable sensors concerning stability and sensitivity. The compositions of P3HT dissolved in dichlorobenzene (DCB) and the blend of P3HT and phenyl-C61-butric acid methyl ester (PCBM) with ratio 3:1 dissolved in DCB could be operated for at least 6hrs in tissue culture medium. The composition P3HT in chloroform (CHCl_3) in contrast was only stable under very restricted conditions. During irradiation all device configurations showed repeatable behaviour; no damage by ionising radiation in the range up to 2Gy was observed. Depending on the transistor configuration the sensors showed high sensitivity to pH and ion concentration changes but also aging effects. All transistors worked properly in the pH range from pH 4 to pH 10. Though, the

blend made from P3HT:PCBM exhibited non-reproducible behaviour, probably caused by aging effects. Devices made from P3HT in CHCl_3 and P3HT in DCB showed sensitivity to all tested ions in a concentration range from 10^{-3}M to 10^{-5}M . With the sensors made from P3HT in DCB changes in the calcium concentration in the range of cellular communication processes, which means down to $2.5 \cdot 10^{-7}\text{M}$, could be detected. The device made of 1wt% P3HT in DCB suits best for the desired application, since it fulfils all needed requirements. Furthermore, based on the presented results, a sensing model was proposed. It is assumed that diffusion of the ions into to polymer film or adsorption on to the surface creates the measured signal depending on the ion in the solution.

As a further step towards a biosensor, an optical approach for the detection of calcium fluxes inside the cell was developed. An increase in the fluorescence of non-irradiated cells was visible after the addition of medium of irradiated cells. The combination of optical and electrical measurements might help to decode the measured cell signals during an irradiation experiment. In a last step, the possibility to run the devices with cells adherently grown on the sensor surface was proved and the effect of the cells on the sensors was determined.

Zusammenfassung

Die durchschnittliche Strahlenbelastung der Bevölkerung in Deutschland durch ionisierende Strahlung liegt bei rund 4.1mSv pro Jahr. Ungefähr die Hälfte, 2mSv, ist bedingt durch natürliche Hintergrundstrahlung, der restliche Anteil stammt von künstlichen Quellen. Der Hauptanteil der künstlichen Strahlenbelastung ist bedingt durch medizinische Anwendungen. Die lokale Strahlenbelastung reicht hier von ungefähr 1mSv im Zahnmedizinischen Bereich bis hin zu Dosen von 30mSv bei einer Schädel Computertomographie. Bis jetzt sind die Effekte geringer Dosen ionisierender Strahlung, kleiner 100mSv, auf den Organismus unbekannt. Aus diesem Grund ist es von allgemeinem Interesse, vor allem die biologischen Effekte durch geringe Dosen in diesem Dosisbereich zu bestimmen um Risikovorhersagen treffen zu können. Das existierende Konzept eines linearen Dosis-Wirkungs-Verlaufs, welcher für mittlere bis hohe Dosen gültig ist, trifft für den geringen Dosis Bereich nicht zu. Mit bisher verwendeten retrospektiven Analysen konnten keine eindeutigen Ergebnisse für den Dosis-Wirkungs-Verlauf erzielt werden, denn gerade in diesem Bereich beeinflussen Effekte wie die adaptive Zellantwort, Zellanomalien, „Bystander Effekte“ und genomische Instabilität den Dosis-Wirkungs-Verlauf. Da die meisten Effekte auf der zellulären Ebene auftreten, wurde ein Sensor für zeitaufgelöste Messungen, basierend auf dem organischen Polymer poly(3-Hexylthiophen) (P3HT), entwickelt. Es wurde gezeigt, dass die Sensoren den speziellen Anforderungen für den Einsatz in Bereich der Strahlenbiophysik, wie Biokompatibilität, Stabilität im Zellkulturmedium und unter ionisierender Strahlung, sowie pH- und Ionen-Sensitivität genügen. In dieser Arbeit wurden organische Materialien wegen ihrer verschiedenen Vorteilen gegenüber anorganischen Materialien zur Herstellung der Bauteile verwendet. Die Sensoren wurden hinsichtlich der oben genannten Anforderungen ausgiebig charakterisiert. Des Weiteren wurde das Sensor-Verhalten bezüglich der Dünnschicht-Morphologie der Polymerschicht untersucht.

In dieser Arbeit konnte die Biokompatibilität der verwendeten organischen Materialien bewiesen werden. Es wurde gezeigt, dass die Zellen sehr gut auf den chemisch oder physikalisch funktionalisierten organischen Oberflächen anwachsen und dass das Transistormaterial selbst die lebenden Zellen in keiner Weise beeinflusst. Durch die Verwendung verschiedener Polymer-, und Lösungsmittel-Kombinationen zur Transistorherstellung war es möglich die Sensoren in Bezug auf Stabilität und Sensitivität anzupassen. Die Kombination aus P3HT gelöst in Dichlorbenzol (DCB) sowie ein Gemisch aus P3HT und Phenyl-C₆₁-Butylsäure Methylester (PCBM) im Verhältnis 3:1 gelöst in DCB konnte mindestens 6 Stunden im Zellkulturmedium

betrieben werden, wohingegen die Kombination P3HT in Chloroform (CHCl_3) nur unter sehr bestimmten Bedingungen stabil war. Während einer Bestrahlung mit bis zu 2Gray zeigten alle Kombinationen reproduzierbares Verhalten und wurden nicht durch die ionisierende Strahlung zerstört. In Abhängigkeit des Transistoraufbaus zeigten die Sensoren hohe pH- und Ionen- Sensitivitäten, aber auch Alterungseffekte. Alle Transistoren konnten in einem pH-Bereich von pH 4 bis pH 10 betrieben werden. Die Mischung aus P3HT:PCBM zeigte kein reproduzierbares Verhalten, wahrscheinlich bedingt durch Alterung. Sensoren, welche aus P3HT in CHCl_3 oder P3HT in DCB hergestellt wurden wiesen eine gute Sensitivität auf alle getesteten Ionen, in einem Bereich von 10^{-3}M bis 10^{-5}M , auf. Mit den Sensoren basierend auf P3HT in DCB konnten Kalzium-Konzentrationsänderungen im Bereich von zellulären Kommunikationsprozessen, also bis zu $2.5 \cdot 10^{-7}\text{M}$, detektiert werden. Der Aufbau basierend auf 1% P3HT in DCB eignet sich am besten für die gewünschte Anwendung, da er alle benötigten Anforderungen erfüllt. Des Weiteren wurde anhand der präsentierten Ergebnisse ein Messprinzip vorgeschlagen. Es wird angenommen, dass das gemessene Signal durch die Ionen auf zwei Arten erzeugt wird: Diffusion in das Polymer oder Anlagerung auf dessen Oberfläche, abhängig vom jeweiligen Ion in der Lösung.

Ein weiterer Schritt in Richtung eines Biosensors wurde durch die Entwicklung einer *in situ* Vorgehensweise zur optischen Detektion des Kalzium-Ionenstroms innerhalb der Zelle gemacht. Eine Zunahme der Fluoreszenz von unbestrahlten Zellen konnte nach Zugabe von Medium bestrahlter Zellen beobachtet werden. Die Kombination optischer und der elektrischer Messungen könnte dazu beitragen während eines Bestrahlungsexperiments gemessene Signale zu entschlüsseln. In einem letzten Schritt wurde gezeigt, dass es möglich ist, die Sensoren mit den angewachsenen Zellen zu betreiben. Der dabei auftretende Effekt der Zellen auf den Sensor wurde bestimmt.

Acknowledgments

Die vorliegende Arbeit wurde unter der Leitung von Privatdozent Dr. Stefan Thalhammer am Helmholtz Zentrum München in Zusammenarbeit mit der Universität Augsburg und der Technischen Universität München durchgeführt. Ohne die Unterstützung, die ich von vielen Seiten erfahren habe wäre die Arbeit nicht zustande gekommen.

Besonderer Dank gilt Privatdozent Dr. Stefan Thalhammer für die Überlassung des Themas, die wissenschaftliche Anleitung und die Betreuung der Arbeit. Durch Ihn hatte ich die Möglichkeit an internationalen Konferenzen teilzunehmen und mich somit weiter zu entwickeln. Durch seine kritischen Denkanstöße lernte ich, manche Problemstellung aus einem anderen Blickwinkel zu betrachten. Ich habe viel von Ihm gelernt und konnte mich bei Fragen stets an Ihn wenden.

Bei Privatdozent Dr. Giuseppe Scarpa des Lehrstuhls für Nanoelectronics der Technischen Universität München möchte ich mich herzlich bedanken. Er hat die vorliegende Arbeit mit entwickelt und betreut und stand mir immer mit Rat und Tat zur Seite. Mille Grazie!

I want to thank Prof. Kubota for the possibility to work in his lab at Unicamp in Campinas. The time there enabled me to experience a scientific and personal development.

Sehr herzlich möchte ich mich bei allen jetzigen und ehemaligen Kolleginnen und Kollegen der Arbeitsgruppe Strahlenbiophysik des Instituts für Strahlenschutz am Helmholtz Zentrum München bedanken. Davon besonders Norbert Menzel, Gerolf Lieckfeld, Helmut Niedermayer, Denis Adigüzel, Markus Hofstetter und Elisângela Linares. Bei Problemen und Fragen konnte ich immer zu Ihnen kommen und wurde von ihnen unterstützt. Auch für die Ablenkung in den Pausen oder den hilfreichen Diskussionen bin ich sehr dankbar.

Des Weiteren möchte ich mich bei meinen Kollegen des EP1 der Universität Augsburg, vor allem Susanne Braunmüller und Jörg Kinzel bedanken. Großer Dank gilt auch meinen Kollegen des Lehrstuhls für Nanoelectronics der TUM, vor allem Eduardo Martín Rodríguez, Anandi Yadav und Alexandra Münzer die mich herzlich in ihrer Arbeitsgruppe aufgenommen haben und einen großen Beitrag zum Gelingen der Arbeit geleistet haben.

Bei Dr. Otmar Schmid vom Helmholtz Zentrum München möchte ich mich für die Möglichkeit der Nutzung seines Labors und dem Interesse an meiner Arbeit bedanken.

Herzlicher Dank gilt den Sekretärinnen Frau Pedone, Frau Cevik und Frau Weik.

Für die technische Unterstützung und die immer vorhandene Hilfsbereitschaft möchte ich mich bei Alexander Hupfer, Sidonie Lieber und Rosi Heilmann bedanken.

Bei Teresa Neumaier möchte ich mich für die seit dem 1. Semester andauernde Freundschaft bedanken. Bei Problemen war sie immer für mich da.

Ganz besonders bedanken möchte ich mich für die wertvolle moralische Unterstützung meiner Familie und meiner Freunde, insbesondere während der letzten Phase der Fertigstellung der Arbeit. Ich konnte mich immer auf sie verlassen.

Von ganzem Herzen möchte ich meinem Freund Tobias Gutberlet danken... für Alles. Ohne seine Geduld und Unterstützung wäre ich nie so weit gekommen.

Table of Contents

Abstract	5
Zusammenfassung	7
Acknowledgments	9
Table of Contents	11
1 Introduction and Scope of the Work	13
2 Theoretical Background	17
2.1 Organic Electronics	17
2.1.1 Chemical Background	17
2.1.2 Charge Transport Models	19
2.1.3 Organic Field-Effect Transistors	20
2.2 Cell-Cell Communication	23
2.3 Ionising Radiation	26
2.4 Biological Consequences	27
2.5 Dose-Risk Relation Curves and Non-Targeted Effects	28
3 Materials and Methods	32
3.1 Organic Field-Effect Transistors	32
3.1.1 Organic Materials	32
3.1.2 Fabrication	33
3.1.3 Set-Up and Measurement Performance	35
3.2 Tissue Culture	36
3.2.1 Handling of Cells	36
3.2.2 Cell Splitting	36
3.2.3 Bio-Functionalisation.....	37
3.2.4 Fluo-3 Staining	37
3.2.5 Immunocytochemistry	38
3.2.6 Three Colour Staining	39
3.3 Microscopy	40
3.3.1 Atomic Force Microscopy.....	40
3.3.2 Optical Microscopy.....	40
3.3.3 Confocal Microscopy.....	41
3.3.4 Data Acquisition	41
3.4 Irradiation Source	42
3.5 Zeta Potential Measurements	42
4 Results and Discussion	43
4.1 Technological Optimisation	43
4.1.1 Set-Up.....	43
4.1.2 Characterisation of the Different Transistor Configurations	48
4.2 Demands for Application in Radiation Biophysics	58
4.2.1 Biocompatibility	58
4.2.2 Stability in Tissue Culture Medium.....	63
4.2.3 Stability under Ionising Radiation.....	71
4.3 Sensitivity in Aqueous Conditions	80
4.3.1 pH Sensitivity	81
4.3.2 Ion Sensitivity	86
4.4 Sensing Principle	100
4.5 Towards a Biosensor	108
4.5.1 Transparent Electrodes.....	108
4.5.2 Approach for the Optical Detection of Calcium Fluxes	111
4.5.3 Medium Transfer Experiments	114

4.5.4 Effect of Cells on Sensor	117
5 Summary	123
6 Outlook	127
Literature	129
Appendix	135
A) List of Abbreviations	135
B) List of Materials	139
C) Lab-intern protocol: Method for fluorescence evaluation	145
D) Curriculum Vitae	147

1 Introduction and Scope of the Work

The public exposure caused by ionising radiation in Germany is around 4.1mSv per year (1, 2). About 2mSv are generated by natural background radiation, like radon, terrestrial and cosmic radiation. The remaining part is due to man made radiation, caused by nuclear facilities, atomic fall out, research and medical applications. Hereby, medical imaging causes the highest part of about 2mSv. In Germany, around 130 million X-ray images are taken per year. One third of them are taken in the dental field of application with doses smaller than 1mSv. Though, depending on the examination, local body exposure can range up to 30mSv e.g. for a cranial computer tomography (CT) or thorax CT (3). Nowadays the effect of low doses of ionising radiation smaller than 100mSv on the organism or single cells is unknown. For risk prediction, effects of ionising radiation in the medium to high dose regime determined by epidemiological studies from the atomic bomb survivors in Hiroshima and Nagasaki are extrapolated to the low dose regime. Since, it is not known if this relationship holds also for the low dose regime, several research groups investigated this effect retrospectively. Different biological endpoints that mean the occurrence of a disease, a symptom, or a laboratory abnormality, were identified and analysed. These endpoints are for example damage of the deoxyribonucleic acid (DNA), protein expression, chromosomal aberration or genomic instability. However, these retrospective studies indicate different results and therefore, a novel approach to examine the effect of low doses of ionising radiation is needed (4). An online approach seems promising, since biological systems, from cells to tissue are very complex and dynamical systems and respond to intracellular and extracellular inputs. One way of the cells to respond to an extracellular input is via the so-called cell-cell communication process. Hereby, different messengers like for example ions, are transferred directly between cells or via the extracellular matrix. This communication process is probably altered during or after the exposure to ionising radiation and is hence a suitable endpoint for online analysis with a biosensor.

The major feature of a biosensor (BS) is the presence of a biological sensing element that interacts selectively with the target analyte. The analysed samples may be cell cultures, human samples, food samples or environmental samples. The bio-receptors, for example nucleic acids, cells, antibodies or enzymes are coupled to the electrical interface and react to a specific binding. A transducer translates the biological response into a measurable optical or electronic signal (5) which is then displayed for the user. Figure 1 shows the different components of a biosensor.

generation of electrons, which can be collected by a metal electrode. The measured current is directly proportional to the amount of glucose in the blood. Here, the generated electrons are the analysed end point (see Figure 2).

One type of electrochemical BSs, the chemical sensitive field-effect transistors (ChemFET), can be distinguished e.g. between ion sensitive field-effect transistors (ISFETs) (9-11), or enzyme-immobilised FETs (EnFET) (12-14) which are specialized for detection of specific bio-molecules using enzymes. With these sensors it is possible to detect pH value changes, ionic strength and also biochemical reactions. For organic ChemFETs detection limits down to the parts-per billion range of different analytes like glucose or cysteine were reported (15). Cell based sensors are sensors that involve living biological cells. They monitor physiological changes of living cells induced by exposure to environmental perturbations such as toxicants, pathogens or other agents. Fromherz first showed that it is possible to measure action potentials of neurones with silicon based FET devices (16). Also with other inorganic devices, like AlGaN/GaN or carbon nanotube (CNTs) FETs it is possible to record and activate action potentials of neurones that are attached to the active area of the sensor (17, 18).

Disadvantages of inorganic materials are high fabrication cost and difficult fabrication processes. Organic materials can be easily processed with techniques like spin coating, spray coating or inkjet printing. The size of the sensor can easily be adapted to the favoured application. Biosensors made from organic material could also be used as body implantable sensors because they can be applied on flexible substrates. Furthermore the low production costs allow the use as disposable test systems in the diagnostic which would address the increasing interest in low-cost point-of-care analysis (19). The polymer backbone is carbon based similar to biological materials (20) and the "soft" nature of organics is better compatible with tissue than traditional "hard" electronic material. The most important advantage of conducting polymers is the ability to conduct both electronic and ionic carriers. In life processes ions are important carriers of information, therefore, a material that is able to exchange ionic for electronic carriers, constitutes the ideal connection between the biological and the electronic world (5). In addition, the high sensitivity of the organic molecules to physical and chemical influences is one important property in favour of using organic materials for biosensors. Moreover, the chemical and physical properties of polymers can chemically be tailored to enhance sensitivity and selectivity. All these advantages make organic materials a perfect choice for biosensors used to measure cell-cell communication processes fast, online and cheap and determine with it the effects of low doses of ionising radiation on cells or tissue.

Scope of the Work

Up to now, there does not exist a set-up to determine the effects of ionising radiation in the dose regime between the natural background radiation and some mSv on the organism. Nonetheless, it is of general interest to know these effects for risk prediction. For example, this is necessary to define threshold values for the work in nuclear facilities and for the general public.

Until now, only retrospective analysis is possible. Here, various changes or damages in cell culture, tissue or whole animals are examined after irradiation. The problem hereby is that the analysis is hindered because of the always-present background radiation and the lack of assays which are sensitive enough to measure the relevant cellular alterations (21).

Another way would be an online approach, but so far, the technology is still missing. The goal here is to measure time resolved changes in the cellular microenvironment, so-called cell-cell communication processes, directly during the irradiation experiment. This might lead to an understanding of the cell-cell communication process and could help to understand the induction of different diseases such as cancer (22).

The aim of the work is to fill this gap by developing a novel sensing approach based on organic material, which is capable for online cell measurements in radiation research. Therefore, different hurdles for the electronic device need to be overcome. The sensors have to be biocompatible and stable in complex tissue culture medium, since the cells will be seeded directly on the active area. Another demand is the stable working under ionising radiation. Furthermore, the experimental set-up has to be designed sensitive enough to pick up very small signal changes in the range of cell-cell communication processes. Consequently, it is necessary to develop an understanding of the underlying working principles of these devices and their dependence on various fabrication and measurement conditions.

2 Theoretical Background

2.1 Organic Electronics

In recent years, the use of organic electronics in food and environmental monitoring (23) or as bio-sensors (5) has steadily increased. Besides low-cost and large-area fabrication capability, they offer a unique opportunity when used in sensing applications (24, 25). The semiconducting material acts both as active transport layer and sensing component and the molecular structure and morphology can be adjusted and modified to fine-tune the chemical and physical properties. The combination of ion and electron transport can be used to examine biological events and processes where ions are important messengers (5, 26).

2.1.1 Chemical Background

The semiconducting behaviour of organic polymers is derived from a specific bonding arrangement with alternating single and double bonds, called conjugated π system. After Hückel, they are aromatic compounds consisting of cyclic molecules, where $4n + 2$ ($n = 0, 1, 2, \dots$) π -electrons are delocalised over the whole molecule and can be described by sp^2 hybridisation. The formation of these systems can be explained by the electronic configuration of the binding carbon atoms, which is $1s^2 2s^2 2p^2$ for a free carbon atom. This means the 1s, 2s and 2p orbitals are each occupied by two electrons. Two neighbouring carbon atoms form a double bond via sp^2 hybridisation. One s- and two p-orbitals (p_x and p_y) form three coplanar orbitals. Furthermore, a σ -bond is formed. The two p_z -orbitals remain perpendicular to this plane and when they overlap, a so-called π -bond is formed (see Figure 3). Due to the interaction with the unpaired electron of the neighbouring carbon atom, a splitting of the energy level in a bonding π - and anti-bonding π^* -orbital is formed. These are referred as highest occupied molecular orbital (HOMO) and lowest unoccupied molecular orbital (LUMO). The HOMO level can be seen as analogue to the valence band and LUMO to the conducting band in inorganic semiconductors. Nevertheless, an important difference to inorganic semiconductors is the fact, that HOMO and LUMO do not form extended band states at fixed energies but localised states with a given energetic distribution.

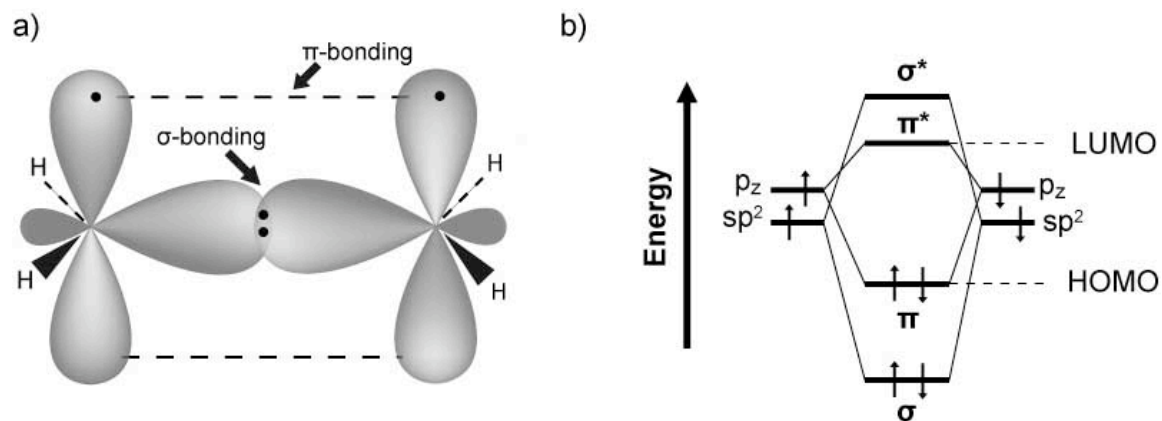


Figure 3 Schematic sketch of the sp^2 -hybridisation of ethene: a) formation of σ - and π - bonds, b) energy level diagram illustrating the bonding and anti-bonding molecular orbital (adapted from (27)).

Important for the semiconducting properties is the fact that the π -bond is significant weaker than the σ -bond. This is because the p_z -orbitals show a less pronounced overlap than the sp^2 -hybridised orbitals. The energy gap between the HOMO and the LUMO is relatively small, between 1.5 and 3eV. Therefore, only a small energy is necessary to lift the electrons occupying the π -orbital into the π^* -orbital. Electrons in the π^* -orbital are considered as delocalised and can travel along the backbone of the polymer (27). This property leads to fluorescence or semiconducting behaviour of the organic material.

There are two classes of materials used for organic electronics: small molecules and polymeric materials (28). Figure 4 shows the most commonly used organic materials: the polymer Poly(3-hexylthiophene) (P3HT) (Figure 4a) and the molecule pentacene (Figure 4b), where the alternating arrangement of single and double bonds can easily be seen.

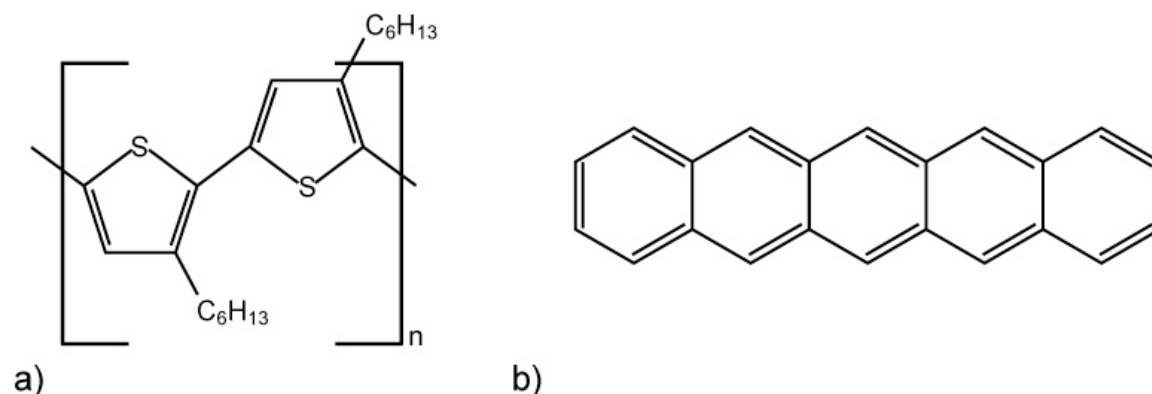


Figure 4 Most commonly used semiconducting materials a) monomer repeat unit of P3HT and b) pentacene. The alternating arrangement of single and double bonds can easily be seen.

P3HT and pentacene are p-type materials, which means the charge carriers inside the material are holes. There are also n-type polymers, like phenyl-C61-butric acid methyl ester (PCBM), where electrons act as charge carriers. Blends of PCBM and P3HT are often used to realise ambipolar transport, which means the transport of positive and negative charge carriers at the same time. Applications for ambipolar transport are for example in solar cells (29, 30).

During the synthesis of P3HT the thiophene rings polymerise to long chains between the 2- and 5-position. Thereby, three different couplings of the monomers are possible, 2,5' or head-tail (HT), 2,2' or head-head (HH) and 5,5' or tail-tail (TT). With a higher amount of HT coupling in the polymer, the intra- and intermolecular order is higher. When the HT coupling is greater than 95%, the polymer is called regioregular (rr-P3HT). As a result of this highly ordered structure high field-effect mobilities and reasonable on/off ratios are gained when used as semiconducting material in transistor structures (31). Furthermore, its high solubility in various organic solvents and good film forming properties makes it attractive as solution processable semiconducting polymer (32). Therefore, rr-P3HT is used in this work. Additionally, blends from P3HT:PCBM and dibenzotetrathiafulvalen (DB-TTF) were used. Details to PCBM and DB-TTF can be found in the materials and methods part, chapter 3.1.1.

2.1.2 Charge Transport Models

Up to now charge transport in organic semiconductors is not completely understood (28, 29). However, it is possible to distinguish between disordered amorphous polymers and highly ordered organic single crystals. In amorphous polymers charge transport is possible in two ways. The first is along the backbone of the polymer in one molecule, which is called transport in conjugation direction. The second transport mechanism is between the localised states in molecules due to so-called "hopping transport" (28, 33, 34). Hopping transport is temperature dependent and the charge mobility in amorphous polymers increases with increasing temperature (28). Whereas highly ordered molecular crystals are showing mobilities that decrease with increasing temperature, indicating a band-like transport (29). The polymer microstructure plays a fundamental role in controlling inter-chain charge hopping and with it the carrier mobility (35). Figure 5 shows a schematic of the crystallite structure in polythiophenes. Transport in conjugation direction, that means along the backbone of the polymer is a fast transport direction. Due to supramolecular ordering, the π -orbitals overlap partially which assists inter-chain transfer in π - π stacking direction. In the third transport direction, the insulating

alkyl chains inhibit charge transport and therefore the mobility in this direction is the lowest (35, 36).

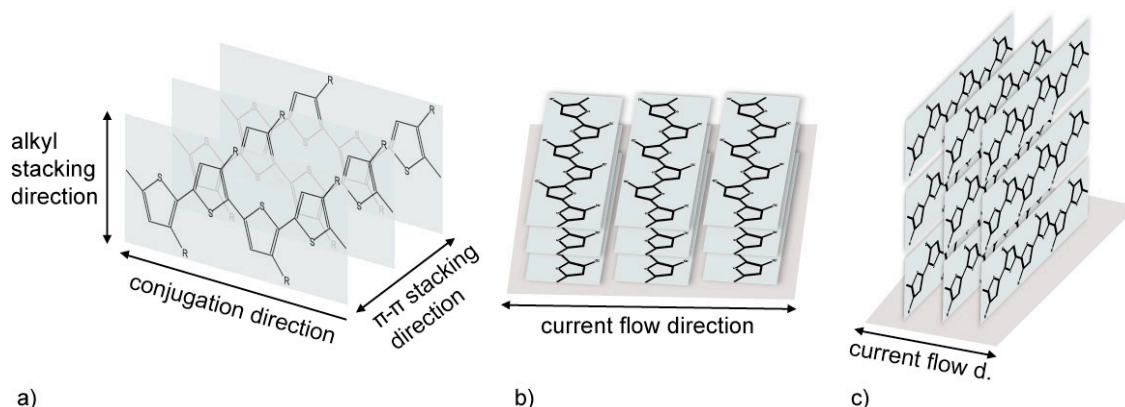


Figure 5 Schematic of crystallite structure in polythiophenes: a) shows the different transport directions. Depending on the orientation transport is b) slower (plane-on structure), or c) faster (edge-on) structure (adapted from (35)).

The microstructure and hence the mobility, can be adjusted by the choice of solvents and fabrication conditions (29). Several studies showed that the microstructure depends on different parameters like: the molecular weight (M_w) of the used polymer, the regioregularity of the starting polymer, the casting technique (like spin-coating, drop casting and printing) and casting temperature, the used solvent and the substrate (35-38).

2.1.3 Organic Field-Effect Transistors

A field effect transistor (FET) is a simple electronic device, consisting of three metal electrodes, a thin semiconductor layer and a dielectric. The dielectric separates the gate electrode from the semiconducting material (39). In organic field-effect transistors (OFET) the semiconducting material is replaced with organic semiconductors. Figure 6 shows the most commonly used structures (29, 30).

With applying a drain-source voltage, charges are injected in the conducting channel directly at the semiconductor-dielectric interface between the two electrodes. The density of charge carriers in the channel is modulated by the applied gate voltage (28). Depending on the device geometry transistors can show very different behaviour (29, 40, 41). This is caused by the way charges are injected into the channel and also by the dielectric/semiconductor and electrode/semiconductor interfaces. Different morphologies may exist at the top and bottom surface of the semiconductor film and trap states may

be introduced during metal evaporation on organic semiconductors of top contact transistors (29).

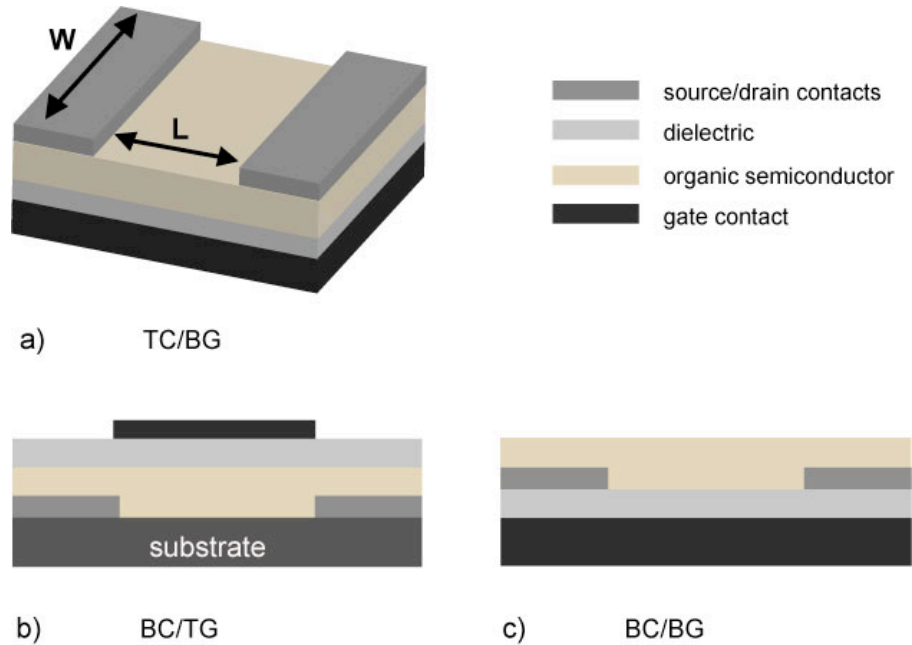


Figure 6 Common field-effect transistor configurations: a) top contact/bottom gate (TC/BG) with indicated channel length (L) and width (W), b) bottom contact/top gate (BC/TG) and c) bottom contact/bottom gate (BC/BG) (adapted from (29)).

OFETs are characterised by different device parameters:

- the mobility μ , which is the measure of how easy the charge carriers move within the semiconducting layer in response to an electrical field
- the on/off ratio, which is the ratio of the current in the conductive “on” state to the device’s “off” state and shows how fast the sensor switches
- the threshold voltage V_T , at which the device turns on, allowing passage of current through the semiconductor channel.

These characteristics are extracted from the output and transfer characteristics of the device (30, 39). The output characteristic (Figure 7a) is the plot of the drain-source current, I_{DS} , versus drain-source voltage, V_{DS} at various gate voltages, V_G . The transfer characteristic is the plot of I_{DS} versus V_G at different fixed V_{DS} and is shown in Figure 7b).

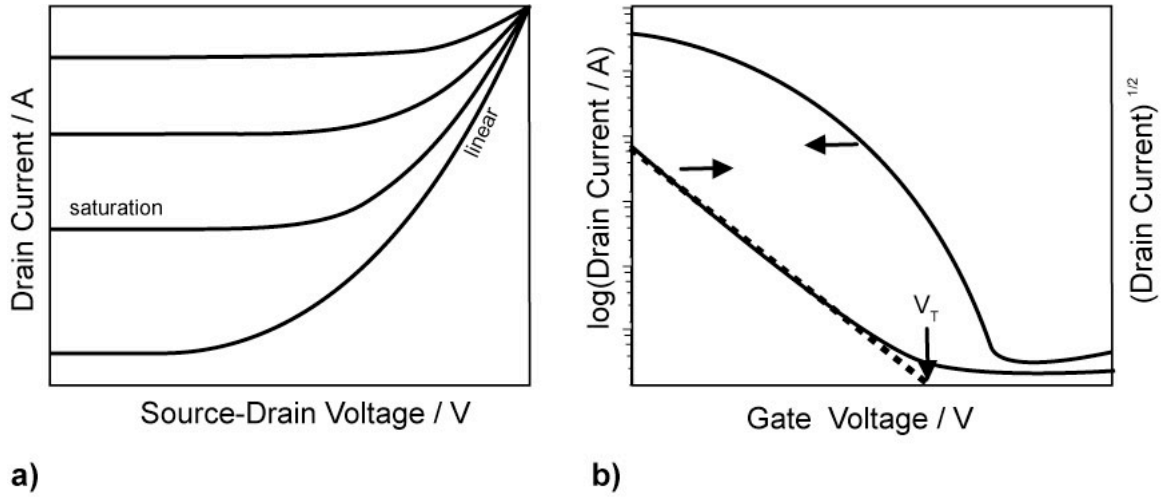


Figure 7 a) Typical output characteristic with the linear and saturation regime and b) transfer characteristic of a p-type organic field-effect transistor.

At low V_{DS} , I_{DS} increases linearly with V_{DS} and is approximately determined from the following equation (see (29)):

$$I_{DS} = \frac{WC_i}{L} \mu (V_G - V_T) V_{DS} \quad (1.1)$$

where L is the channel length, W is the channel width, C_i is the capacitance per unit area of the insulating layer, V_G is the gate voltage, V_T is the threshold voltage and μ is the field-effect mobility. The field-effect mobility can be calculated in the linear regime from:

$$\mu_{lin} = \frac{\partial I_{DS}}{\partial V_G} \frac{L}{WC_i V_{DS}} \quad (1.2)$$

At $V_{DS} = V_G - V_T$, the current cannot increase significantly anymore and saturates ($I_{DS,sat}$); by substituting V_{DS} with $V_G - V_T$ the saturation current can be obtained:

$$I_{DS,sat} = \frac{W}{2L} \mu_{sat} C_i (V_G - V_T)^2 \quad (1.3)$$

In the saturation regime, the square root of $I_{DS,sat}$ is directly proportional to V_G . A gate voltage dependent saturation mobility (μ_{sat}) can be extracted:

$$\mu_{sat}(V_G) = \frac{\partial I_{DS,sat}}{\partial V_G} \frac{L}{WC_i} \frac{1}{(V_G - V_T)} \quad (1.4)$$

The transistor behaviour depends on the used materials for the contacts, the active material and the dielectric. For the contacts usually gold, doped polymers (39) or indium tin oxide (ITO) (42, 43) are used. The most commonly used material is gold, because its

work function is close to the HOMO level of many organic semiconductors and therefore charges can easily be injected in the semiconducting layer since a good ohmic contact is formed (30, 39). In poly(3-hexylthiophene) the LUMO level is about 2.9-3.3eV and the HOMO level is about 4.9-5.2eV. The work function of gold is around 5.1eV. In Table 1 commonly used materials for the different transistor components and their effect on the transistor performance are listed.

Table 1 Commonly used materials for the different transistor components and their effect on the transistor performance.

component	material	effect on
active material	small molecules like pentacene (29); semiconducting polymers like rr-P3HT (34), or single crystals like DB-TTF (29)	μ , V_T
isolator	inorganic insulators: SiO ₂ (34), Al ₂ O ₃ (44), Si ₃ N ₄ , or polymeric insulators like PMMA or PVP(45)	C _i , driving voltage μ ; V_T , polymer orientation/morphology
contacts	high work function metals like Au (also Pt (46) and Ag (47)) or conducting polymers (39) like PEDOT:PSS (48), or ITO (42, 43)	injection of charge carriers
substrate	often gate electrode highly doped Si, or flexible foils (49, 50)	orientation/morphology of polymer if directly processed on top

In addition, the dimensions of the device play an important role for device performance. Reducing the dimensions from the μm scale to the nm scale can further improve sensitivity and allow single molecule detection (19). It also was shown, that organic transistors can be used as pH electrodes (10) or are able to detect changes in biological relevant glucose and cysteine molecules (15). This leads to the assumption that these kinds of sensors are capable to detect messenger molecules and relevant ions during cell-cell communication processes.

2.2 Cell-Cell Communication

Cell communication is a complex system that governs basic cellular activities and coordinates cell actions. The ability of cells to perceive and correctly respond to their microenvironment enables cells to control their behaviour in order to secure the wellbeing of the whole organism. Errors in cellular information processing are responsible for diseases such as cancer, autoimmunity and diabetes (51). By understanding cell signalling, diseases might be treated more effectively (52). Therefore, one interesting endpoint to investigate could possibly be altered cell-cell communication.

Cell-cell communication mechanisms depend on the one hand on extracellular signal molecules, which help to connect neighbouring or more distant cells with each other. Furthermore, cell-cell communication depends on intercellular proteins, which enable the cells to react to the received signals. Figure 8 shows the three phases of cell signalling, which always works the same way. This signal transduction pathway was explored by Earl Sutherland who gained the Nobel Prize in 1971 for his discovery (53). At the first phase, the reception, the signal molecule binds at the receptor protein. Then, the transduction takes place. It is a step-by-step process where the last molecule in the pathway triggers the third phase, the cell response. This response may be differentiation, division and the regulation of specific functions like gene expression or even apoptosis, the so-called programmed cell death, which inhibits incorrect replication of highly damaged cells (51).

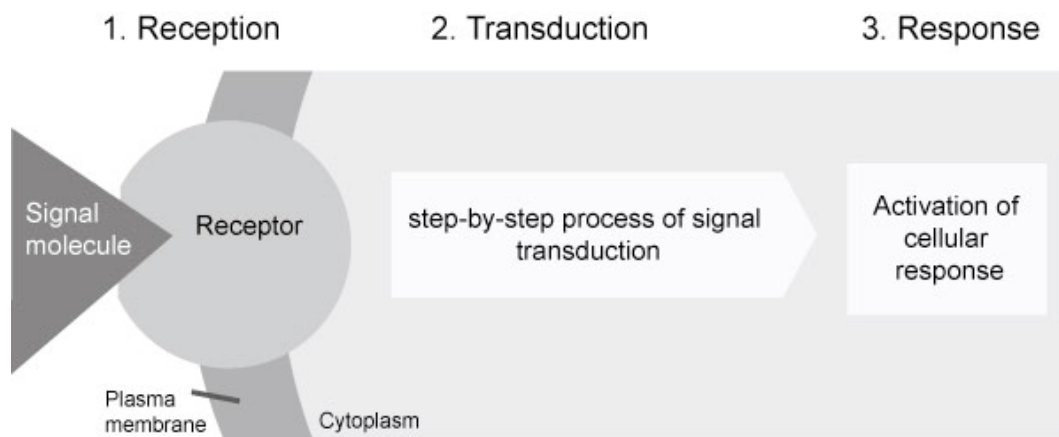


Figure 8 The three phases of cell communication. With the first phase, the reception, extracellular signal molecules bind to a receptor protein, which leads to the translation of the signal. In the last phase, the cell response to the signal and changes their behaviour (adapted from (51)).

Cell communication can take place between cells in direct contact (juxtacrine signalling) or between distant cells and depends on interactions between cells, like gap junctions, cell adhesion molecules or interactions with the extracellular matrix. To connect neighbouring cells with each other, so-called gap junctions are formed, which are very important for cell-cell communication. They can precisely be formed or aborted and allow various second messengers like cyclic adenosine monophosphate (cAMP), inositol triphosphate (IP₃), or calcium ions (Ca²⁺), to pass freely between the cells. Extracellular signalling is distinguished in signalling between distant cells, the so-called endocrine signalling and neighbouring cells, the paracrine signalling. Endocrine signalling is the transport of hormones via the blood stream to far distant cells. Paracrine signalling is the release of first messengers, like growth factors, neurotransmitters or clotting factors, into the extracellular medium. These messengers arrive at the cell surface and either quickly

move into the cytoplasm or produce a second messenger, which activates the intracellular signalling (signal transduction). One very prominent second messenger is Ca^{2+} . It is a highly manifold intracellular signal, which operates over a broad time range from milliseconds up to 24 hours and regulates many different cellular processes, including proliferation, metabolism, muscle contraction, gene transcription and apoptosis (54, 55). This is possible, because the cells are able to shape the specifications of the Ca^{2+} signals that means the amplitude, speed and duration resulting in spikes, waves and oscillations. When gap junctions connect cells, intracellular waves can also spread to neighbouring cells, to create intracellular waves (56). Furthermore, the spatial dimensions can be controlled. Neurones, for example, can generate Ca^{2+} signals that are either restricted to a small volume of about $0.1\mu\text{m}^3$, or large signals that can spread over some $100\mu\text{m}$ (55). In resting cells, the cytosolic free Ca^{2+} concentration is maintained at approximately $0.1\mu\text{M}$. During an “on” mechanism, the Ca^{2+} concentration can increase up to $> 1\mu\text{M}$ induced by entry of external Ca^{2+} and the release of internal Ca^{2+} that is stored in the endoplasmic reticulum (ER), mitochondria or buffers (54, 55, 57, 58). During the “off” mechanism, Ca^{2+} is removed from the cell via ion pumps back in the Ca^{2+} stores or via the $\text{Na}^+/\text{Ca}^{2+}$ exchanger to the outside, which is the so-called Ca^{2+} burst. Figure 9 shows the different Ca^{2+} pathways and typical concentrations activating different cellular responses (54).

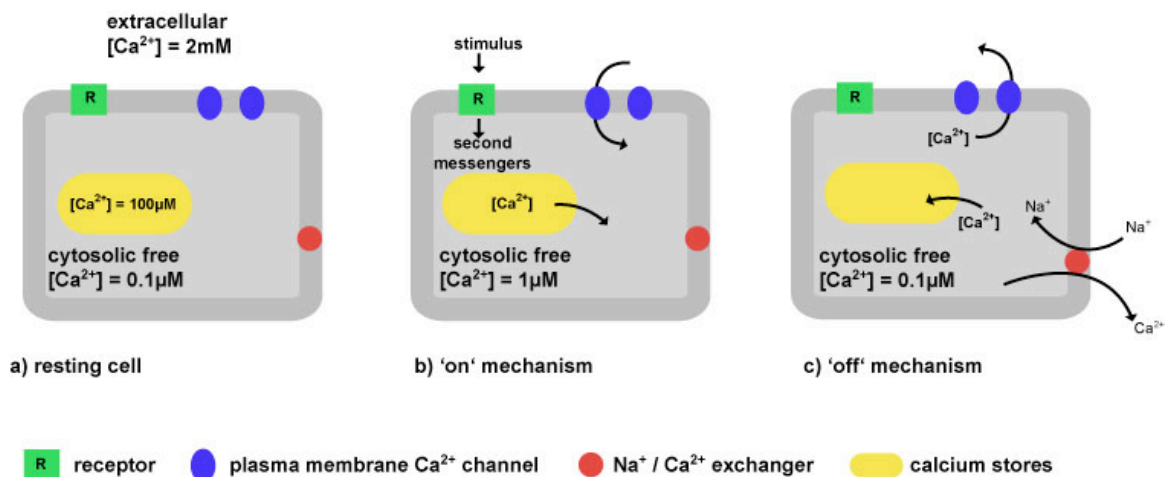


Figure 9 Simplified sketch of calcium-signalling dynamics. Different Ca^{2+} -pathways and typical concentrations inside and outside of the cell: a) resting cell, b) after stimulus and c) “off” mechanism (adapted from (54)).

Cell survival is dependent on calcium homeostasis, whereby the calcium fluxes during the “off” reactions exactly match those during the “on” reactions (54). Furthermore, it was shown, that a rise in cytosolic free Ca^{2+} can also be caused by ionising radiation (59). Therefore, Ca^{2+} fluxes during the “off” mechanism of the cell caused by irradiation

could be used as an endpoint and might be detected with a sensor, which is highly sensitive to calcium ions.

Alteration in the cell-cell communication process is not the only effect of ionising radiation on the cellular system. Direct and indirect interactions lead to multitude of effects and are discussed in the following.

2.3 Ionising Radiation

Radioactivity is the spontaneous decay of unstable atomic nuclei by emitting of ionising radiation. The different kinds of ionising radiation are particle radiation, like α - and β -radiation or neutrons and electromagnetic radiation like γ - and X-ray-radiation. During the interaction of ionising radiation with matter, energy is transferred to the atoms or the molecules of the matter. Particle radiation directly transfers its energy to the electrons of atoms or molecules next to the particle trajectory. The energy transfer of the electromagnetic radiation takes place via three physical processes, the photo effect, the Compton effect and the pair building. During the photo effect, an electron is removed from the inner shell by a photon at energies up to 50keV. At energies up to 100keV the Compton effect occurs. It is the inelastic scattering of photons at weakly bound electrons from the outer shell. Here, a part of the photon energy is propagated to the electron, which is removed from the atomic shell; the atom is ionised. The third process, pair building, occurs at high energies in the range of MeV and is a spontaneous formed electron-positron pair in the electrical field of the atomic nucleus (60). During all three processes atoms and molecules along the trajectory of X-ray and γ -radiation are ionised. Thereby, secondary electrons are generated whose effects are about a multiple higher and fundamentally responsible for radiation-induced transformation in the absorbing biological material. The linear energy transfer (LET) is a measure of the energy transferred to a target per unit length along a charged-particle track. The unit of the LET is keV/ μ m. In biological systems, the caused damage depends on the amount of ionisation events, thus, on the LET of the ionising radiation. Radiations with a high LET, like α -radiation, are more damaging to a biological system per unit dose than radiation with a low LET, like X-ray or γ -radiation. Furthermore, the relative biological effectiveness (RBE) depends on the amount of absorbed radiation in tissue. The unit of the dose is Gray (Gy). One Gray is defined as the energy absorbed per unit mass (J/kg). To consider the biological effectiveness for the different kinds of radiation the equivalent dose H is introduced. It is defined as the product of the absorbed dose D and a quality factor Q, which depends on the quality of the radiation:

$$H = Q \cdot D \quad (2)$$

Typical values of Q for the different radiations are listed in the table below (Table 2).

Table 2 Quality factors for different types of radiation (61)

Type of radiation	Radiation weighting factor
Photons, all energies	1
Electrons, all energies	1
Neutrons, depending on energy	5-20
Alpha particles	20

The unit of the dose equivalent is Sievert (Sv). Since Q is dimensionless, H has the same dimension like the energy dose: J/kg (62, 63).

2.4 Biological Consequences

Ionising radiation can directly interact with biological material and cause damage by ionisation of the macromolecules, like DNA or proteins. The interaction with the biological material can also happen via an indirect way. During indirect interaction, water molecules are ionised and thereby highly reactive radicals and compounds are generated. This process is called radiolysis of water. The generated radicals, like e_{aq}^- , which is a highly reactive electron with a hydration shell, OH^* and OH^\cdot , then chemically react with the biological material which can lead to DNA damage. Since eukaryotic cells consist to 70-80% of water indirect ionisation is the more prominent effect (63).

The process of physical and biological radiation effects can be classified in different phases characterised by different time scales. The first phase is the physical phase, which starts at the initial event and lasts up to 10^{-12} s. In this phase ionisation and excitation processes as well as radical formation takes place. In the physical-chemical phase, which last from 10^{-6} s up to seconds, the radical interaction takes place. Here, the damage in the molecular level, like DNA and protein damage and in the sub-cellular level like damage to cell membranes, nucleus and chromosomes takes place. The next phase lasts for several minutes after radiation exposure and includes enzymatic effects like damage repair. The biological phase can last from hours to many years and can also be present in the next generation. It includes cellular effects, like alteration of the cell-cycle and apoptosis, dysfunction of tissue, organs and the central nervous system as well as whole body effects, like life time reduction, death and mutation in genotype (60). Of central importance for the radiation effect on the cellular level are radiation-induced transformations at the macromolecular building blocks, the nucleic acids and

proteins. Radiation-induced damage of the nucleic acid have a dominant effect because the nucleic acid is carrier of the genetic code (DNA) and important for protein synthesis (ribonucleic acid, RNA) (51).

The DNA consists of two antiparallel double strands organised in a double helix. A sequence of the four different bases Adenine, Thymine, Guanine and Cytosine encodes the genetic information. Damage of the sugar-phosphate backbone can lead to breaks of the DNA strands and with it to loss of genetic information. DNA damage is differentiated in single-strand (SSB) and double-strand break (DSB), depending if only one strand or both DNA-strands are damaged. Since DNA replicates in a semi-conservative fashion base damage and SSB repair is relatively easy. If one strand is damaged, the intact opposite strand can be used as a template for direct repair (64). DNA DSBs are considered to be the most biologically damaging lesion produced by ionising radiation. If left unrepaired, DSBs can result in permanent cell cycle arrest, induction of apoptosis, or mitotic cell death caused by loss of genetic material. If repaired incorrectly, they can lead to induction of cancer through translocations, inversions, or deletions (65). The amount of DSBs is a measure for the damage within the cell and depends on the radiation dose. A dose of 1Gy of ionising radiation induces around 30-40 DSB and 1000 SSB per cell (65, 66). Therefore, reliable repair mechanisms have been developed, to secure the genetic information and with it the survival of the organism (64). Rothkamm and Löbrich showed, that after a repair time of 24hrs after irradiation with different doses, 1 DSB is left unrepaired in 10 cells which corresponds to the natural background level of DSBs per cell (66). For DSB repair, a large number of proteins is required. When the damage is localised, the specific DNA repair molecules, like Rad52, bind at or near the site of damage including other molecules, like the histone H2AX, to bind and form a complex that enables the actual repair to take place. These protein complexes, so-called radiation-induced foci (RIF) are in the size of some mega base pairs (21) and can indirectly be visualised through immunostaining with antibodies against the protein of interest (65, 67) (see chapter 3.2.5.). One of these proteins is the p53 binding Protein 1 (53BP1). If the damage of the cellular DNA is too drastic, the cell is able to initiate apoptosis, the so-called programmed cell death, thereby eliminating itself to ensure genomic stability (64).

2.5 Dose-Risk Relation Curves and Non-Targeted Effects

In terms of ionising radiation effects it is differentiated between deterministic and stochastic effects. Deterministic radiation effects occur above a threshold dose, which depends on the radiation (like type, dose and duration), on the cell itself, (like age, tissue

type, genetic background and physiological status) and on the surrounding microenvironment (2, 63, 68). If the exposure to ionising radiation is low, the effects can be compensated by repair mechanisms. Therefore, below the threshold dose, deterministic damages cannot be observed retrospectively. Stochastic effects, however, are subjected to a statistical distribution. That means it exists no threshold dose below no risk occurs and the damage is stochastically distributed. Furthermore, with increasing dose, the probability of damage increases. The dose-risk relation in the low-dose regime is still not completely determined. Five different and partly contradictory dose-risk curves were proposed from different authors shown in Figure 10. These different assumptions are based on different experimental results, which were gained partly under different conditions (69).

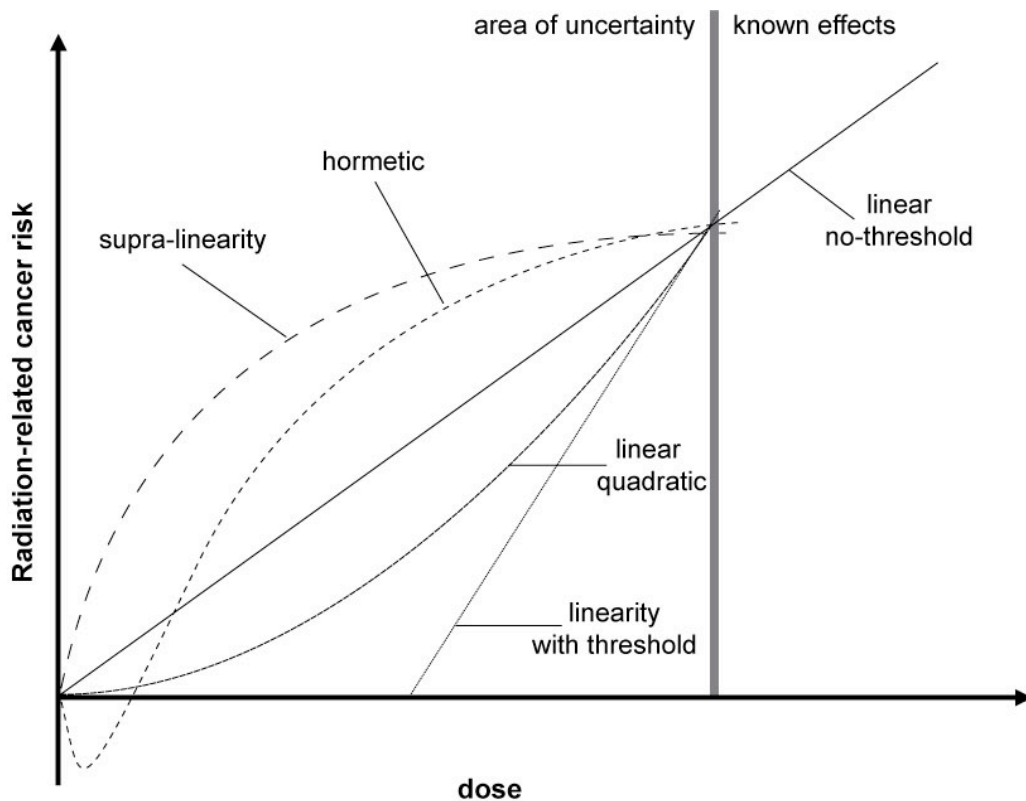


Figure 10 The curves are showing different possible models in the low dose regime for the correlation between radiation-related cancer risk and dose (adapted from (70)).

The most conservative model is the linear non-threshold model (LNT). Here, the increased risk is proportional to the radiation dose without a threshold. For this hypothesis data from epidemiological studies, for example of the atomic bomb survivors in Hiroshima and Nagasaki (1) of the high dose regime of 500mSv and more is taken and extrapolated to the low dose regime. This linear behaviour is assumed from the

stochastic nature of ionising radiation energy deposition, but there are uncertainties at low doses (70).

The effects of low doses could be overestimated, which is indicated in the threshold and hormetic models. In the threshold model exists a threshold dose below which the risk of a particular radiation-induced endpoint is zero (71). The hormetic model describes behaviour where small doses may have a beneficial effect on the organisms. This curve progression is possible, but not widely accepted. Laboratory studies showed that after a first irradiation with a low dose followed by an irradiation with a medium or high dose less damage occurred than after only one irradiation with the same medium or high dose. This behaviour is called adaptive response (2, 72). Acute dose-effects, like radiation-induced leukaemia (73) and chromosomal aberration induction (74) have been extensively analysed and can be well described by the linear quadratic curve.

Furthermore, it is possible that the effect of low doses is underestimated. This results in a supra-linearity curve. Epidemiological and laboratory studies showed such a curve progression, which was interpreted in several ways. One interpretation is that a small subpopulation exists within a population that showed a hypersensitivity to radiation. As another reason for the non-linear relationship between dose and risk in the low dose regime the so-called bystander effect (75-77) and other non-targeted effects are assumed. A central paradigm in radiation sciences has been that the energy from radiation must be deposited in the cell nucleus to generate damage (78). However, research in the last years showed, that damage is also caused in cells that are not directly hit by ionising radiation, especially in the low dose regime (<100mSv) (78). These effects are called non-targeted effects. They include genomic instability occurring in the progeny of irradiated cells, bystander effects or chromosome damage in not-directly hit cells. All these effects might represent an initiation event for carcinogenesis and with it increases the cancer risk.

The radiation-induced bystander effect describes the impact on non-irradiated cells by the signal generated from directly irradiated cells. It is an effect of cell-cell communication that takes place via signals generated by the irradiated cells, like released factors in the surrounding medium or via gap-junctions. The non-irradiated cells show signs of genetic instability or die (79, 80). Different effects are observed in different cell types and depend on the cell type producing the bystander signal after irradiation and the cell type receiving the bystander signal (78). Some examples for radiation-induced bystander effects are apoptosis (76, 81-83), chromosomal aberrations (84, 85) and genomic instability (83, 85, 86). Furthermore, Ca^{2+} seems to play a role as intercellular messenger for the mediation of the bystander effect. Some studies showed

that intracellular calcium fluxes precede the induction of responses in bystander cells exposed to signals from irradiated cells (83, 87). Calcium was also found to be involved in the production of the bystander signal (88). This was affirmed by experiments showing that the bystander response could be inhibited when the non-irradiated cells were treated with calcicludine, which is a calcium channel blocker (89). Therefore, the examination of cell-cell communication processes, for example calcium pathways, might help to understand the dose-risk relation in the low dose regime.

3 Materials and Methods

3.1 Organic Field-Effect Transistors

3.1.1 Organic Materials

a) Poly(3-hexylthiophene)

P3HT is a conjugated p-type polymer with the empirical formula $C_{10}H_{14}S$ and a molecular weight of about $M_w = 17.500\text{g/mol}$. It consists of polymerised thiophene rings and hydrophobic alkyl side chains ($-CH_3$). During the polymerisation process of P3HT the thiophene rings connect to long chains. During this process, it is possible that the alkyl remainder is randomly distributed and the polymer is regiorandom. When HT-coupling is greater than 95%, the polymer is called regioregular (rr-P3HT). With a higher degree of order the polymer shows higher mobilities. The chemical structure of P3HT can be found in chapter 2.1.1, Figure 4a.

b) Phenyl-C61-butric acid methyl ester

Phenyl-C61 acid methyl ester is a fullerene derivate of the C_{60} buckyball. It is an n-type organic material and is often used in organic solar cells or flexible electronics in combination with a p-type material. It is soluble in dichlorobenzene. Its empirical formula is $C_{72}H_{14}O_2$ and it has a molecular weight of $M_w = 910.88\text{g/mol}$. Figure 11 shows the chemical structure of PCBM.

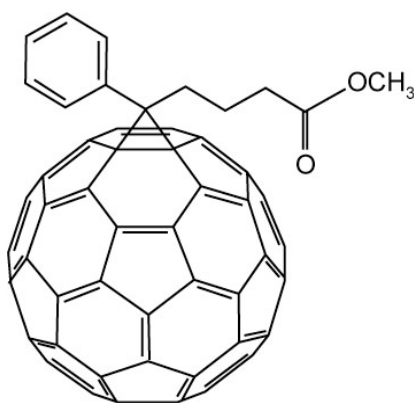


Figure 11 Chemical structure of PCBM.

c) Dibenzotetrathiafulvalen

DB-TTF is a p-type small molecule with the empirical formula $C_{14}H_8S_4$ and the molecular weight $M_w = 304.37\text{g/mol}$. DB-TTF is dissolved in toluene or DCB. Figure 12 shows the chemical structure.

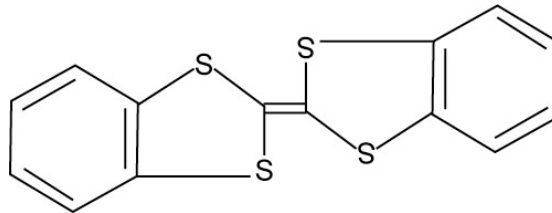


Figure 12 Chemical structure of DB-TTF.

3.1.2 Fabrication

The used device geometry of the OFETs is the bottom contact/bottom gate structure because it reduces fabrication complexity and enables direct access to the active semiconducting layer to investigate its structure and morphology and how those characteristics relate to the device's electrical properties (41). With the use of an interdigitated electrode structure it is possible to enlarge the channel width without the need to produce large devices.

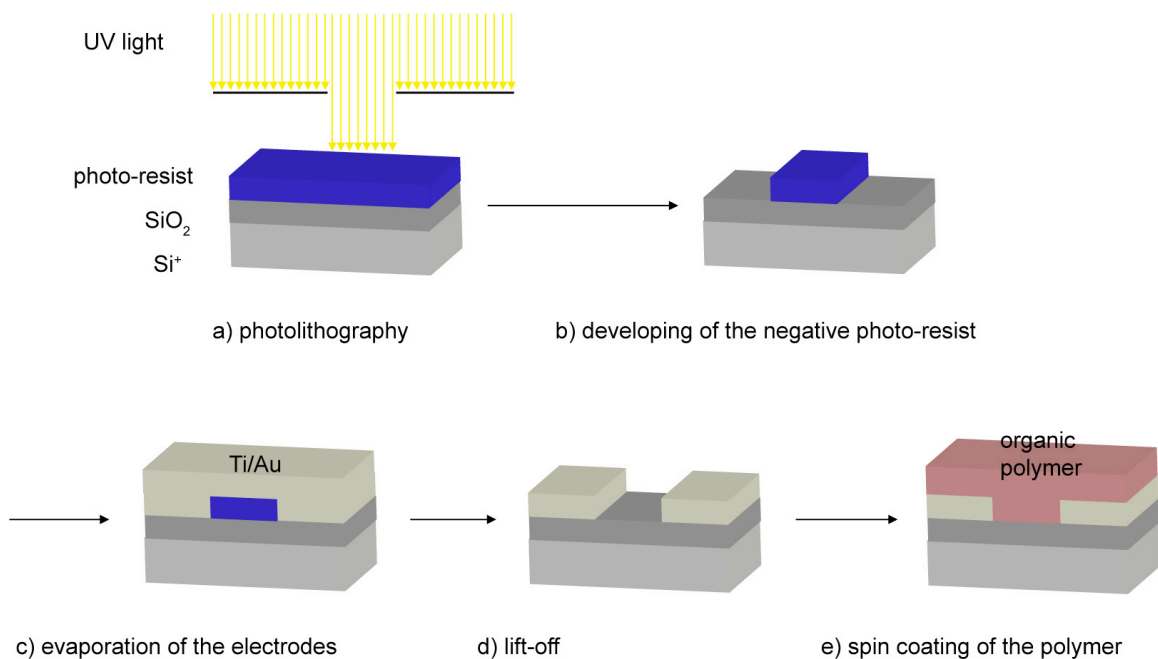


Figure 13 Different fabrication steps of an OFET.

To deposit the electrode structure on the silicon-substrate either sputtering technique or evaporation deposition was used. With this technique it was possible to produce transistors with different channel length (10 μ m, 20 μ m, 50 μ m and 100 μ m). The evaporated electrodes of the OFETs were performed with standard photolithographic process. Figure 13 shows the different fabrication steps of the OFETs followed by the used protocol.

Materials:

- Substrate
- Acetone
- Isopropanol
- Photo-resist
- Shadow mask
- Developer

At first the substrate was cleaned in an ultrasonic bath for 10min in acetone followed by 10min in isopropanol. After that, the sample is dried under nitrogen flow. Then the photo-resist was applied on the substrate surface, coated at 3000rpm for 30s and dried on the pre-heated hot plate at 100°C for 120s. After a cooling step of 5min, the sample was placed in the mask-aligner with the photo-resist face upwards. The mask was blown clear and placed on top of the substrate facing downwards and weighted down with a glass slide. Then the sample surface was exposed with UV for 50s. To develop the photo-resist, the substrate was slewed in the developer for 55s, washed with pure water for 2-3min and dried under nitrogen flow. The next step was the evaporation of the electrode structure. For this a thermal evaporation chamber (Leybold) was used. At first titanium or chrome was evaporated as adhesion promoter (0.2 Å/s), after that the gold was evaporated (1.0 Å/s).

For the lift-off, the substrate was placed and slewed in acetone on the hot plate at 90°C for 3min. Then the substrate was taken from the hot plate, washed with acetone and placed in the ultrasonic bath until the electrodes became visible. After that, the sample was washed with acetone and dried under nitrogen flow.

For the last step, the spin coating, the polymer was dissolved in a solvent. In Table 3 the different settings for the different solvent/polymer combinations are listed.

Table 3 Different settings for spin coating.

Polymer	Solvent	Mixing	Settings spin coater	Treatment
P3HT	DCB	10min ultrasonic bath	1000rpm, 90sec	3hrs @ RT and 15 min @ 150°C
P3HT	CHCl ₃	15min stirrer or 5min ultrasonic bath	2000rpm, 30sec	10min @ 60°C
P3HT:PCBM	DCB	24hrs, 800rpm, 60°C	1000rpm, 90 sec	3hrs @ RT and 15 min @ 150°C
P3HT:DB-TTF	toluene	24hrs, 800rpm, 60°C	1000rpm, 90sec	3hrs @ RT and 15min @ 150°C

The sample was placed centred on the chuck of the spin coater. The dissolved polymer was taken with a syringe, pressed through a filter on the sample surface and the spinning process was started immediately. To receive solvent-free polymeric layers thermal treatments were used.

3.1.3 Set-Up and Measurement Performance

Characterisation of the transistors were performed at the Institute of Nano-Electronics at the “Technische Universität München” with a Keithley Semiconductor Characterization System 4200-SCS or at the “Helmholtz Zentrum München” with two Keithley 2400 source meter controlled by in-house Lab View programs. To characterise the OFETs, output- and transfer characteristics were recorded.

For characterisation with the Keithley 2400 source meter and the experiments in liquids the transistors needed to be contacted. To characterise the transistors relating to ion or pH sensitivity static and online measurements were performed. For the static measurements the output-characteristic was recorded before and 15min after exposure to the sample solution. Every data point was recorded for at least 1sec to ensure a stable measurement. For online measurements, a constant drain-source and gate voltage was applied to the transistors while recording the drain-source current. With varying the sample solution (pH, ion concentration) the drain-source current was modulated. The shift in drain current shows the response of the OFETs.

To determine the effect of the cells on the OFETs transistors were characterised before and after seeding cells on the surface. Furthermore characterised before and after trypsination of the adherent grown cells was performed.

3.2 Tissue Culture

3.2.1 Handling of Cells

For all experiments with cells L929 mouse fibroblast were used. The cells were cultivated at 37°C, with 95% humidity and 5% CO₂ in a cell incubator. Handling of the cells and preparation for the biocompatibility tests were performed under sterile conditions. Therefore, preparation was done under a flow hood, which was decontaminated with UV light for at least 10min before and after use. Furthermore, the bench was cleaned with 70% ethanol before working under the hood and again after finishing the preparations. All materials used in the flow hood were cleaned with 70% ethanol before placing them in the flow hood.

3.2.2 Cell Splitting

Materials:

- RPMI Medium supplemented with 10% FBS Superior and Penicillin/Streptomycin
- PBS
- Trypsin 0.25%

At first, RPMI medium, PBS and trypsin were heated up to 37°C. The old medium in the tissue culture flask was removed and then the cells were washed with PBS (3.5ml for 25cm² flasks and 10ml for 75cm² flasks). After that, trypsin (0.7ml for 25cm² flasks and 2ml for 75cm² flasks) was added to the cells and cells were incubated for 3min in the incubator. After 3min, cells detached from the surface and fresh RPMI medium was added (3.5ml for 25cm² flasks and 10ml for 75cm² flasks) to stop the effect of the trypsin. To determine the cell concentration in the cell suspension a “Neubauer Zählkammer” was used. The counting was performed following the usual protocol (90). After preparing an new flask with fresh medium (3.5ml for 25cm² flasks and 10ml for 75cm² flasks) 0.5-2ml of the cell suspension (depending on the concentration) were added in the new flask and again cultivated (91). The cell splitting had to be carried out 2-3 times a week to keep the confluence of the cells between 10% and 100%.

3.2.3 Bio-Functionalisation

Bio-functionalisation was used to enhance cell adhesion on the polymeric surface. Functionalisation was performed either chemically with protein-based coatings or physically with plasma oxidation.

a) Protein-Based Coatings

Materials:

- Collagen
- Poly-L-lysine or
- Fibronectin:HBSS 1:80

The samples were rinsed with 70% ethanol and then decontaminated with UV light for 20min. Thereafter, the different proteins, fibronectin, collagen or poly-L-lysine, were applied on the surface. The protein coatings were incubated for 30min, fibronectin and collagen at 37°C in the incubator and poly-L-lysine at room temperature in the flow hood. After incubation, the solutions were removed and cells could directly be seeded on the functionalised surfaces.

b) Plasma Oxidation

For plasma oxidation a Plasma-Processor 500-E (Technics GMBH Europa) was used. The settings to functionalise the surface were: 150W/0.3Torr/1min, (these settings depend on used set-up and need to be tested when using another set-up). After the plasma treatment, the sample was rinsed with 70% ethanol and sterilised for 20min under UV light in the hood. Cells were directly seeded on the surface.

3.2.4 Fluo-3 Staining

For online measurement of Ca^{2+} fluxes during exposure to different noxa intracellular Ca^{2+} was stained with the fluorochrome Fluo-3.

Materials:

- PBS w/o Ca^{2+}
- DMSO
- RPMI Medium

- Fluo-3 fluorochrome

First the “staining medium” was prepared under sterile conditions. It is composed of 3-5µmol DMSO and 5mmol Fluo-3 in RPMI Medium. 1.5h before the experiment, the tissue culture medium was removed from the cells. Then, the cells were rinsed with PBS and incubated with the “staining medium” at 37°C. After an incubation time of 30-60min, the staining medium was removed and the cells were rinsed with PBS w/o Ca²⁺. New RPMI medium, without fluorochrome, was applied to the cells and further incubated for 30min at 37°C in the incubator. Directly after the last incubation step, the experiment was performed.

3.2.5 Immunocytochemistry

For staining of radiation-induced foci (RIFs) a set of two antibodies was used. The primary antibody binds to the antigen of interest, here the protein accumulation of 53BP1. The secondary antibody binds to the primary antibody and makes a fluorescent detection possible (Figure 14).

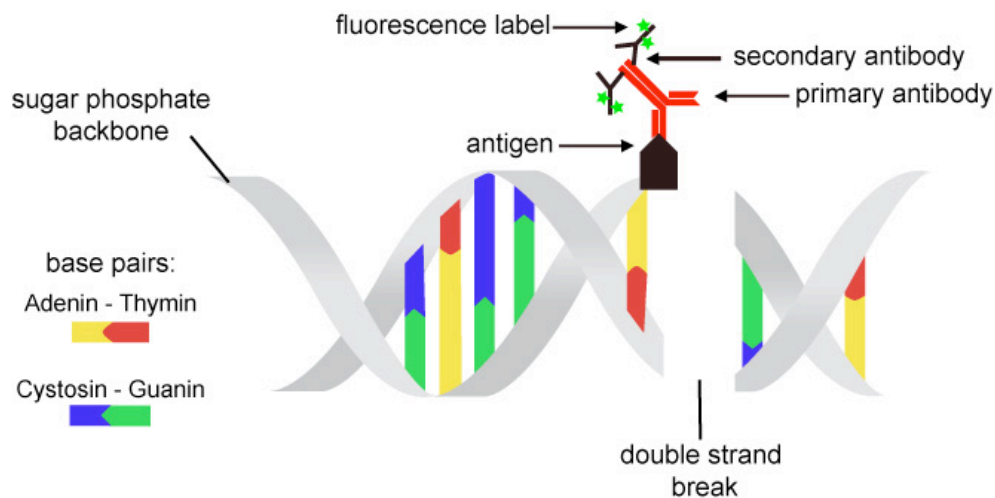


Figure 14 Schematic illustration of the DNA double helix with the sugar phosphate backbone, the base pairs and double strand break with radiation-induced focus: the antigen is recruited to the DSB, at the antigen binds the primary antibody and at this the secondary antibody with the fluorescent label (92).

Materials:

- 2% Paraformaldehyde in PBS
- PBS
- 0.15% Triton X in PBS
- 0.1% BSA in PBS

- Primary antibody (1:100 in PBS)
- Secondary antibody (1:200 in PBS)
- Hoechst 33342 (1:500 HBSS)
- Vectashield mounting medium
- Cover slide

To determine the amount of RIFs, cells were fixed with 2% Paraformaldehyde for 15min at room temperature. The fixation process was stopped with PBS. After that the cells were washed three times with PBS and then permeabilised three times with 0.15% Triton X 100 for 5min at room temperature. To avoid unspecific binding, the cells were blocked three times with 0.1% BSA for 10min at room temperature. The next step was the incubation with primary antibody (rabbit polyclonal anti 53BP1) for 1h at room temperature. Thereafter, the cells were washed 5min with PBS, 10min with 0.15% Triton X 100, 5min with PBS and 7min with 0.1% BSA. Then the samples were incubated with the secondary antibody (Alexa Fluor 488 conjugated anti-rabbit IgG) for 1h at room temperature. This step was followed by another washing step with PBS and the incubation with the Hoechst 33342 intercalating dye for 10min at room temperature. Finally cells were washed with PBS, mounted with the Vectashield mounting medium and covered with a cover slide. The samples were kept in the dark at 4°C until examination with the confocal microscope.

3.2.6 Three Colour Staining

To examine the cells grown on the polymeric surface a three-colour staining was performed. With this method it is possible to stain the cell nucleus (Hoechst 33342), the cell membrane (DiO) and the F-Actin (Rhodamin Phalloidin) of the cell and determine changes in the morphology.

Material:

- DiO (1:200 in RPMI Medium)
- 2% Paraformaldehyde
- PBS
- 0.1% Triton X
- Rhodamin-Phalloidin (1:40 in PBS)
- Hoechst 33342 (1:500 HBSS)
- Vectashield mounting medium
- Cover slide

First RPMI Medium of cells was removed. Then, cells were incubated with DiO in RPMI for 20min at 37°C in the incubator. Thereafter, medium with DiO was removed and cells were fixed with 2% Paraformaldehyde for 15min at RT. The fixation was stopped with PBS and cells were washed twice with PBS. Cells were permeabilised with 0.1% Triton X for 5min. After removing Triton X, Rhodamin-Phalloidin was added and incubated for 20min at RT. Then, cells are washed again twice with PBS. To stain the nucleus, Hoechst 33342 was incubated for 10min at RT. Finally cells were washed with PBS, mounted with 10µl of Vectashield mounting medium and covered with a cover slide. The samples were kept in the dark at 4°C until examination with the confocal microscope.

3.3 Microscopy

3.3.1 Atomic Force Microscopy

Depending on the sample properties and the required resolution a particular imaging mode was chosen. The samples were analysed with a JPK Nanowizard 1 mounted on an inverted microscope (Zeiss Axiovert 100). Data analysis was performed with JPK data analysis software. Cells were fixed with 2% paraformaldehyde or glutaraldehyde before scanning as described before (4.1.4). The polymeric samples were analysed without any further treatment. Table 4 summarises the settings used for the different applications:

Table 4 Used settings for different applications

Sample	Mode	Resonance frequency	Spring constant	Experimental condition
Fixed Cells	(intermittent) contact	17-24kHz	0.1-0.2N/m	liquid
Polymer surface	Intermittent contact	265-400kHz	20-75N/m	ambient air

3.3.2 Optical Microscopy

To control cell growth on the different polymer samples, optical microscopy was used. The examination was performed either with or without further treatment of the cells.

Depending on the samples either a transmitting light microscope (Axio Observer Z1) or a reflected-light microscope (Zeiss Axiotron) was used. For the Fluo-3 fluorescence experiment a mercury lamp (HBO 100) and filter sets (AHF Fluo 3 Filterset Basic) were used. A Rolera-XR CCD camera was used for documentation controlled by the software

QCapture Pro 6.0. Data analysis was performed with ImageJ and Adobe Photoshop CS3.

3.3.3 Confocal Microscopy

The confocal microscopy is a technical approach to optimise the recording of three-dimensional samples. The analysis with a confocal microscope is a point-wise approach in the focal plane. This prevents the detection of background fluorescence as well as out-of-focus fluorescence and improves the contrast of the image. With the confocal microscope a z-stack from the sample was recorded.

Confocal microscopy was used to detect RIFs and to analyse the morphology of the cells (3-colour staining). The samples were stained and fixed as described before (4.1.4. and 4.1.5.). A Zeiss LSM 510 with a 63x water objective was used. For the different dyes different filter sets were used. The different settings are listed in the following table (Table 5).

Table 5 Settings for confocal microscopy.

Dye	Stained Component	Laser	Filter Configuration	Laser Power	Pinhole
Alexa Fluor 488 Ex: 488nm Em: 519	Foci	Argon	HFT 488/543 NFT545 Mirror LP530	25-35%	1.2
Hoechst 33342 Ex: 764nm Em: 465nm	Cell nucleus	Titanium Sapphire	HFT/KP 700/514 Mirror Mirror BP 435-485	90-100%	8-10
DiO Ex: 488 Em: 510	Cell membrane	Argon	HFT 488/543 Mirror NFT 490 BP 505-530	40-40%	1.2
Rhodamine-phalloidin Ex: 550nm Em: 580nm	F-Actin	Argon	HFT 488/543 Mirror NFT 490 BP 565-615	30-40%	1.2

3.3.4 Data Acquisition

AFM images were analysed with provided JPK software.

Confocal images and fluorescence images were analysed with Adobe Photoshop and with ImageJ software.

3.4 Irradiation Source

For all irradiation experiments a Stabilipan TR300f X-ray machine was used. With this machine it was possible to adjust the acceleration voltage and current. The dose was measured with a Diamantor M4 dose area meter, which recorded the applied dose and the irradiation time. The dosimeter was calibrated with regard to the distance of the sample to the X-ray source.

3.5 Zeta Potential Measurements

Zeta Potential Measurements were performed with a Zetasizer ZS+ (Malvern Instruments Ltd, Germany).

Materials:

- Trypsin
- RPMI
- PBS
- 0.154mol NaCl
- Capillary cells DTS 1061

First cells were trypsinated and the cell amount determined (see 3.1.1.1). Then, cells were centrifuged and supernatant cell medium was removed. Cells were resuspended in physiological sodium chloride solution (0.154mol NaCl in H₂O). After that cells were centrifuged again to remove the complete RPMI medium to avoid unwanted electrochemical reaction during the Zeta Potential measurement. A concentration of about 10⁶ cells/ml was adjusted. Cells were kept at 37°C before, during and after the measurement. For the measurement 750-800µl of the cell suspension was filled in the appropriate cuvettes, measurements were performed and repeated 3 times. Zeta potentials were calculated from the Smulchowski equation.

After the measurement cells were dyed with 2% trypan blue in PBS to determine the amount of dead and living cells with a "Neubauer Zählkammer".

4 Results and Discussion

The aim of this work was to develop a new sensing approach based on organic polymers for the application in radiation research. Therefore, different transistor configurations were prepared, characterised and the suitability of the devices for applications in radiation research were tested.

At first technological optimisation including set-up, device geometry and device materials are presented. In the second part the suitability of the sensors to meet the essential demands necessary for the use as a sensor in radiation biophysics is examined. These demands are biocompatibility, stability in tissue culture medium and stability under ionising radiation. Additionally, the sensitivity of the different compositions in terms of pH and ion concentration changes is characterised and a sensing principle based on the achieved results is presented. The last part focuses on the further development towards a biosensor. First results for transparent devices are shown. Moreover, an optical approach for the detection of calcium fluxes caused by external stimuli was developed and the effect of the cells on the sensor was determined.

4.1 Technological Optimisation

In this chapter the different optimisations are described. Different polymers and substrates were used. A sample holder for easy, fast and reproducible contacting was constructed and the device geometry was adjusted. Furthermore, the different transistor configurations were characterised.

4.1.1 Set-Up

For all experiments, a bottom gate/bottom contact structure was used. Figure 15 shows the device geometry. The electrodes had an interdigitated electrode structure (IDES) with different geometrical details given in Table 6.

Table 6 Geometrical data of the used IDES.

Channel length L	W/L	Number of fingers
10 μ m	53700	90
20 μ m	13350	45
50 μ m	2100	18
100 μ m	510	9

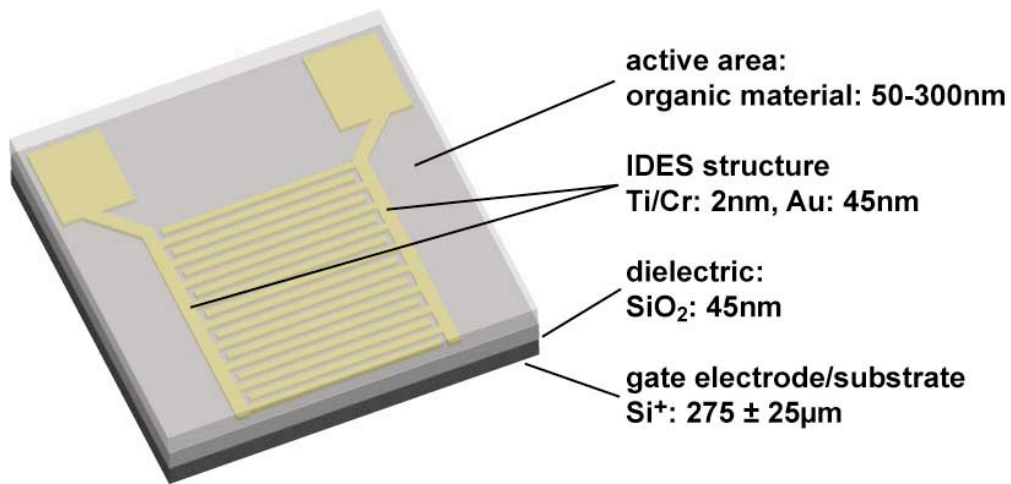


Figure 15 Schematic of the layer-by-layer structure of the organic field-effect transistor with gate, dielectric, source and drain electrodes as well as the polymeric layer.

In the first layout 6 transistors were placed on one wafer. The transistors had different channel lengths of 10µm, 20µm, 50µm and 100µm, resulting in different W/L ratios. Transistors with channel length 20µm and 50µm showed the best performance. For a better comparability, it was decided to use transistors with one fixed channel length. With the possibility to print the shadow mask on a foil the device geometry could easily be adjusted. For an easy contacting, the contact pads were adapted and only transistors with 50µm channel length were used. Furthermore, the whole wafer was used and nine instead of six transistors could be placed on one wafer. Figure 16 shows the two device geometries with the different contact pads. Further details about transistor preparation can be found in 3.1.2.

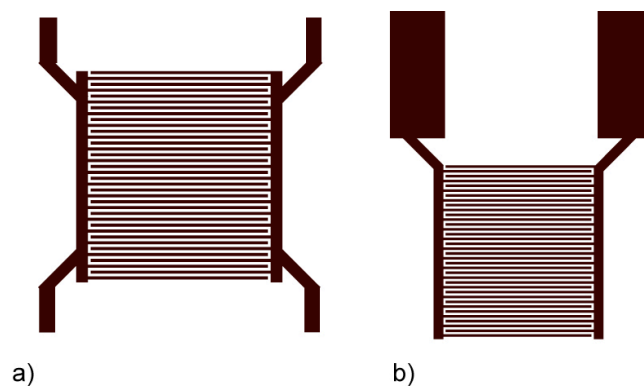


Figure 16 Geometry of “old” and “new” transistors. For easy contacting, the contact pads were enlarged

4.1.1.1 Sample Holder

A precondition to perform measurements in liquids was to passivate the transistor connections from the liquid. Only the active area should be in direct contact to the liquids. For the first experiments, the transistors were contacted with gold wires and silver glue and passivated with silicone rubber, later also called “old” way of contacting. The different steps to contact and passivate the transistors this way are shown in Figure 17.

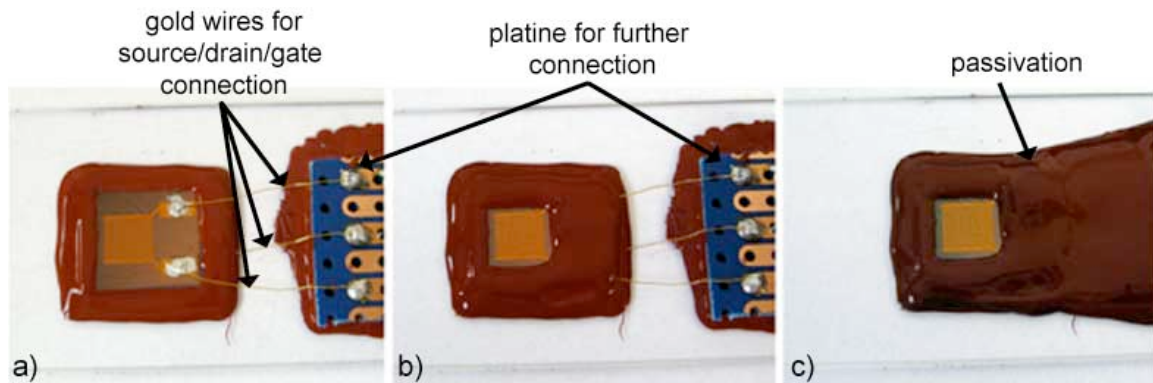


Figure 17 Different steps of transistor contacting with gold wires and silver conductive varnish and passivation of the transistor connections from the liquid.

Figure 17a) shows the fixed transistor on a glass slide. The gate was connected with silver conductive varnish to the gold wire, which was soldered to the plate. Also the source and drain contacts were connected via gold wires to the plate. From the plate different linkages could be soldered to connect the transistor with the measurement set-up. For measurements in liquids either only the contacts (Figure 17b) or the whole sample was passivated with silicone rubber depending if only the active area or the whole sample was exposed to liquid media. Using this technique, often problems occur like short circuit between the gate electrode and the source or drain electrode. Moreover, leaking currents caused by a poor passivation arose.

To get reproducible and reliable results a sample holder was constructed. With the sample holder fast and easy contacting of two transistors could be performed at once. Furthermore, the sample holder could be combined with a flow chamber, which was mounted on the sample holder with a connection piece made from polydimethylsiloxane (PDMS). Figure 18 shows the sample holder with two OFETs and the flow chamber.

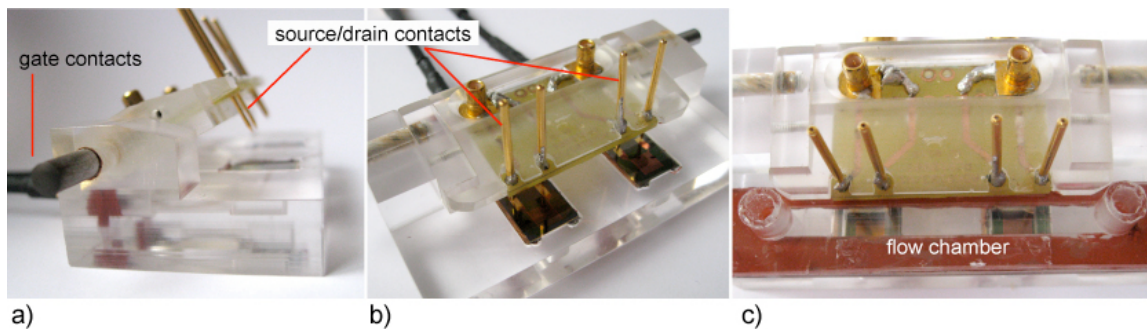


Figure 18 Sample holder for easy and fast contacting of the OFETs (with flow chamber): a) side view, b) top view with source, drain and gate contacts and OFETs and c) flow chamber mounted on sample holder.

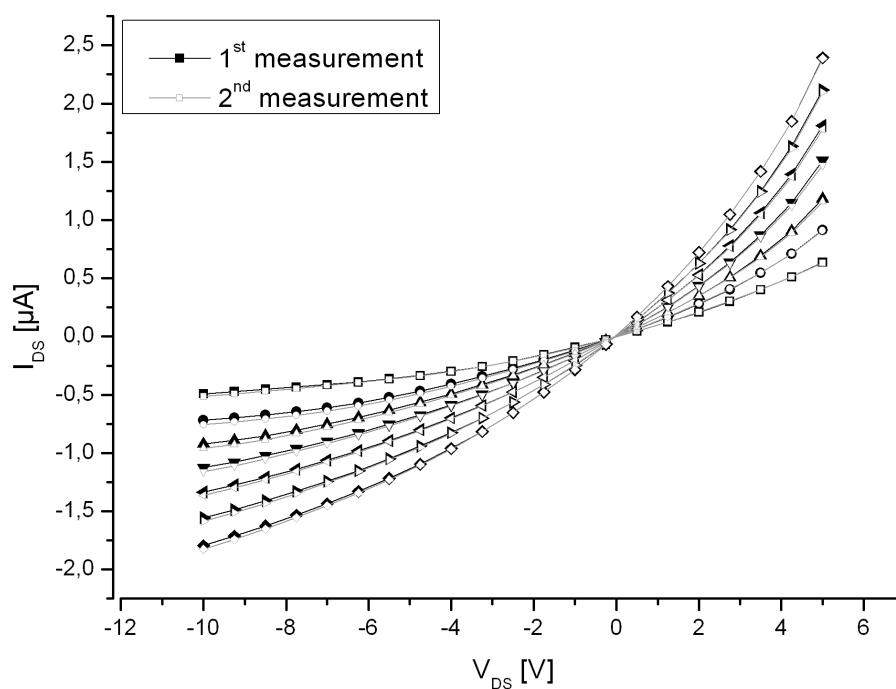


Figure 19 Output characteristic of the OFET transistor mounted into the sample holder. After the 1st measurement, the transistor was removed, again adjusted into the sample-holder and the measurement was repeated. The sample-holder enables reproducible measurements. Here, a device made from 2wt% P3HT in DCB with $L = 50\mu\text{m}$ was used and V_G was decreased from 2V to -10V in -2V steps, V_{DS} was decreased from 5V to -10V in -1V steps.

A transistor was placed in the sample holder and the output characteristic was recorded at room temperature with the drain-source voltage being decreased from 5V to -10V in steps of -1V, while the gate voltage was decreased from 2V to -10V in steps of -2V. After the measurement the transistor was removed, placed again in the sample holder and the measurement was repeated. In Figure 19, it clearly can be seen that the two characteristics of the transistor are almost identical. Therefore, the sample holder ensures reproducible contacting of the transistors.

4.1.1.2 Comparison of Different Transistors

In this work, two types of silicon wafers were used. On the one hand highly doped p⁺ Si wafers with an electrical conductivity of 10000 S/m and a SiO₂ layer with a thickness of 45nm. On the other hand p⁺ doped wafer from the “Bundeswehr Universität München” (UniBW) with a SiO₂ layer thickness of 50nm. The different wafer should not result in different transistor performance since the differences are very small. Nevertheless, the transistors produced on the different wafers are compared with each other.

At first transistors from different wafers were compared with each other to see if there was an effect from the wafer (see Figure 20).

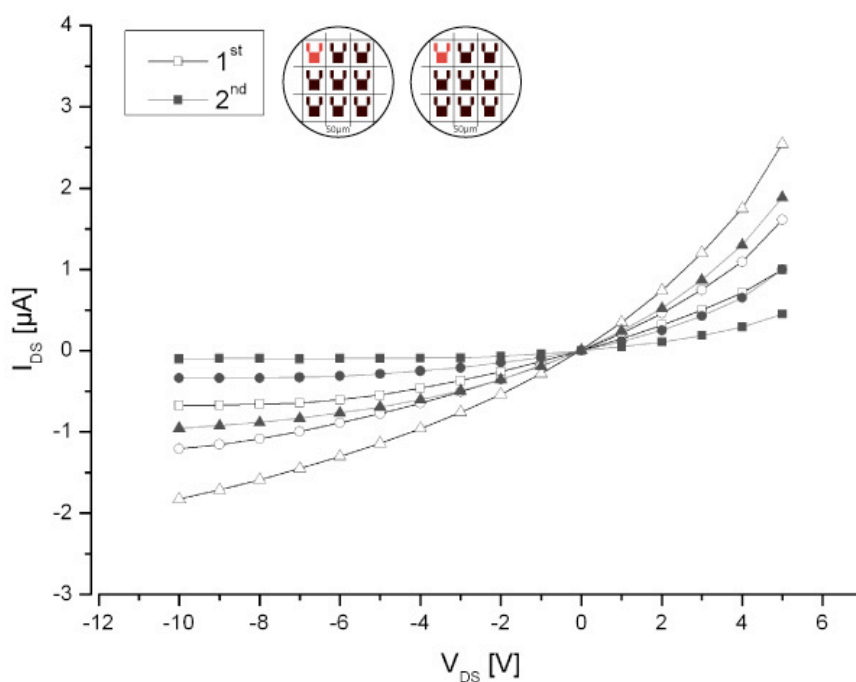


Figure 20 Comparison of two transistors of different wafers. “1st” was made of highly doped wafers and “2nd” of UniBW wafers. A clear shift in the output characteristic is visible. The transistors were made of 1wt% P3HT in DCB and had a channel length $L = 50\mu\text{m}$.

Here, “1st” represents a transistor made of a highly doped wafer and “2nd” is a transistor of a UniBW wafer. The output characteristic was recorded at room temperature with the drain-source voltage being decreased from 5V to -10V in steps of -1V, while the gate voltage was decreased from 2V to -10V in steps of -2V. Here, only the graphs of the gate voltages $V_G = -2, -4$ and -10V are shown. The variation in the output characteristic is obvious. and of about $1\mu\text{A}$ at $V_{DS} = -10\text{V}$ and $V_G = -10\text{V}$. This can be caused either by the different used wafers or by variations during the processing steps. To verify if this effect is caused by the different used wafers, transistors of one wafer were compared (see Figure 21).

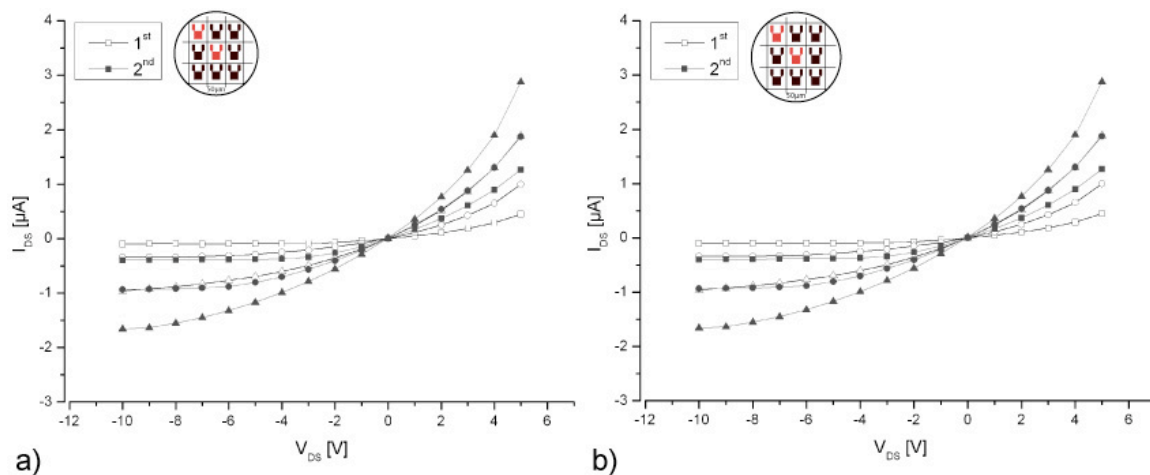


Figure 21 Comparison of two transistors of the same wafer: a) UniBW and b) highly doped wafer. Again, a clear variation in the transistor characteristic is visible. The transistors were made of 1wt% P3HT in DCB and had a channel length $L = 50\mu\text{m}$.

It clearly can be seen, that the transistors' output characteristics of different transistors of one wafer are not identically. This might be caused by the evaporation process or by spin coating. For the evaporation process on a foil printed masks were used. It is possible that not all structures are completely identically. Furthermore, it is possible, that impurities adhered to some of the structures causing slightly different electrode structures. After spin coating, sometimes artefacts like so-called comets or an inhomogeneous polymer layer could be observed which might result in different transistor behaviour. Since, the output characteristics between different transistors of one wafer vary as much as the characteristics of the different wafers, it is not further distinguished between the two types of wafers used in this work. Nevertheless, the different behaviour of the transistors needs to be kept in mind when transistor performance is analysed. Moreover, the processing steps needs to be optimised for future work.

4.1.2 Characterisation of the Different Transistor Configurations

Up to now, there exists no standard set-up configuration for an OFET used as biosensor in radiation experiments. Therefore, a suitable set-up needed to be designed. Since it is known that a fast response is obtained when the signal process occurs directly at the surface of the sensor (93) a bottom contact/bottom gate structure was chosen where the active area will be in direct contact to the electrolyte. Since the device properties, like stability and sensitivity depend heavily on the organic thin-film, different polymer and solvent configurations were prepared. It is known that the properties of used solvent (for

example polarity and hence the solubility of the polymer) and the processing parameters affect the thin-film morphology and with it, the transistor performance (35, 37, 94, 95). To create tuneable sensors different configurations were chosen, which are as follows:

- a) P3HT in chloroform (CHCl_3)
- b) P3HT:PCBM in dichlorobenzene (DCB)
- c) P3HT in DCB
- d) DB-TTF and P3HT:DB-TTF in toluene

The different OFET-configurations were prepared, characterised and the suitability of the devices for applications in radiation research was tested. In the next part the different set-up configurations are presented and discussed.

Once the transistors were fabricated as described in chapter 3.1.2, their basic characterisation was performed to ensure the proper working of the devices. The output characteristic of the transistors was measured at room temperature with the gate voltage being decreased from 2V to -10V in steps of -2V, while drain-source voltage was decreased from 0V to -10V in steps of -1V. The sweep delay was kept at 1sec and the holding time before measuring the output characteristics was 1msec.

a) Characterisation of the composition P3HT in CHCl_3

P3HT dissolved in CHCl_3 was used since it is known that transistors made from this configuration show promising transistor properties like relatively high mobility and stability in water (15). Therefore, first tests were performed with this configuration. Transistors made of 1wt% and 2wt% P3HT in CHCl_3 solutions were characterised. At first, the polymer layer was examined (Figure 22). It clearly can be seen, that a homogenous layer for both wt% was formed on top of the electrodes. Furthermore, the thicknesses of the layers were determined with AFM as described in 3.3.1 since it is an important parameter of device performance (96). For 2wt% P3HT in CHCl_3 a thickness of 300nm was measured, which is about double as thick as for 1wt% P3HT in CHCl_3 , 150nm.

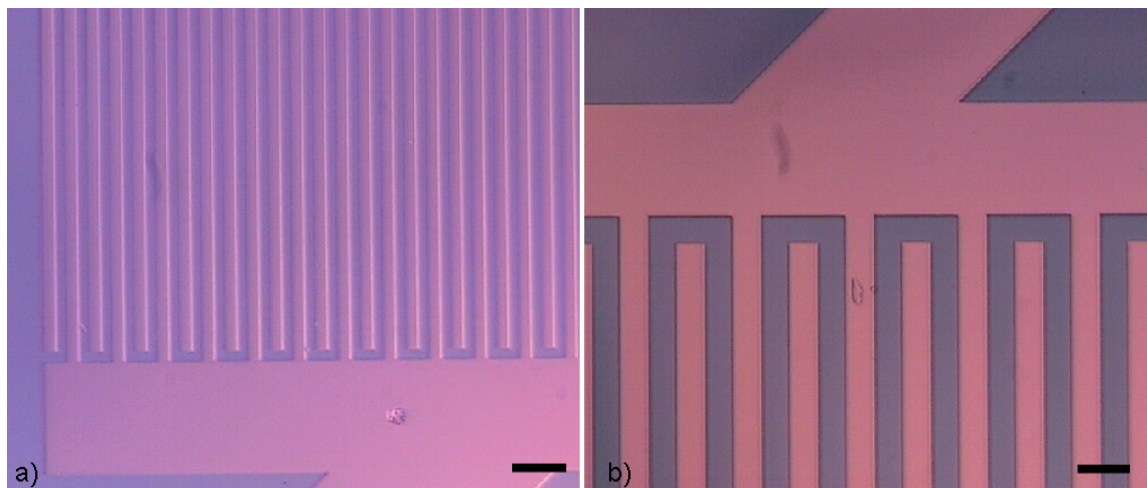


Figure 22 Optical images of the transistor surface take with 10x objective of a) 1wt% P3HT in CHCl_3 with $L = 20\mu\text{m}$ and b) 2wt% P3HT in CHCl_3 with $L = 50\mu\text{m}$. On both electrode structures, the polymer is forming an homogenous layer. The scale bar represents $100\mu\text{m}$.

The following graphs show the output characteristic of OFETs made of 1wt% (Figure 23) and 2wt% (Figure 24) P3HT in CHCl_3 . Measurements were performed as described in the introduction of this chapter.

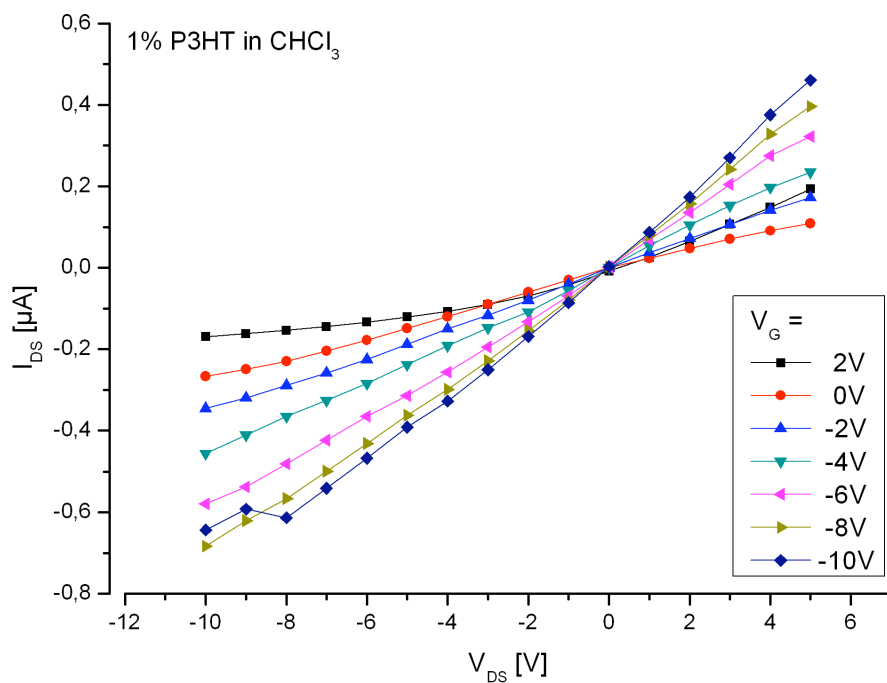


Figure 23 Output characteristic of a transistor made of 1wt% P3HT dissolved in CHCl_3 with channel length $L = 50\mu\text{m}$. V_G was decreased from 2V to -10V in steps of -2V, while V_{DS} was decreased from 5V to -10V in steps of -1V.

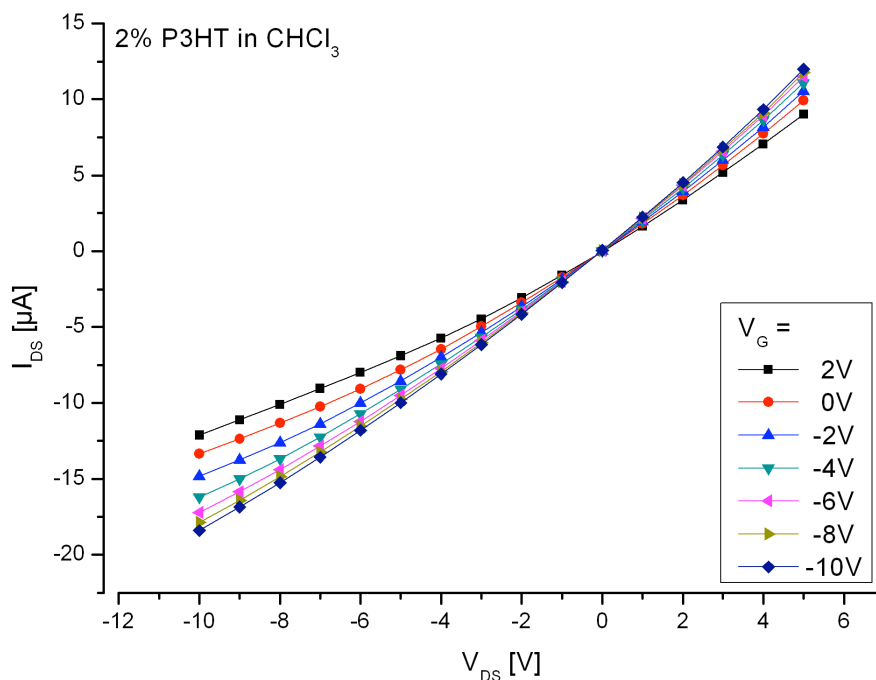


Figure 24 Output characteristic of a transistor made of 2wt% P3HT dissolved in CHCl_3 with $L = 50\mu\text{m}$. V_G was decreased from 2V to -10V in steps of -2V, while V_{DS} was decreased from 5V to -10V in steps of -1V

The transistors made from 1wt% P3HT showed low source-drain currents, but good transistor behaviour with a well-defined linear and saturation regime. The transistors made from 2wt% P3HT showed about one order of magnitude higher source-drain currents and there is no saturation regime visible.

b) Characterisation of the composition P3HT:PCBM in DCB

Preliminary results showed P3HT is an optically active material. When a transistor made from P3HT is excited with light the drain-source current increases and after excitation the current decreases again. The increase in the drain-source current caused by light is relatively fast, whereas the decay after turning the light off is relatively slow. For measuring online cell-cell communication processes during irradiation experiments, the transistor should switch as fast as possible. Then the decay after the irradiation does not superimpose the cell signals. Since it is known that blends of p- and n-type materials responses very fast to optical excitation, blends of P3HT and PCBM were prepared in different ratios: 1:1, 3:1 and 10:1. The transistor performance (Figure 25) and the response to UV light and white light were examined (data from white light is shown in Figure 26, results from UV light are not shown but exhibited the same behaviour).

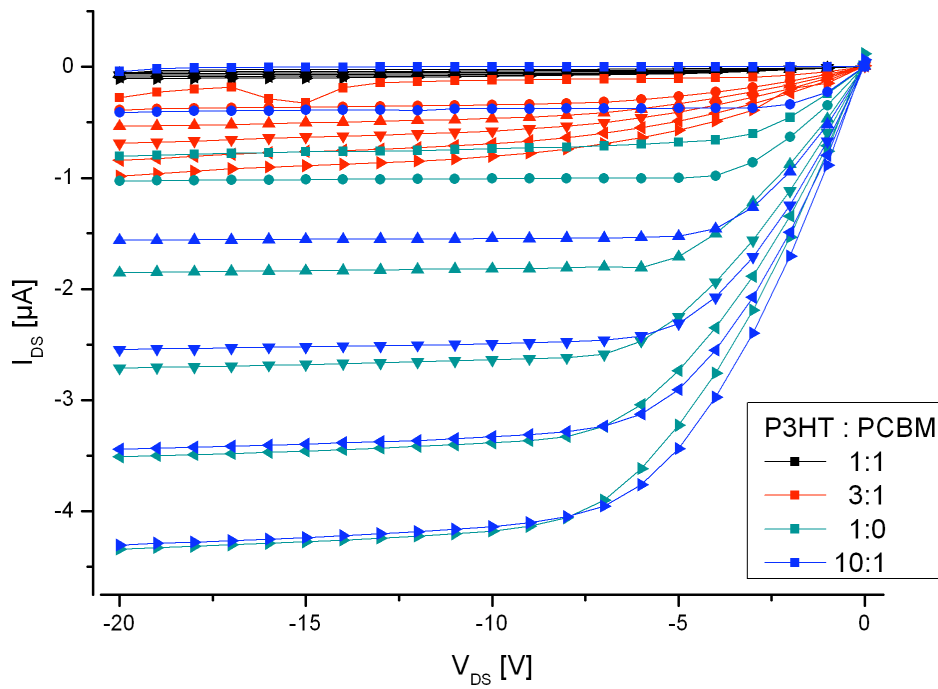


Figure 25 Comparison of the output characteristics of P3HT and P3HT:PCBM blends in DCB with the different ratios: 1:0, 1:1, 3:1 and 10:1. V_G was decreased from 5V to -20V in -5V steps and V_{DS} was decreased from 0V to -20V in steps of -1V. $L = 20\mu\text{m}$. With increasing amount of PCBM the transistor performance is reduced.

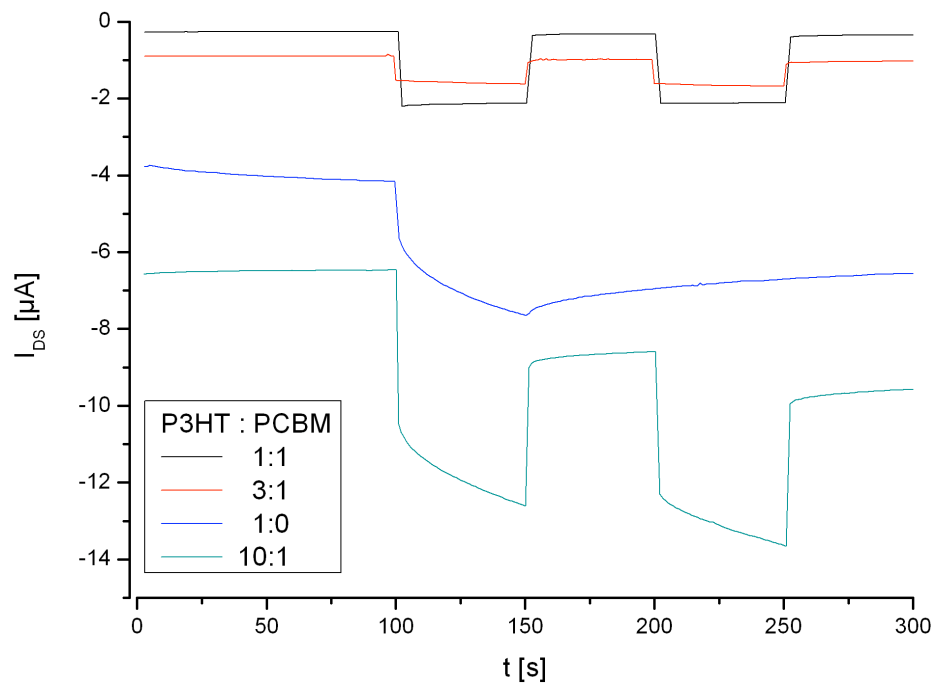


Figure 26 Comparison of the sensitivity to white light exposure of P3HT and P3HT:PCBM blends in DCB with the different ratios 1:0, 1:1, 3:1 and 10:1. $V_{DS} = -10\text{V}$, $V_G = -5\text{V}$ and $L = 20\mu\text{m}$. With increasing amount of PCBM the transistor response is faster the whit light exposure.

Output characteristics were recorded with the gate voltage being increased from 5V to -20 V in steps of -5V, while source-drain voltage was increased from 0V to -20V in steps of -1V. For the UV/white light characterisation the modulation of the drain-source current with respect to light exposure at fixed drain-source voltage $V_{DS} = -10V$ and a gate voltage of $V_G = -5V$ was measured (Figure 26). It is obvious that with an increasing amount of PCBM the transistor reacts faster on the radiation but the transistor performance is reduced. PCBM is an n-type material, which means that the charge carriers are holes. In combination with P3HT ambipolar transport is realised. The dielectric SiO_2 is known to trap negative charges (97) which might reduce the drain source-current with increasing amount of PCBM. Furthermore, gold is not the appropriate electrode material as its work function (5.1eV) is not close to the HOMO level of PCBM, which is around -6.1eV (98). Therefore, charge injection is reduced, which also alters the drain-source current. Based on these results and the fact that the drain-source current remains constant during excitation and returns to its initial value, it was decided to use the blend ratio 3:1. The transistor performance during X-ray radiation is characterised in chapter 4.2.3.

Furthermore, the transistor surface was examined optically (Figure 27). A homogenous layer was formed. The brighter and darker shades are typical for this blend.

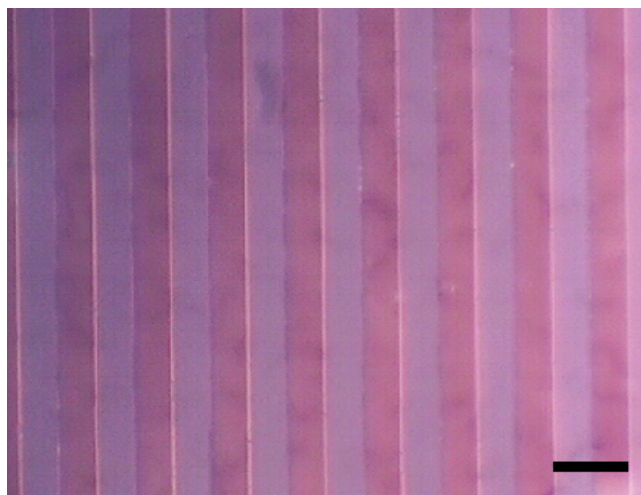


Figure 27 Optical image of the surface of a transistor made of P3HT:PCBM 3:1 in DCB with $L = 50\mu m$ taken with 10x objective. The brighter and darker shades are typical for this blend. The scale bar represents $100\mu m$.

c) Characterisation of the composition P3HT in DCB

Since the used solvent plays an important role in transistor performance, P3HT was also dissolved in DCB to examine the difference to P3HT dissolved in $CHCl_3$. After preparation as specified in chapter 3.1.2 the transistors were characterised as described

in the introduction of this chapter. The next graphs are showing the output characteristics of 1wt% and 2wt% P3HT dissolved in DCB (Figure 28 and Figure 29).

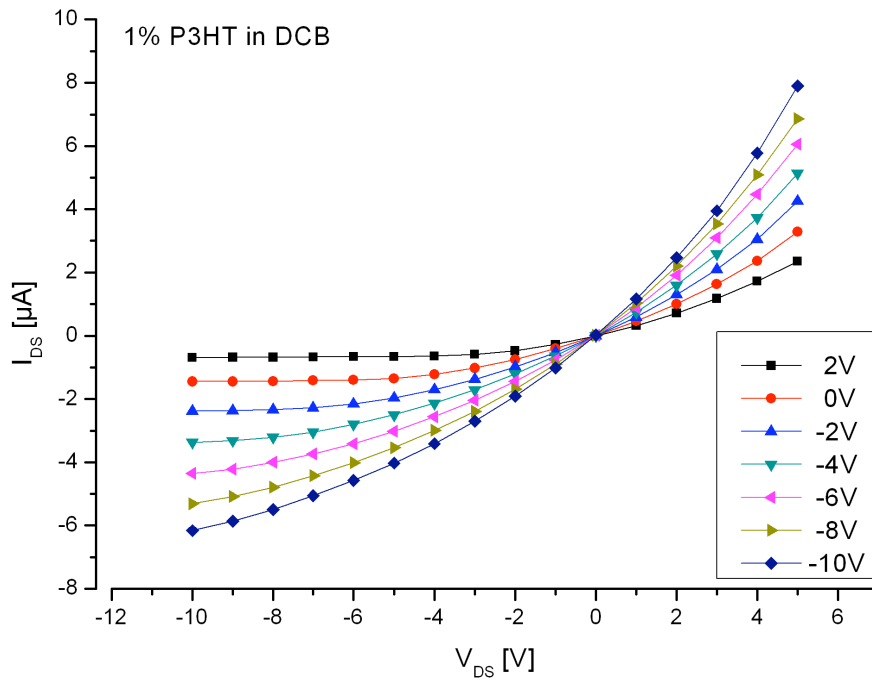


Figure 28 Output characteristic of an OFET made of 1wt% P3HT dissolved in DCB with channel length $L = 50\mu\text{m}$. V_G was decreased from 2V to -10V in steps of -2V, while V_{DS} was decreased from 0V to -10V in steps of -1V.

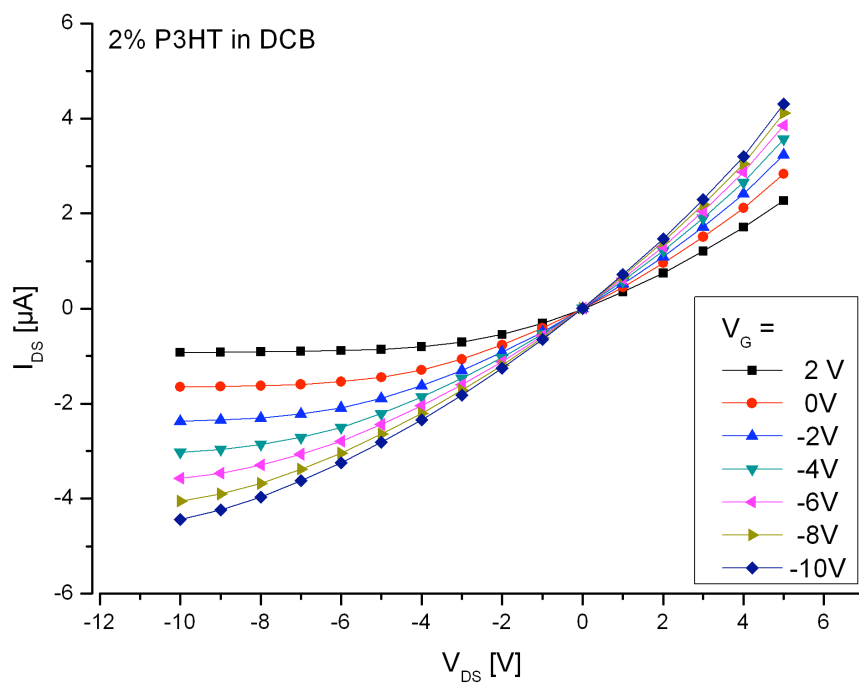


Figure 29 Output characteristic of an OFET made of 2wt% P3HT dissolved in DCB with channel length $L = 50\mu\text{m}$. V_G was decreased from 2V to -10V in steps of -2V, while V_{DS} was decreased from 5V to -10V in steps of -1V.

Both transistors are showing good transistor behaviour with linear regime and saturation regime. Here the transistors are almost in the same source-drain current regime with 1wt% showing a slightly higher current. Furthermore, the optical image of the transistor surface shows a homogenous polymer layer with only some non-influencing artefacts (Figure 30). Additionally, the thicknesses of the layers were determined with AFM as described in 3.3.1 as it is an important parameter for device performance (96). For 2wt% P3HT in DCB a thickness of 100nm was measured, which is about double as thick as for 1wt% P3HT in DCB, 50nm.

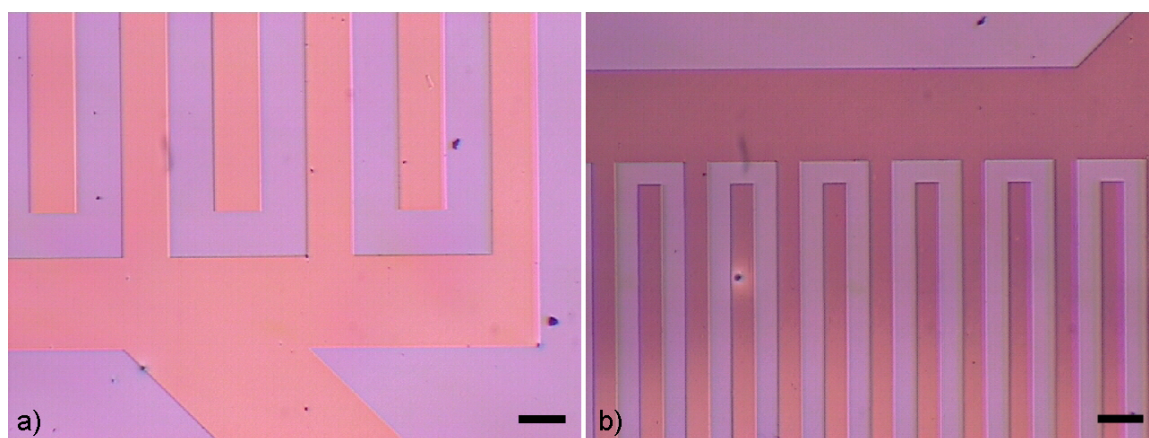


Figure 30 Optical image of the transistor surface of a) 1wt% P3HT in DCB with $L = 100\mu\text{m}$ and b) 2wt% P3HT in DCB transistor with $L = 100\mu\text{m}$ taken with 10x objective. The black dots in a) are dirt particles, the black dot on top of the electrode in b) is a non-influencing artefact from spin-coating. The scale bar represents $100\mu\text{m}$.

d) Characterisation of the composition DB-TTF and DB-TTF:P3HT in toluene

DB-TTF is, like P3HT, a solution processable p-type material. During the evaporation process of the solvent, the polymer DB-TTF forms crystals. The mobility inside the crystals ranges up to $1\text{cm}^2/\text{Vs}$ and therefore, DB-TTF is often used for single-crystal field effect transistors (99). Due to these properties, DB-TTF was used as conducting material in our set-up configuration. Figure 31 shows the top view of a transistor made from DB-TTF. Crystals with different lengths were formed and the orientation of the crystals is not ordered. Since charge transport is anisotropic, which means it is high along the crystals and low between the crystals, the transistor performance will be affected by the crystal geometry and orientation. Most important is that no homogenous layer is formed and it can clearly be seen that the electrodes are not completely covered with polymer. This will be a problem for measurements performed in liquid, since the electrodes will be in direct contact to the analyte resulting in an additional current through the analyte that probably influences the measured signal. Furthermore, when cells are grown on the transistor surface, they will be in direct contact to the electrodes,

which might result in cell signals caused by the applied drain-source voltage and not by the ionising radiation.

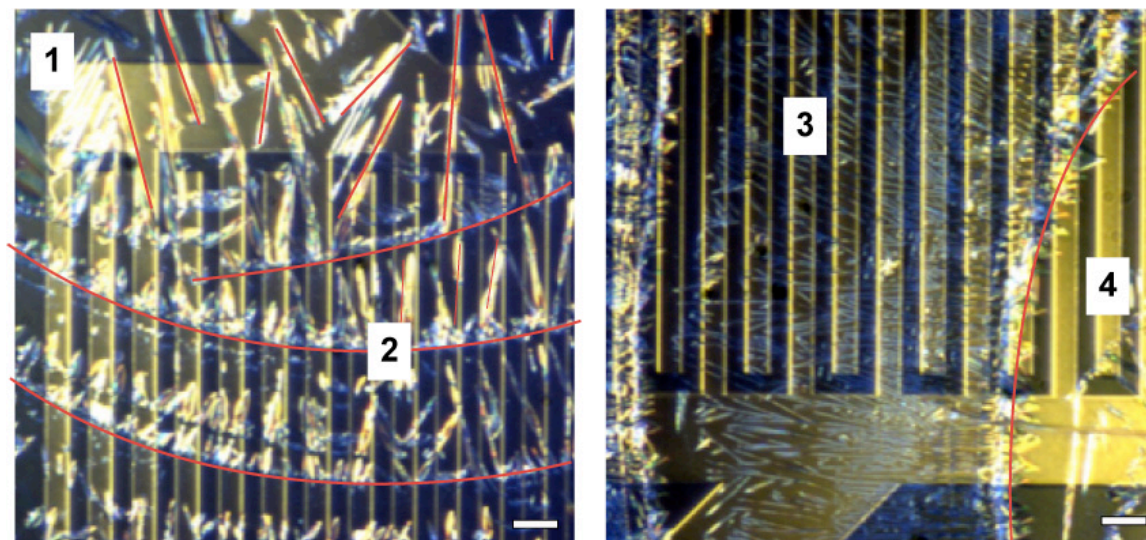


Figure 31 Optical images of the surface of a transistor made of DB-TTF in toluene with $L = 50\mu\text{m}$ taken with 10x objective. Here, four different regions of crystal orientation could be observed indicated with red lines: 1) no order in crystal orientation, 2) some order in crystal orientation, 3) region with almost uniform layer and 4) area where the electrode is not completely covered with polymer. The scale bar represents $100\mu\text{m}$.

To overcome these problems, a blend of DB-TTF and P3HT with a ratio of 1:1 dissolved in DCB was prepared. The next image (Figure 32) shows the polymer surface.

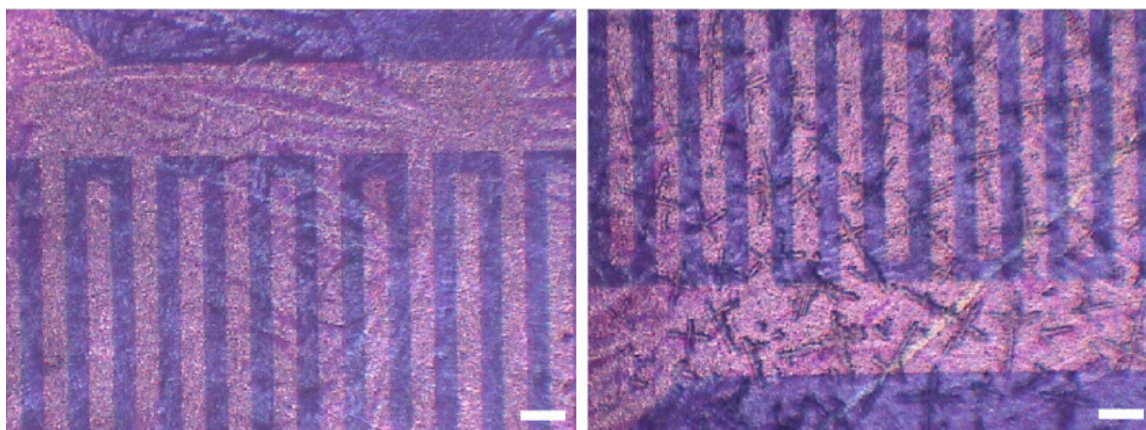


Figure 32 Optical image of P3HT:DB-TTF 1:1 in toluene surface taken with 10x objective. Again, no homogenous polymer layer was formed, but the electrodes are completely covered with polymer. Different regions with different crystal orientations can clearly be seen. The scale bar represents $100\mu\text{m}$.

By using this blend the electrodes were completely covered with polymer. However, the polymer still did not form a homogenous layer. There were regions with different crystal orientation, which will result in alterations in charge transport and therefore in the device

performance. It will be almost impossible to produce reproducible results with this polymer blend.

Summary

All transistors, which were electrically characterised, showed a positive threshold voltage, since the silicon dioxide was not treated separately. Already at zero gate voltage, a clearly conducting channel could be seen. Therefore, a low working point for drain-source current measurements could be chosen which is important for measurements in liquids to avoid unwanted electrochemical reactions and the activation of attached cells. Since problems with the reproducibility of transistors made from DB-TTF occurred, this configuration was not further characterised. Only the following configurations showed promising results and were used for further characterisation: 1wt% and 2wt% P3HT in CHCl_3 , 1wt% and 2wt% P3HT in DCB and 1wt% P3HT:PCBM 3:1 in DCB.

4.2 Demands for Application in Radiation Biophysics

To be able to use OFETs as biosensors in radiation biophysics, different requirements have to be matched. The sensor needs to be biocompatible, stable under the measurement conditions and furthermore capable to pick-up small pH changes and variations of the concentration of ions. This chapter deals with the suitability of the different transistor configurations for application in radiation-biophysical research. Biocompatibility studies and tests about stability in tissue culture medium as well as under ionising radiation are presented. Therefore characterisation of the sensor before and after exposure to the analyte of interest was performed and online measurements with a fixed drain-source and gate voltage during exposure to the analyte or X-ray radiation. At first, the results of the biocompatibility tests are presented.

4.2.1 Biocompatibility

Processing of the used non-toxic polymers (P3HT, PCBM, DB-TTF) relies on organic solvents like chloroform, toluene or dichlorobenzene, which are usually toxic for living cells. Consequently, a thermal treatment under nitrogen atmosphere above the boiling point of the used solvent was used to remove residues of the solvents from the polymeric layer. Details of the preparation can be found in chapter 3.1.2. Extracellular physical surface parameters (like wettability, surface energy, charge, roughness, modulus or exposure of chemical groups) affect cell biology of adherent grown cells and thus, are important for cell growth and development (26). Hence, biocompatibility studies and biofunctionalisation of the polymer surfaces were performed. For this purpose, the polymer was coated onto glass substrates and adherent growing L929 mouse fibroblasts were cultivated on the surface. Details about the cultivation process can be found in 3.2.1.

For the first biocompatibility test, cells were plated on the samples without any further treatment besides the solvent removal under nitrogen atmosphere (see. chapter 3.1.2). After cultivation time of 24h at 37°C the cells were examined and an optical image was taken (Figure 33 b).

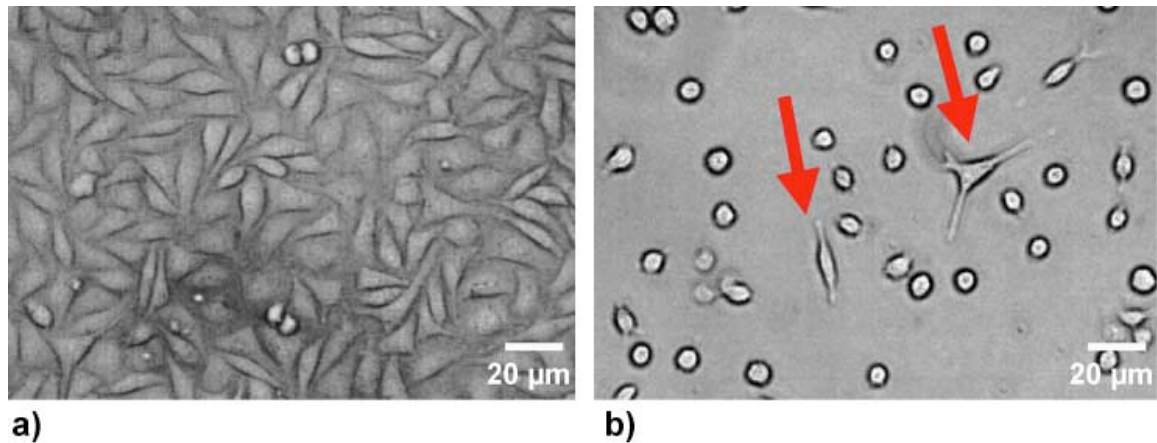


Figure 33 Optical image of L929 mouse fibroblast cultivated for 24hrs a) in a tissue culture flask and b) on P3HT surface without further treatment taken with 20x objective. The red arrows indicate cells that could already adhere to the untreated polymer surface.

Figure 33 shows the morphology of L929 mouse fibroblast grown in a tissue flask as reference (a) and on the polymeric surface (b). In Figure 33a), the cells are forming a confluent monolayer and are having their typical spindle-like shape. On the polymer surface, no confluent monolayer could be formed after a cultivation time of 24hrs. However, a few cells, indicated by the red arrows, could adhere to the surface. This experiment showed that it is possible to cultivate living cells on P3HT surfaces, but the adhesion is delayed. Furthermore, the survival rate of the cells was too low to perform reliable long-term experiments. The formation of a healthy morphology and a stable sticking of cells to the polymer surface represents a necessary precondition for all further studies of chemical and physical interactions between organism and electro-active polymers. Consequently, bio-functionalisation of the polymeric surface was performed to enhance cell adhesion on the polymer surface.

It was shown, that the hydrophobicity of the surface influences the interaction with the attached living cells. The rise in hydrophilicity favours adhesion of several cell types (100). Untreated P3HT shows a very hydrophobic surface due to methyl groups facing to the surface. Therefore, chemical and physical functionalisation was performed (see chapter 3.2.3). For chemical functionalisation, protein based coatings, like fibronectin, collagen and poly-L-lysine were used. Fibronectin is one of the extracellular matrix proteins that separates and supports the organs and tissues of an organism. It plays a major role in cell adhesion, growth, migration and differentiation and is commonly used as model protein for studies of cell interactions on surfaces (26). The structural protein collagen is found in the connective tissue of mammals. Collagen is the main component of connective tissue and affects cell-cell and cell-matrix communication and cell adhesion. Poly-L-lysine is a positively charged amino acid chain, which is widely used as a coating

to enhance cell attachment and adhesion to plastic ware and glass surfaces. For the physical functionalisation, a well-controlled oxygen plasma oxidation was performed. Here, the uncharged, hydrophobic P3HT methyl groups $-\text{CH}_3$ partially react with O^- to uncharged, hydrophilic $-\text{OH}$ groups, similar to the reaction of polydimethylsiloxane in oxygen plasma (101). A water droplet was placed on top of the P3HT surface before and after plasma oxidation and the contact angle (ϕ) between the P3HT surface and the water was examined (Figure 34). The contact angle is the angle between the liquid droplet and the surface and depends on the interaction between the two substances at the contact area. The lesser the interaction, the major is the contact angle. It clearly can be seen, that the contact angle is significantly reduced by the functionalisation. This means, the interaction between the surface and the liquid droplet was increased via changing the surface properties from hydrophobic to a rather hydrophilic.

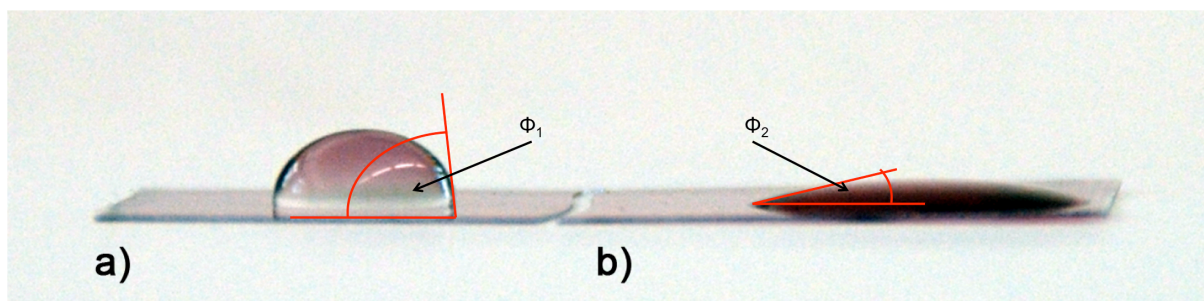


Figure 34 Contact angle (ϕ) of water droplet on P3HT surface a) before any treatment and b) after plasma oxidation. The hydrophobic surface gets more hydrophilic.

For the biocompatibility study the cells were cultivated on the different functionalised surfaces. Figure 35 shows the result after an incubation time of 24hrs. The images show that the cells attached very well to the pre-treated polymer surfaces. The cells have their spindle-like shape. It is apparent from the images that the cells attach and differentiate equally well on collagen (c), fibronectin (b) and plasma (d) and more poorly on poly-L-lysine (a). To assure that cells adhere to a sample surface, a formation of adhesion complexes that interact with proteins from the sample surface has to be achieved. When cells are seeded on the samples, the surface of the sample becomes coated with proteins from the culture medium before cells have the possibility to adhere. With changing the surface properties of the polymer by plasma treatment a better wetting was reached. Since wetting influences the protein adsorption onto the surface it also influences cell adhesion. With improved wetting, more proteins can be adsorbed onto the sample surface. A polar or charged surface will generally result in a higher degree of wetting as compared to non-polar surfaces (26).

In the case of the chemical functionalisation additional binding regions are formed by the coatings. The reason for the poor adhesion on poly-L-lysine functionalised surfaces might be that the poly-L-lysine itself was not well adsorbed to the hydrophobic surface and therefore only few additional binding sites for the formation of adhesion complexes were formed.

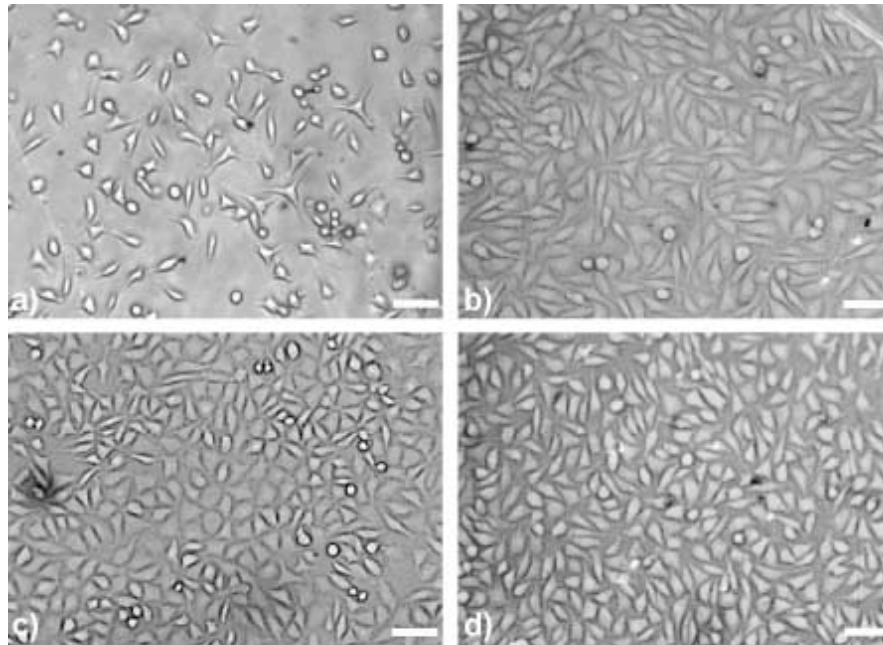


Figure 35 Optical images of L929 mouse fibroblast cultivated on the different functionalised P3HT surfaces taken with a 20x objective; a) poly-L-lysine, b) fibronectin, c) collagen and d) plasma treatment. The cells exhibit their healthy spindle like shape and grew equally well on all surfaces except poly-L-lysine. The scale bar represents 100 μ m.

To observe the cell morphology more precisely, AFM imaging studies and confocal microscopy studies were carried out on the L929 fibroblast after a cultivation time of 24hrs. Therefore, the cells were fixed with glutaraldehyde or paraformaldehyde. Both are known to provide excellent structure preserving properties (102). 3D AFM image of cells on a collagen pre-treated P3HT chip are shown in Figure 36a). From the magnified AFM picture it is apparent that the morphology of the cells is not influenced by the surface treatments and furthermore, no changes on the cell surface are visible. AFM images were recorded as described in 3.3.1. Figure 36b) shows a confocal image of the cells after a three-colour staining (see chapter 3.2.6). The different parts of the cells, like nucleus (here: blue; stained with Hoechst 33342), membrane (here: green; stained with DiO) and F-actin (here: red; stained with Rhodamin-Phalloidin), are showing no morphological changes.

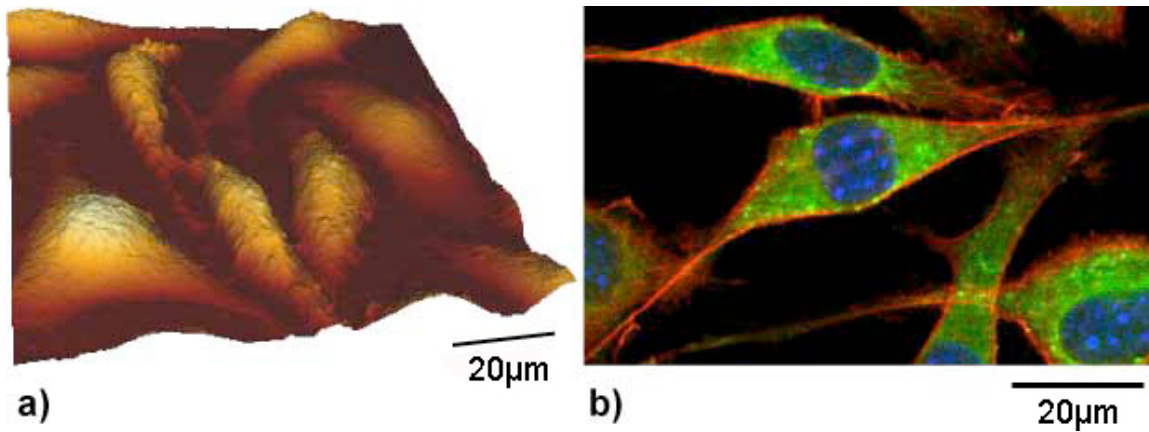


Figure 36 a) 3D AFM and b) confocal fluorescence microscopic image of fixed L929 mouse fibroblast cultivated on functionalised P3HT surface. No morphological changes are visible.

In conclusion, it could be shown that the vital requirement for the usage of polymeric surfaces in direct contact to cells in a biosensor, the biocompatibility, is reached. It was shown, that it is possible to cultivate living cells on polymeric surfaces without altering the cellular morphology. Since the plasma treatment and the functionalisation with fibronectin performed very well, the effect of the functionalisation on the transistor performance was tested and is discussed in chapter 4.3.2. These results are published and further details can be found in (103).

4.2.2 Stability in Tissue Culture Medium

For a lot of applications the analyte of interest must be detected in aqueous conditions. For example biological analytes and biologically derived recognition elements are only active in aqueous media (40). Additionally, for the use as a cell sensor the transistors need to operate in the tissue culture medium (104). Although, ion-sensitive field-effect transistors (9, 10) and sensors used in liquids (105) have been reported, the organic semiconducting layer is normally not directly exposed to the electrolytes and the transduction mechanism is based on the charging effects occurring at the electrolyte/insulator interface. Someya *et al* (106) were the first to explore OFETs operation with the active semiconducting material in direct contact with water. It was shown, that it is possible to operate OFETs in aqueous conditions and detect variations of different analytes like pH, ions or chemicals (15). Nevertheless, tissue culture medium represents a complex mixture of monovalent and bivalent ions, amino acids, carbohydrates and serum proteins that are likely to interact electrochemically with the organic surface (26). Therefore, the sensor performance needs to be examined in tissue culture medium. Up to now, only short-term measurements with the organic material directly exposed to complex tissue culture medium were performed by Lin *et al* (104). Here, an organic electrochemical transistor with PEDOT:PSS as active layer was used. However, the interaction between organic semiconductor and the analyte molecule is still not completely understood. Since long-term stability in aqueous condition is a critical parameter, the possibility to operate the P3HT-based OFET in tissue culture medium is not known. Also the impact of different morphologies on the transistor performance is unknown. Therefore, the different set-up configurations were investigated in tissue culture medium.

Output characteristics and online measurements with constant drain-source voltage were performed in tissue culture medium to test the stability of the sensors in this complex medium. The driving voltage was reduced to $\pm 1V$ to avoid unwanted electrochemical reactions. The duration of the online measurements varied from 5min up to 6hrs. After the exposure, the transistor surface was optically analysed. In case the surface did not show any degradation, the next measurement was performed. The transistors were considered to be stable when a 6-hour measurement could be performed without any electrically or optically degradation of the transistor.

a) Stability Tests of the Composition P3HT in CHCl_3

For the online measurement a constant drain-source voltage was applied and the drain-source current was measured while exposed to tissue culture medium. Figure 37 shows a 2.5hrs measurement of a P3HT CHCl_3 transistor exposed to tissue culture medium. The applied drain-source voltage is $V_{\text{DS}} = 1\text{V}$. It is obvious that the drain-source current decreases with time. This might be caused by the so-called bias-stress effect, which is typical for organic transistors (29, 30) or by doping or charge trapping effects caused by the tissue culture medium. Furthermore, it can be seen that at $t = 2000\text{s}$ the noise level is increasing.

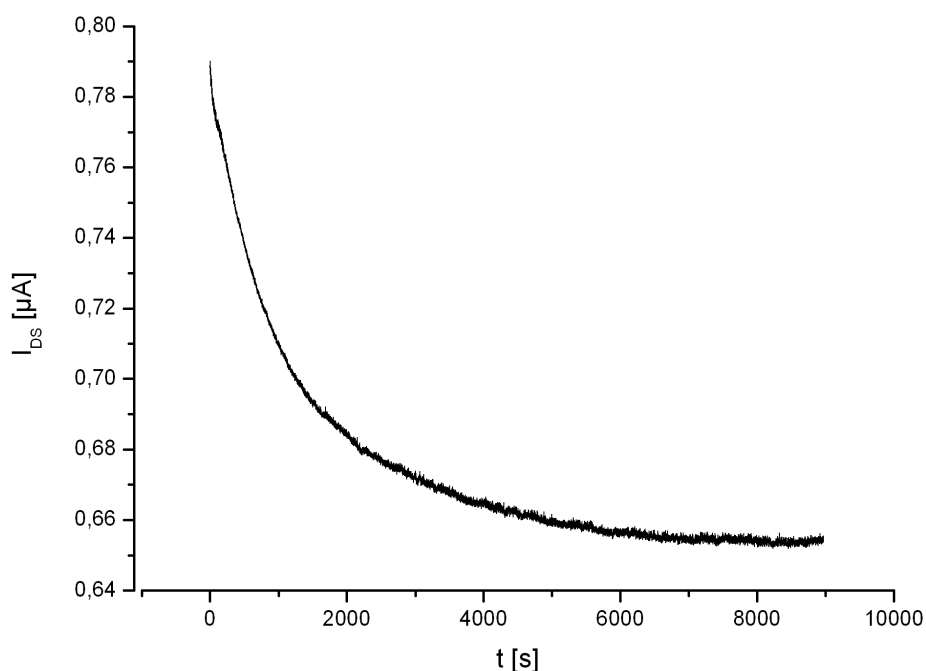


Figure 37 Measurement of drain-source current of a 1wt% P3HT in CHCl_3 exposed to tissue culture medium with $V_{\text{DS}} = 1\text{V}$. The current gets very noisy starting at around 2000s, which might be caused by degradation of the polymer.

By analysing the optical images (Figure 38) taken after different times, it can be seen that the polymer degrades. It clearly can be seen, that just after 1hr, the first changes on the surface occur. After 6hrs whole parts of the polymer delaminated from the electrodes. Furthermore, the polymer on the source electrode partially removed, which can be seen in the lightening of the colour. Since direct current (DC) voltage was applied it is possible that polarisation effects occur, which in turn can damage the polymeric layer by degradation and/or delaminating.

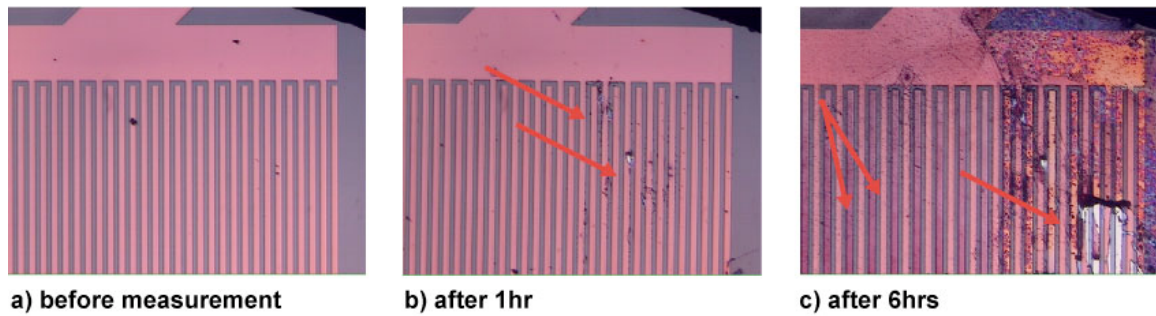


Figure 38 Optical images of the surface of a 1wt% P3HT in CHCl_3 transistor a) before, b) after 1hr and c) after 6hrs of measurement taken with a 10x objective. It can clearly be seen that already after 1hr the polymer surface is damaged. After 6hrs the polymer delaminates from the electrodes. Furthermore from the source electrode polymer is removed indicated by lightening of the electrodes.

As a next step, the different components of the medium were analysed to understand which component of the medium has the negative effect on the transistor. Therefore, solutions containing the components with the highest portion in the tissue culture medium were prepared and measurements were performed as described above. Table 7 summarises the different components and the transistor stability after different times. In the first column the different components of the medium are listed, in the second the transistor degradation. “-” stands for no degradation and “+” for degradation of the transistor. The time in the last column indicates when degradation occurred or how long the transistor was stable.

Table 7 Measurements performed with the different components of tissue culture medium.

solution	degradation	time
PBS	-	2hrs
$\text{C}_6\text{H}_{12}\text{O}_6$ in H_2O	-	12hrs
NaHCO_3	-	6hrs
Amino Acid in H_2O	-	6hrs
Amino Acid in PBS	+	30min
Medium with Pen/FBS	+	5min
Penicillin (Pen in H_2O)	+	4hrs
FKS	+	15min
Medium without FBS/Pen	-	6hrs

Since penicillin and FBS also reacted with the transistors forming either deposits or rivulets on the surface of the transistors, medium without penicillin and FBS were prepared and analysed. Here, the transistor functioned properly even longer than 6hrs. There were some degradation, but the transistor worked fine. Furthermore, the combination of the amino acids and PBS had an effect on the transistor whereas the amino acids dissolved in pure water did not affect the transistor. Since tissue culture

medium is a very complex system it is not understood why the transistors showed this degradation.

Another approach was to apply an alternating current (AC) instead of DC to minimize polarisation effects. By using a frequency of 1Hertz and an amplitude of +/- 1V stable measurements in tissue culture medium up to 12hrs could be performed. Therefore, AC measuring mode could be an option for preventing liquid-related damages and prolonging the lifetime of the device. Further information can be found in the corresponding publication of Scarpa *et al* (107).

b) Stability Tests of the Composition P3HT:PCBM 3:1 in DCB

The following graph (Figure 39) compares 3 measurements as a function of different incubation times with tissue culture medium. The drain-source voltage was reduced to +/- 1V to avoid unwanted electrochemical reactions. The measurement “0 min” was recorded directly after exposure of the RPMI medium on the transistor surface, “15 min” was recorded after the 15-min online measurement and “6 hrs” after the 6-hour online measurement. It is obvious, that the drain-source current is reduced with longer duration of the measurement. This might either be caused by degradation of the polymer or by charge-trapping effects (Figure 39).

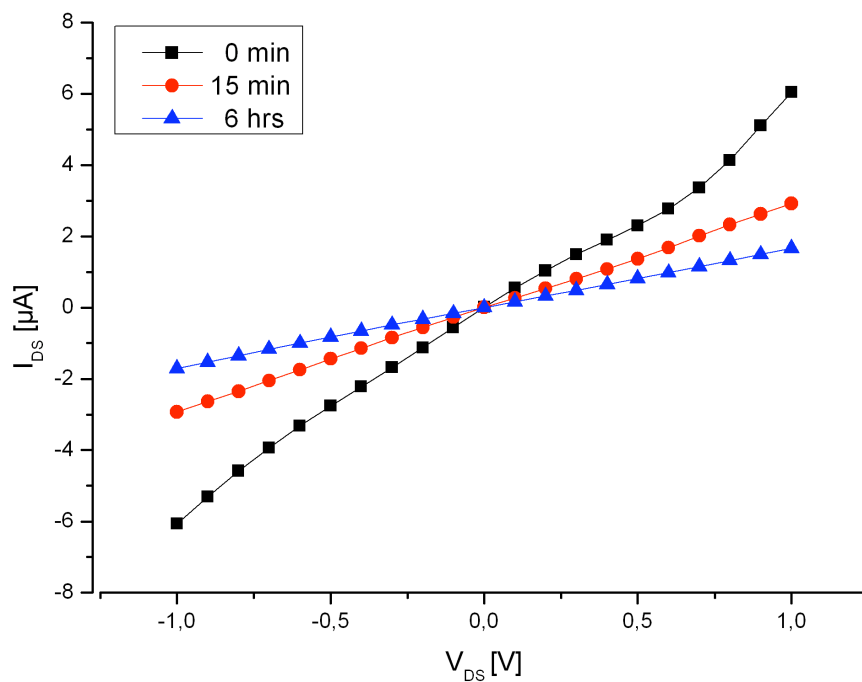


Figure 39 Characteristic of P3HT:PCBM in DCB transistor with $L = 50\mu\text{m}$ after different incubation times with tissue culture medium at $V_G = 0\text{V}$. V_{DS} was varied from 1V to -1V in 0.1V steps.

Next, a constant drain-source voltage of $V_{DS} = -0.5V$ was applied and the drain-source current was measured during exposure to tissue culture medium (Figure 40). The drain-source current decreases with time, indicating a charge trapping effect. The result is consistent with the output measurements shown in Figure 39. The drain-source current shows some noise and is not completely stable. The noise might be caused by poor connection since the “old” way of contacting like described in chapter 4.1.1.1 was used.

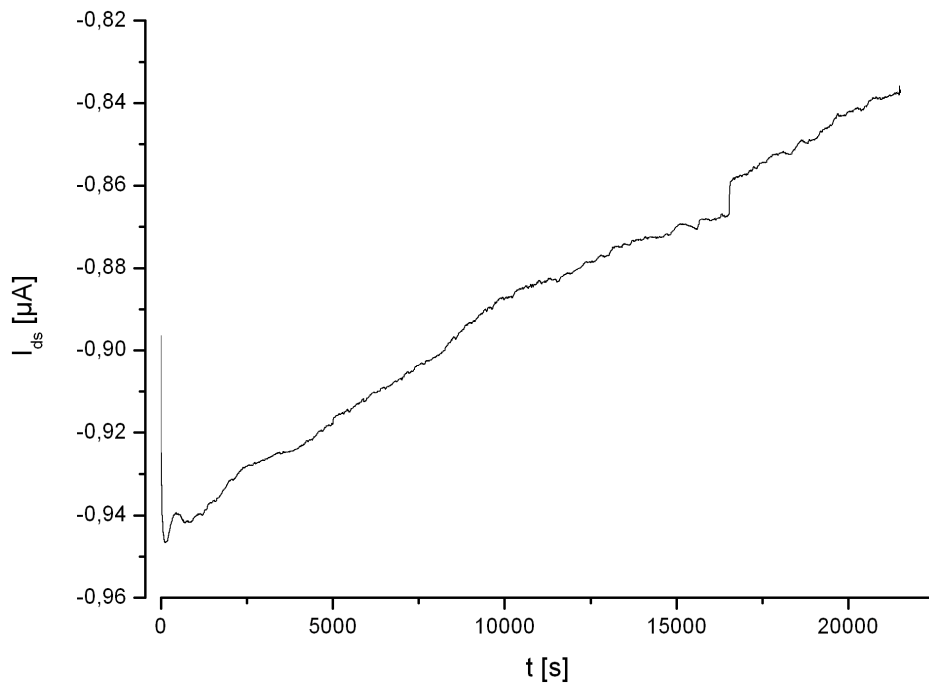


Figure 40 Measurement of drain-source current of a P3HT:PCBM transistor with $L = 50\mu\text{m}$ exposed to tissue culture medium with $V_{DS} = -0.5V$ and $V_G = 0V$. With increasing exposure time the drain-source current decreased, probably caused by charge trapping effects.

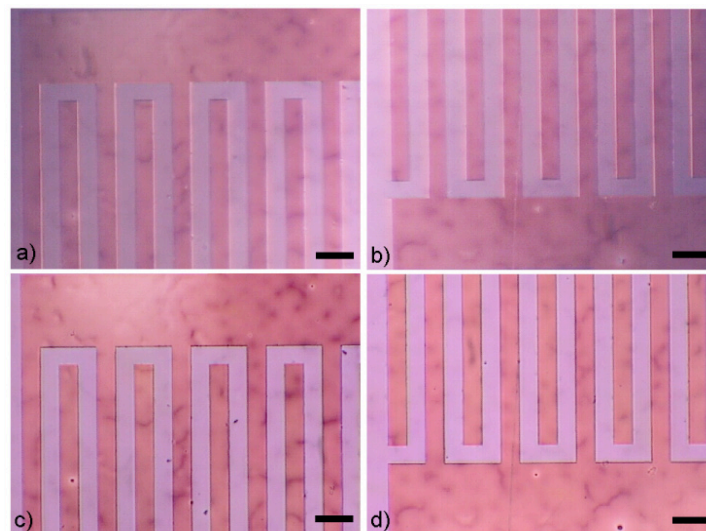


Figure 41 Optical detail image of the surface of an transistor made of P3HT:PCBM in DCB, a), b) before and c), d) after 6-hour measurement in tissue culture medium taken with a 10x objective. It can be seen, that the transistor surface is not degraded during the measurement. The scale bar represents $100\mu\text{m}$.

Figure 41 shows the transistor surface before and after the 6-hour measurement. By comparing the images, it can be seen, that no degradation or even delamination occurred. The brighter and darker shades were typical for the blend P3HT:PCBM.

c) Stability Tests of the Composition P3HT in DCB

At first, output characteristics were recorded directly after exposure to the tissue culture medium, after 15min and after 6hrs as described in the introduction of this chapter (Figure 42).

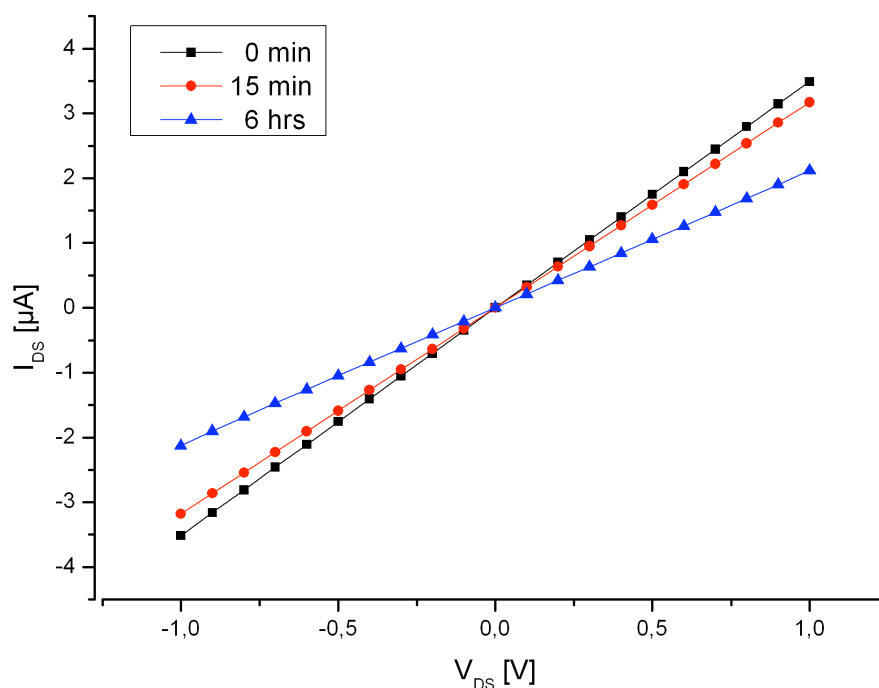


Figure 42 Characteristic of a 2wt% P3HT in DCB OFET with $L = 50\mu\text{m}$ after different incubation times in tissue culture medium at $V_G = -1\text{V}$. V_{DS} was varied from 1V to -1V in 0.1V steps.

Again, the drain-source current decreases with time. Figure 43 shows the corresponding 6-hour online measurement with $V_{DS} = -0.5\text{V}$. The drain-source current is very stable and shows a good signal to noise ratio. Again, the overall drain-source current decreases with time, caused either by the bias-stress effect and/or charge trapping of the tissue culture medium.

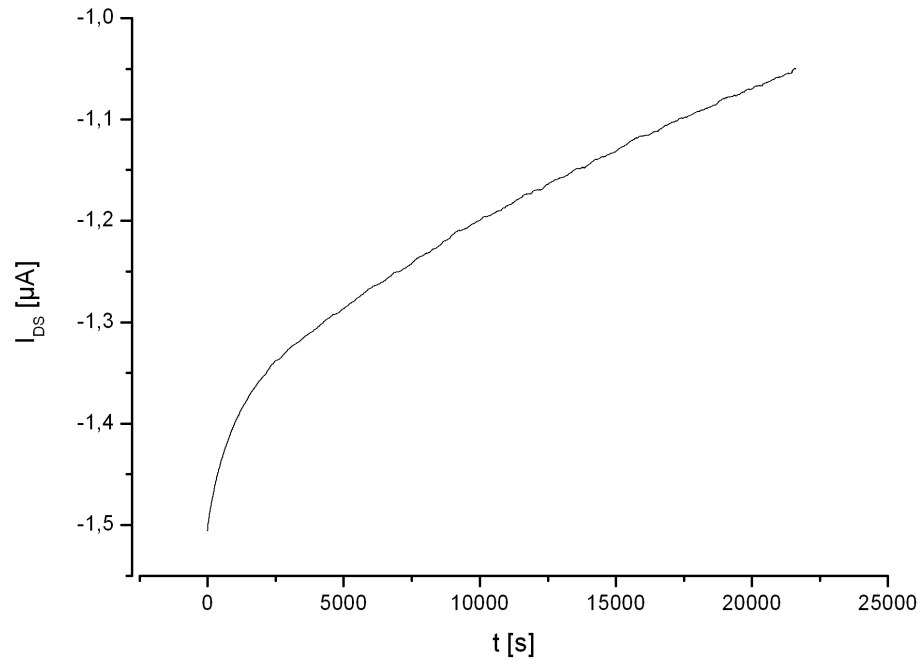


Figure 43 Drain-source current at $V_{DS} = -1V$ of a transistor made of 2wt% P3HT in DCB with channel length of $L = 50\mu m$. The active area was exposed to tissue culture medium during the whole measurement. With increasing incubation time the drain-source current decreases.

With analysis of the transistor surface, it can be seen, that the polymer is not degraded (Figure 44). The dark spots on the surface after 6hrs are probably dried medium and not degradation of the polymer. The spots indicated with the arrow in a) and c) are so-called comets which formed during the spin-coating process.

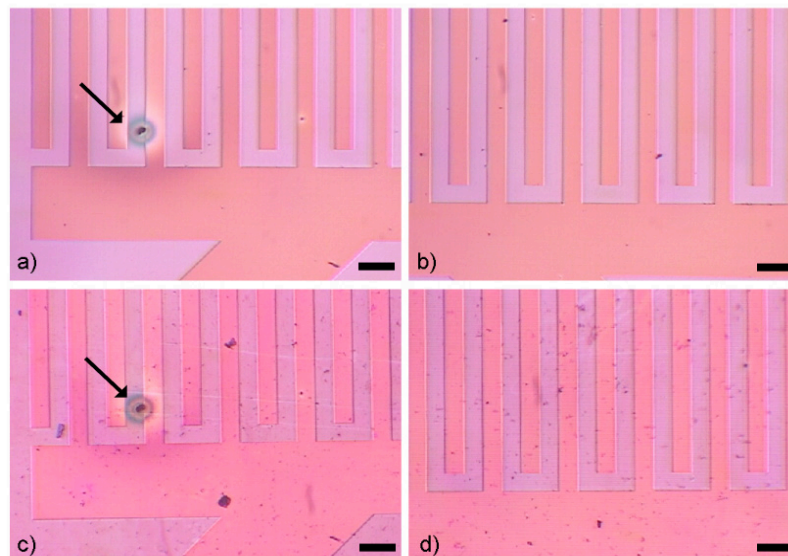


Figure 44 Optical image of a 2wt% P3HT in DCB OFET taken with a 10x objective a), b) before and c), d) after 6-hour measurement in tissue culture medium. No degradation is visible, the dark spots in c) and d) are deposits of dried medium. The spots in a) and c) indicated with the red arrows are artefacts from spin-coating. The scale par represents $100\mu m$.

Summary

During the online measurements, all transistors showed the same trend: the drain-source current decreases. The decrease in I_{DS} is faster than when measured in air, which indicates an interaction of ions from the tissue culture medium with the polymer film. Nevertheless, with varying the solvent for the thin-film preparation, the transistor performance is influenced. The results show, that already the used solvent can tune the transistor stability in tissue culture medium. The configuration P3HT in CHCl_3 is not stable for long-term measurements in tissue culture medium. When instead of CHCl_3 the polymer is dissolved in DCB, the configuration is stable. Reasons therefore might be that a more stable morphology of the polymer was formed. Furthermore, it is possible, that somehow the adhesion of the polymer on the silicon dioxide is enhanced with using DCB instead of CHCl_3 . Also the blend of P3HT:PCBM, dissolved in DCB, is stable. Since it is possible to operate the transistors made from P3HT in CHCl_3 in an altered tissue culture medium, all configurations were further characterised for the application as biosensor.

4.2.3 Stability under Ionising Radiation

To be able to perform reliable cell measurements under ionising radiation with the polymer sensors, the effect of the radiation on the sensors needs to be determined. It is known that the performance of electronic devices degrades with their exposure to ionising radiation (108). Nevertheless, devices made from organic material are already used as radiation detectors. Either by organic photovoltaic devices in combination with scintillating materials (109, 110), or by measuring the change in conductivity of an organic material as function of ionising radiation dose (108). Raval *et al* (108) reported OFET devices based on P3HT which were irradiated with a Cobalt-60 radiation source and doses between $D = 10\text{-}400\text{Gy}$. The reported devices were stable and sensitive to the Cobalt-60 radiation. In our case doses 10-400 times smaller than reported in this study will be used. Therefore, the different set-up configurations used here will probably not show degradation caused by the irradiation. Nevertheless, it is not known if the devices are able to determine the low dose radiation and how the combination of tissue culture medium and ionising radiation affects the device performance.

For device characterisation online measurements during irradiation and output characteristic before and after irradiation were performed. For the online measurement, the device was placed in the irradiation chamber and the measurement was started. After a conditioning time of about 1hour, the X-ray machine was turned on and the sample was irradiated. For the different irradiation pulses distinct energies were used. Instead of a cover plate, which screen the irradiation from the transistor, the X-ray radiation was turned on and off for every irradiation pulse. First experiments were performed in air and then the measurements were repeated in tissue culture medium. These measurements were performed with all three configurations to see, if the thin-film morphologies affects the transistor performance. In the following graphs the red bars indicate the irradiation period for all measurements.

a) X-Ray Characterisation of the Composition P3HT in CHCl_3

A constant drain-source voltage of $V_{\text{DS}} = 3\text{V}$ was applied and the drain-source current was measured online during irradiation with different settings. Three irradiation cycles were performed with the following settings of the X-ray machine: first and second irradiation pulse: 150kV, 18mA, 1.1Gy and the third irradiation pulse: 200kV, 18mA,

1.9Gy. The next graph (Figure 45) shows the drain-source current of the online measurement.

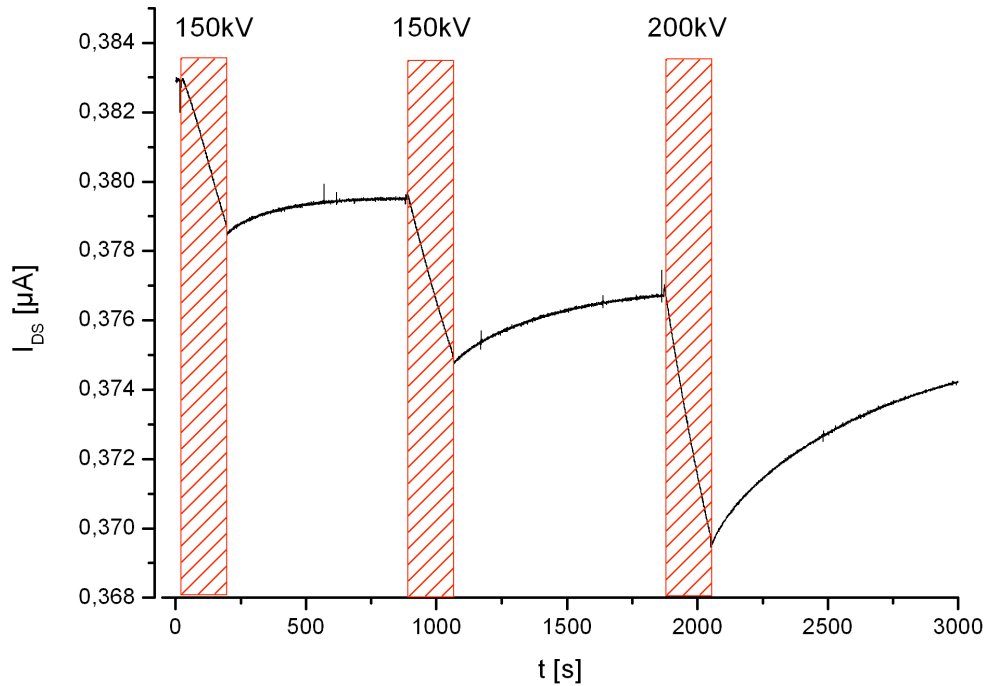


Figure 45 Drain-source current of a transistor with channel length of $L = 50\mu\text{m}$ made of 1wt% P3HT in CHCl_3 during pulsed X-ray radiation with $V_{\text{DS}} = 3\text{V}$ and $V_{\text{G}} = 0\text{V}$. The red bars indicate the radiation.

During the irradiation, a change in the drain-source current is visible. The current decreases during irradiation and increases again afterwards. The recovery after irradiation is much slower than the decay during the irradiation. These variations are very small and in the nA range. Table 8 compares the variation in drain-source current (ΔI) caused by irradiation and the change per Gray ($\Delta I/\text{Gy}$). With increasing dose, the variation in the drain-source current increased, but the change per Gray is not exactly consistent. Nevertheless, the transistors showed a stable performance during the irradiation and were not damaged by the X-rays.

Table 8 ΔI and $\Delta I/\text{Gy}$ for the different irradiations

	1. irradiation	2. irradiation	3. irradiation
ΔI [μA]	0.0045	0.0047	0.0072
$\Delta I/\text{Gy}$ [$\mu\text{A}/\text{Gy}$]	0.004	0.0043	0.0038

The next step was to perform online measurement in tissue culture medium. A constant drain-source current of $V_{DS} = 1V$ was applied and the drain-source current was recorded during irradiation. The settings for the X-ray machine were: 16mA, with varying acceleration voltage from 60-100kV in 20kV steps. The response of the transistor to the X-rays is depicted in Figure 46.

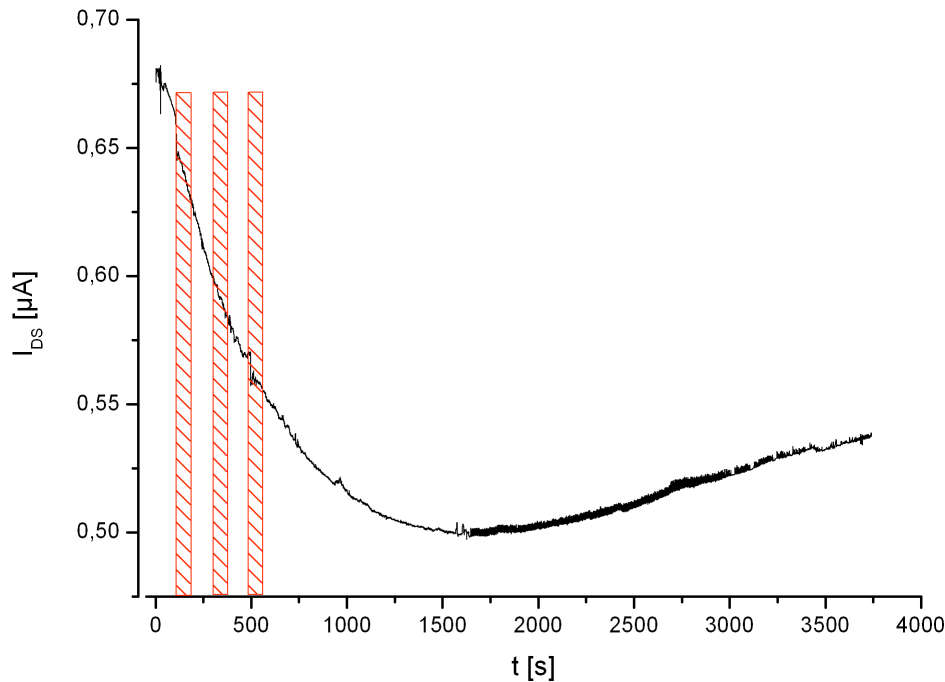


Figure 46 Drain-source current of a 1wt%P3HT in $CHCl_3$ transistor with $V_{DS} = 1V$, $V_G = 0V$ and channel length $L = 50\mu m$ during X-ray radiation in tissue culture medium. The areas highlighted by the red bars show the irradiation. The radiation has no effect on the transistor performance.

We can see that there is no response of the transistor behaviour to the X-rays. An additional effect of the tissue culture medium seems to superimpose the effect of the irradiation. Furthermore, the current is decreasing, but after a certain point the transistor currents starts rising. At this point (around 1500 sec) the polymer layer is degraded due to the tissue culture medium. The rise in the drain-source current can be explained by the fact that during delaminating of the polymer, the electrodes got in direct contact to the culture medium and an additional current through the electrolyte is measured.

b) X-Ray Characterisation of the Composition P3HT:PCBM 3:1 in DCB

A constant drain-source voltage of $V_{DS} = -0.5V$ was applied and the drain-source current was measured during irradiation. Here, the acceleration voltage was kept constant and the tube-current was varied from 4-20mA in 4mA steps. Figure 47 shows the online measurement. The drain-source current decreased during irradiation. With increasing

dose the variation in the drain-source current (ΔI) increases. After irradiation, the drain-source current increased again. It is obvious, that the transistor does not react as fast as during irradiation with white light (see Figure 21). Further comparing both measurements, one can see, that the behaviour during the irradiation differs. While during exposure to UV or white light the drain-source current reached a plateau, during exposure to the X-rays the drain-source current steadily increased. Additionally, during X-ray radiation the drain-source current decreases, whereas during UV or white light exposure the drain-source current increases. Also, after the irradiation, the drain-source current did not get back directly to its starting value like after the irradiation with UV or white light. This increase after irradiation was almost as fast as the decrease during the irradiation.

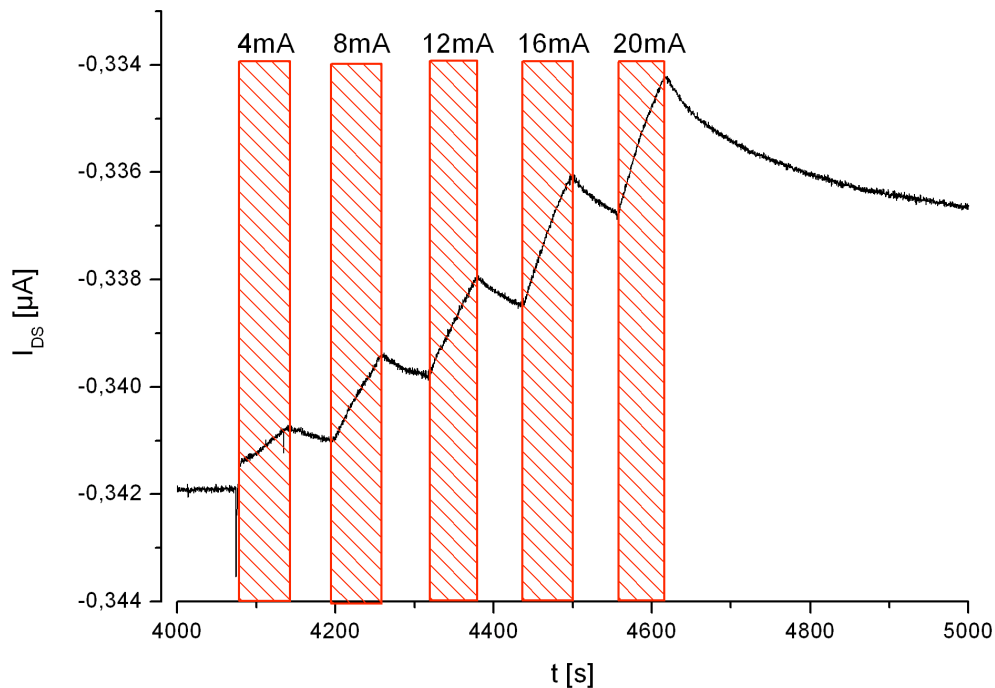


Figure 47 Drain-source current at constant drain-source voltage of $V_{DS} = -0.5V$ and $V_G = 0V$ of an OFET made from P3HT:PCBM 3:1 in DCB during irradiation with different energies. The red bars indicate the irradiation.

The next table (Table 9) summarises the changes in drain-source current (ΔI) and the change per dose ($\Delta I/mGy$) for the presented measurement.

Table 9 ΔI and $\Delta I/mGy$ for the different irradiations

150kV	4mA	8mA	12mA	16mA	20mA
D [mGy]	91.648	180.349	255.678	366.451	436.959
ΔI [μA]	1.18E-3	1.62E-3	1.95E-3	2.4E-3	2.53E-3
$\Delta I/mGy$ [$\mu A/mGy$]	1.28 E-5	8.9 E-6	8.6 E-6	6.5 E-6	5.70 E-6

It can be seen, that ΔI increases with increasing dose, but $\Delta I/mGy$ becomes less with every following radiation. Again, the changes in drain-source current are in the nA range.

To test the stability of this set-up configuration in tissue culture medium, the measurement was repeated in liquid (Figure 48). Like with the composition P3HT in $CHCl_3$, no effect of the X-rays on the transistor is visible. Only a small peak at the very beginning of the irradiation can be seen which might be caused by switching the X-ray machine on.

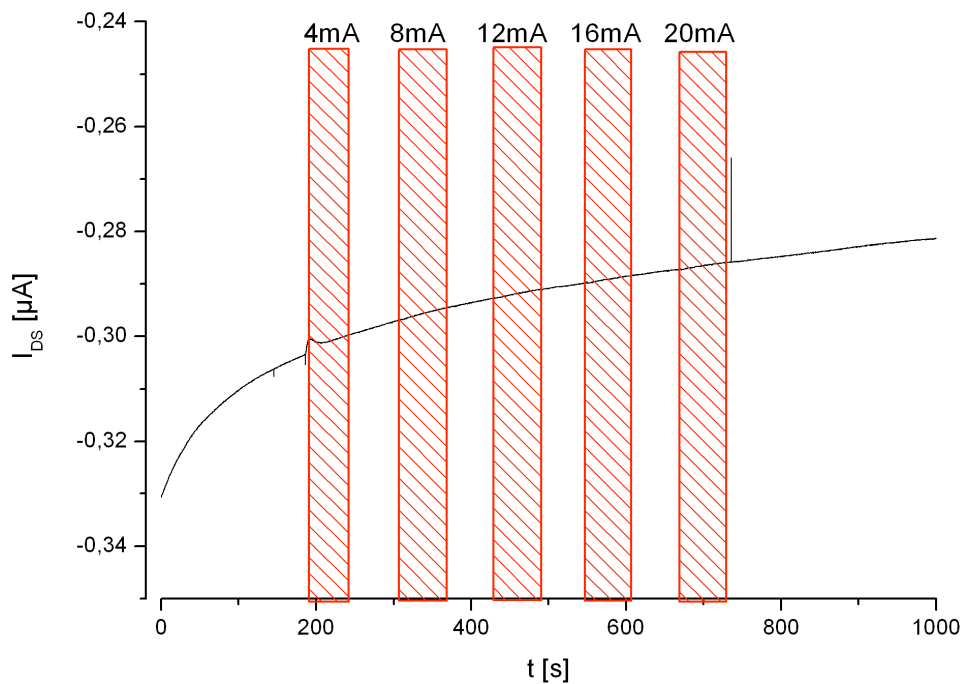


Figure 48 Drain-source current of a transistor P3HT:PCBM 3:1 in DCB and $L = 50\mu m$ exposed to tissue culture medium with respect to irradiation with $V_{DS} = -0.5V$ and $V_G = 0V$. The X-ray machine was operated at 150kV and the accelerating voltage was varied from 4mA to 20mA. The red bars indicate the irradiation.

c) X-Ray Characterisation of the Composition P3HT in DCB

The first experiment was to test if the transistor performance is altered because of X-ray radiation. Therefore, the output characteristic of the transistor was recorded before and directly after irradiation of the transistor. The gate voltage was decreased from 2V to -10V in steps of -2V, while drain voltage was decreased from 0V to -20V in steps of -1V (Figure 49). The X-ray machine was operated at 150kV and 4mA resulting in a dose of $D = 100mGy$.

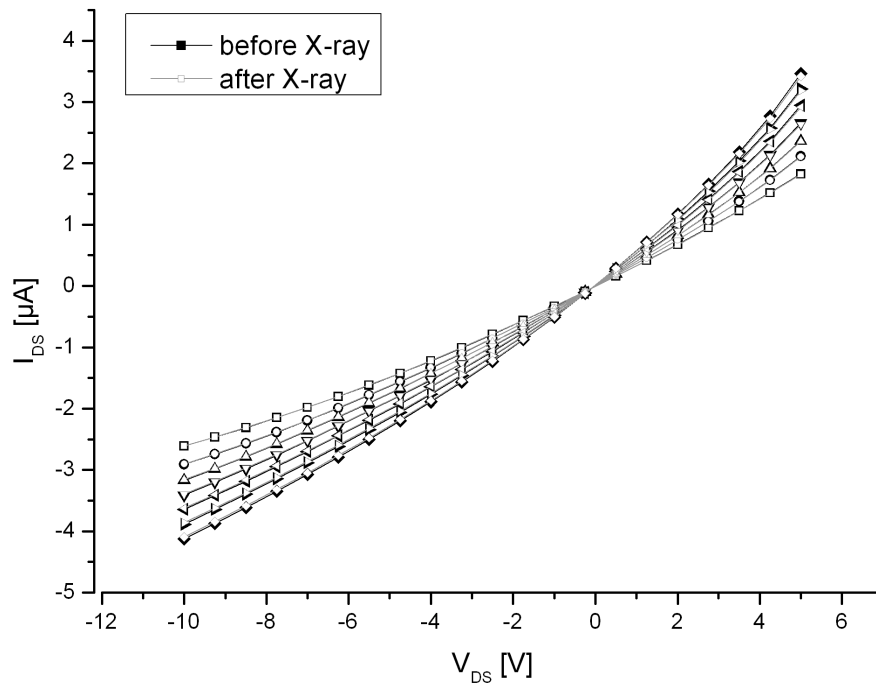


Figure 49 Output characteristics before and after irradiation of a transistor made of 2wt% P3HT in DCB with $L = 50 \mu\text{m}$. No effect of the radiation is visible. The X-ray machine was operated at 150kV and 4mA resulting in a dose of $D = 100\text{mGy}$.

It is obvious that both characteristics are almost identically. Therefore, it can be assumed, that the transistor is not affected or destroyed by the irradiation.

Like for the other transistor configurations also online measurements were performed. A constant drain-source voltage and a constant gate voltage were applied and the drain-source current was measured with respect to the X-rays. Figure 50 shows the measurement with following settings: $V_{\text{DS}} = -0.5\text{V}$, $V_{\text{G}} = -1\text{V}$, 150kV, 4mA and $D = 100\text{mGy}$. The irradiation was repeated two times. Again, the change in drain-source current is very small. ΔI is for the first irradiation is about 0.7nA and for the second irradiation about 0.6nA, which is almost identically. Furthermore, the current decreases continuously during the irradiation. After irradiation, the current increases again, but much slower than the decrease during irradiation.

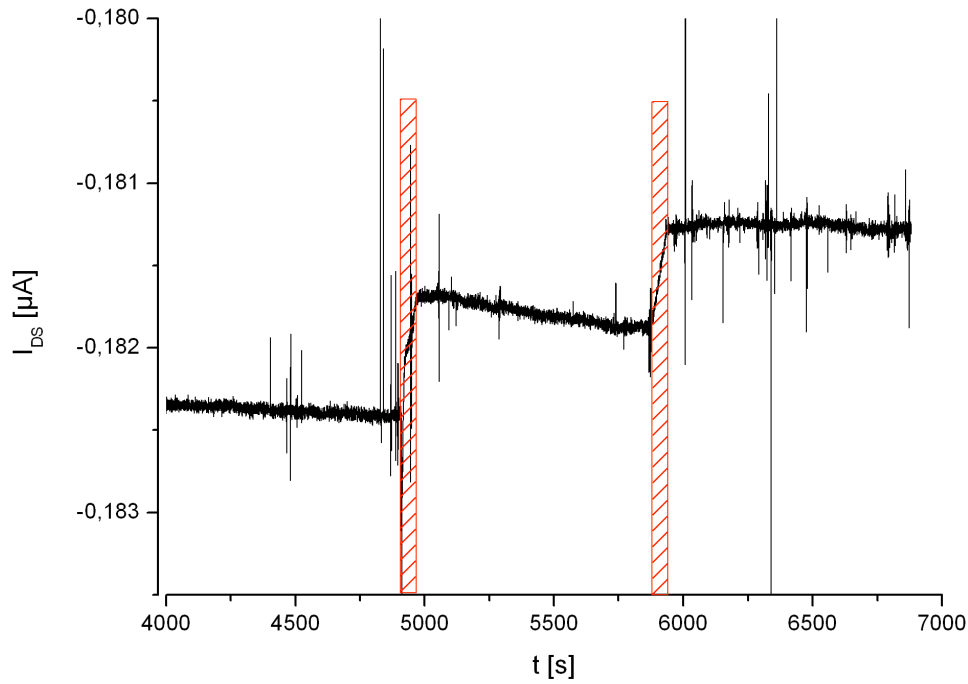


Figure 50 Drain-source current of a transistor made of 2wt% P3HT in DCB with $L = 50\mu\text{m}$, $V_{\text{DS}} = -0.5\text{V}$ and $V_{\text{G}} = -1\text{V}$ during X-ray radiation. Settings of the X-ray machine: 150kV, 4mA resulting in a dose of $D = 100\text{mGy}$ for each irradiation. The red bars indicate the irradiation.

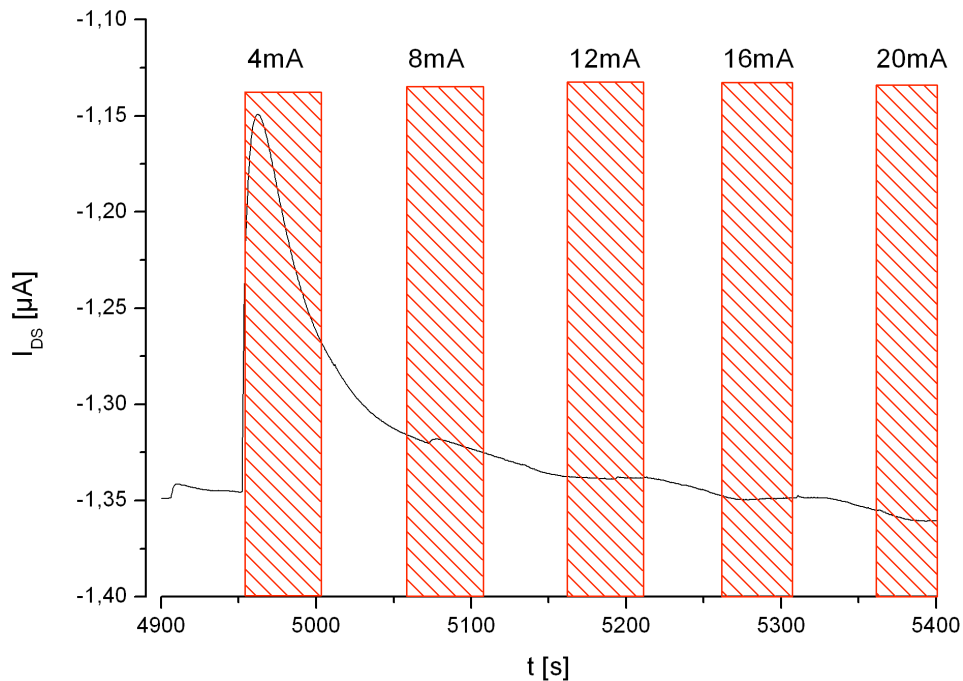


Figure 51 Drain-source current of 2wt% P3HT in DCB transistor with $L = 50\mu\text{m}$ and voltages $V_{\text{DS}} = -0.5\text{V}$ and $V_{\text{G}} = -1\text{V}$ during irradiation while exposed to tissue culture medium. The red bars indicate the irradiation. It is not known what causes the big peak during the first irradiation.

Again, like with the other transistors, a measurement in tissue culture medium was performed. A constant drain-source voltage of $V_{DS} = -0.5V$ was applied and the drain-source current was measured during irradiation. Here, the acceleration voltage was kept constant and the tube-current was varied from 4-20mA in 4mA steps. The measurement can be seen in Figure 51. Turning on the X-ray machine might cause the small peak in the very beginning, but it is not clear, what causes the big peak during the first irradiation since there is almost no visible effect in the drain-source current during all other irradiations.

Summary and discussion

It could be shown that all three configurations react on the X-ray radiation, but the current modulation is in the nA range. When comparing these X-ray measurements with the light measurements a big difference is obvious. During irradiation with light the drain-source current increases caused by excitation of the polymer. Whereas, during irradiation with X-rays the drain-source current decreases. Raval *et al* also reported this behaviour (108). The “on” current decreases after irradiation with increasing dose. They explain the decrease in the drain-source current by accumulation of positive charges in the silicon dioxide due to the ionising radiation. Moreover, the electrical characteristics of the OFETs significantly vary after irradiation. This is oppositional to our results. When recording an output characteristic before and directly after irradiation, no effect on our transistor was visible. Since Raval *et al* used extensively higher doses (up to 4000 times higher) it is possible that the aforementioned effect is persistent. In our case, due to the lower dose, the effect vanishes much faster and is not measurable anymore after irradiation.

For all measurements in culture medium the X-rays have no measurable effect on the drain-source current of the different devices. Since the medium on the transistor surface is only some mm high, it is implausible that it shields the X-rays from the sensor surface. It would be more probably that the medium is ionised and secondary electrons are produced that can interact with the transistors. It is assumed that doping or charge trapping effects caused by the tissue culture medium are much greater than the effect from the ionising radiation and therefore superimpose this effect.

The peaks visible during the first irradiation of the devices made from DCB (P3HT and the blend P3HT:PCBM) exposed to tissue culture medium can not be explained. Since they are not visible in the measurements performed with the devices made of P3HT in

CHCl_3 it seems that the device configuration influences the transistor behaviour. To understand this effect, further characterisations have to be performed in future work.

Summarising, the transistors are not degraded during X-ray radiation in the used dose regime up to 2Gy when measured in air. All transistors showed the same trend: in air, only a small reaction on radiation is visible, exposed to tissue culture medium, no reaction is detectable. By comparing P3HT with the blend P3HT:PCBM it can be seen that the blend reacts faster after irradiation, which is favourable for online measurements. The set-up configuration P3HT in CHCl_3 is not stable when operated in tissue culture medium and under ionising radiation. Therefore, this set-up configuration cannot be used for online cell measurements. By comparing the gained results with the results from the UV/white light irradiation, one can see a difference. During exposure to UV/white light the current increases, while during exposure to X-rays the current decreases. To completely understand the effect caused by the irradiation in air or with tissue culture medium further characterisations have to be done in future work.

4.3 Sensitivity in Aqueous Conditions

The presented results show that the transistors match the preconditions for online cell measurements during ionising radiation, with the exception of P3HT in CHCl_3 . Furthermore, the transistor performance varies with the used processing parameters. As written before, OFETs are already used to detect different analytes like pH, ions or chemicals (15). Nevertheless, it is unclear how the used sensors respond to variations of concentrations of ions or pH and how the response is affected by the thin-film morphology. Therefore, the different set-up configurations with different thin-film morphologies were characterised with respect to pH and variations in the concentration of ions. It is known, that the detection of a “target” analyte involves diffusion of the “target” analyte in the solution onto the sensor surface. In this case the analyte interacts with the surface and results in the modulation of the device characteristics, here the drain-source current. Due to the fact that the sensitivity of the device is limited by the diffusion of the “target” analyte to the sensor surface, the device geometry needs to be optimised to maximise the device sensitivity (111). Here, the used bottom gate/bottom contact structure seems promising since the active area is in direct contact with the solution containing the “target” analyte. Furthermore, the operating conditions also affect the OFET performance (111). For measurements in liquids, the driving voltage was limited to a drain-source voltage of $V_{\text{DS}} = -0.5\text{V}$ to avoid unwanted electrochemical reactions or additional ionic currents to contribute to the sensor signal. Output characteristics and online measurements were performed while exposed to the different solutions.

For the output characteristic, the transistors were first characterised in air. Then, the first solution was placed on to the active area. After an incubation time of 20min, the output characteristic was recorded. After that, the solution was removed, the transistors were washed with water and a new solution was placed on the sensor. These steps were repeated until all solutions were characterised. The range for the measurements is: V_{DS} from 0V to -0.5V, in -0.1V steps and V_{G} from 0V to -3V in -1V steps. For the online measurements, the flow chamber was always used. The measurement was started with a constant drain-source voltage $V_{\text{DS}} = -0.5\text{V}$ and a constant gate voltage $V_{\text{G}} = -1\text{V}$. After a conditioning time of about 1.5hrs the concentration of the ion solutions were altered by purging a new solution through the flow chamber and the drain-source current was measured with respect to these changes. Between measurements with different ions, the transistors were washed with ultrapure water.

4.3.1 pH Sensitivity

The possibility of using OFETs as pH sensors was shown before. For most of the presented data, a set-up configuration was used, where the electrolyte is not in direct contact with the organic material. During our measurements, the polymer will be exposed directly to the analyte and an interaction will take place at the analyte/polymer interface. Therefore the stability of the device in different pH solutions needs to be explored. Furthermore, the effect of the morphology on the transistor performance in aqueous conditions is tested. Since a variation in pH represents a variation in H^+ ions, the devices' sensitivity to monovalent ions was analysed.

The three compositions P3HT:PCBM, P3HT in DCB and P3HT in $CHCl_3$ were analysed. For the characterisation, standard pH solutions with pH 4, 7 and 10 and solutions made from hydrochloric acid and sodium hydroxide were used. pH values were measured using a pH meter, type Cyber Scan 500. Output or online measurements were performed as described in the introduction of this chapter.

a) pH Sensitivity of the Composition P3HT in $CHCl_3$

The next graphs (Figure 52) are showing the characterisation of the transistors made from $CHCl_3$. The measurement was performed as described above with pH standard solutions. The pH sensitivity with an almost linear relation for both transistors is obvious. With decreasing pH, respectively with increasing H^+ concentration, the drain-source current increases. The positive charge (H^+) at the electrolyte/P3HT interface increased the positive charge in the channel and therefore, the drain-source current was enhanced.

The variation in I_{DS} was determined by calculating $\Delta I/I$ for pH 4 and pH 7 at $V_{DS} = -0.5V$ and $V_G = -1V$. For 1wt% in $CHCl_3$ $\Delta I/I$ is $0.7\mu A$ while for 2wt% in $CHCl_3$ $\Delta I/I$ is $0.25\mu A$. This behaviour is consistent with already published data (39). With increasing film-thickness the interaction between the analyte and the conducting channel is reduced resulting in a smaller sensor response. The measurements were reproducible and further details can be found in the publication of Scarpa *et al* (107).

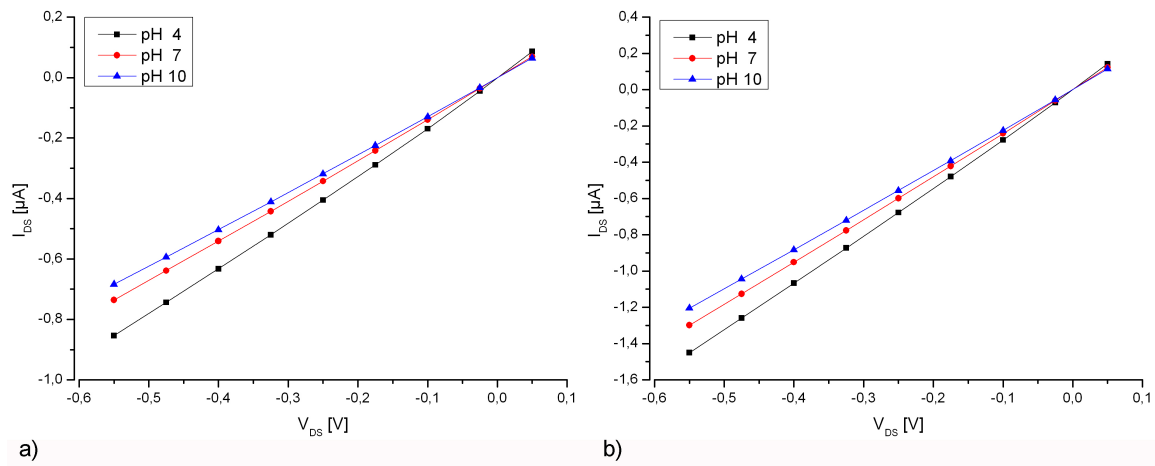


Figure 52 Characteristic of a) 1wt% P3HT and b) 2wt% P3HT in CHCl_3 transistors at different pH values with $V_G = -1\text{V}$ and $L = 50\mu\text{m}$. An almost linear pH dependency is visible.

b) pH Sensitivity of the Composition P3HT:PCBM 3:1 in DCB

Using the polymer blend P3HT:PCBM no reproducible results could be recorded. The next two graphs are showing exemplarily two pH measurements of two transistors (Figure 53).

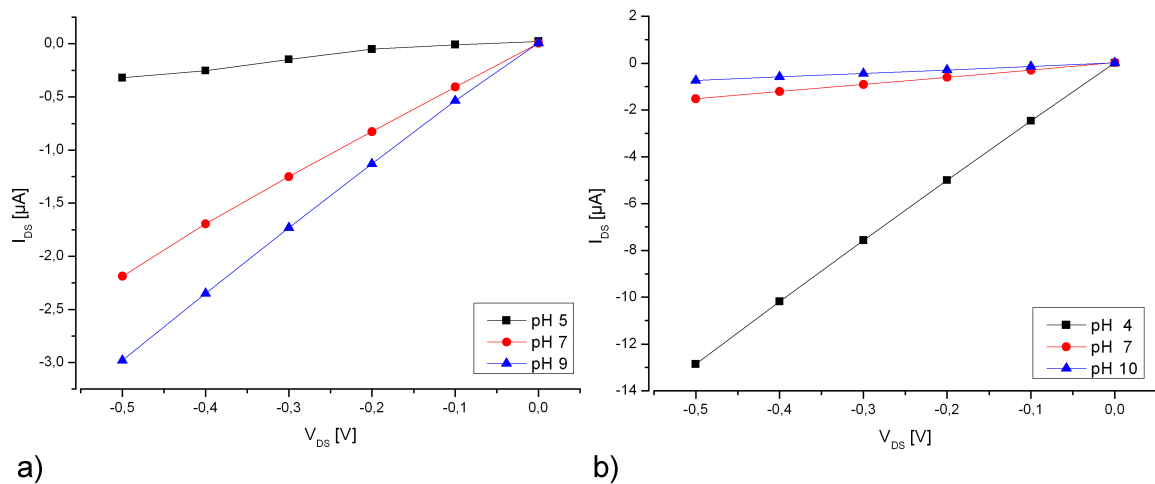


Figure 53 Characteristic of a) 1wt% ($L = 50\mu\text{m}$) and b) 2wt% ($L = 20\mu\text{m}$) P3HT:PCBM 3:1 in DCB with respect to different pH values at $V_G = -1\text{V}$. V_{DS} was reduced from 0V to -0.5V in -0.1V steps.

Regarding the measurements by its own pH sensitivity seems obvious. By comparing the measurements with each other one can see that in the first measurement, the drain-source current decreases with increasing pH and in the second one I_{DS} decreases with decreasing pH. The latter was performed with a transistor from the same wafer only a

few days later. No reproducible measurements could be performed with this device configuration. It is assumed that due to storage under ambient conditions oxygen doping aged the device. The variation in the absolute current is caused by the device geometry. The first transistor had a channel length of $20\mu\text{m}$, the second of $50\mu\text{m}$.

As a next step, the variation of the drain-source current with respect to pH value changes was recorded. Therefore, one acidic solution (0.1M hydrochloric acid) and one basic solution (0.1M sodium hydroxide) were prepared. A fixed drain-source voltage $V_{\text{DS}} = -0.5\text{V}$ and gate voltage $V_{\text{G}} = -1\text{V}$ were applied and the transistor was immersed in to the solution. The pH was changed in small steps from pH 5 to pH 9 by adding either the acidic or the base solution. The pH was measured using a pH meter (type Cyber Scan 500) and the results are shown in Figure 54. The first measurement shows an increase of I_{DS} with increasing pH, the second and third first an increase and starting at around pH 6 a decrease in I_{DS} . By comparing these three measurements and the two above it is obvious that the blend is not suitable for pH sensing.

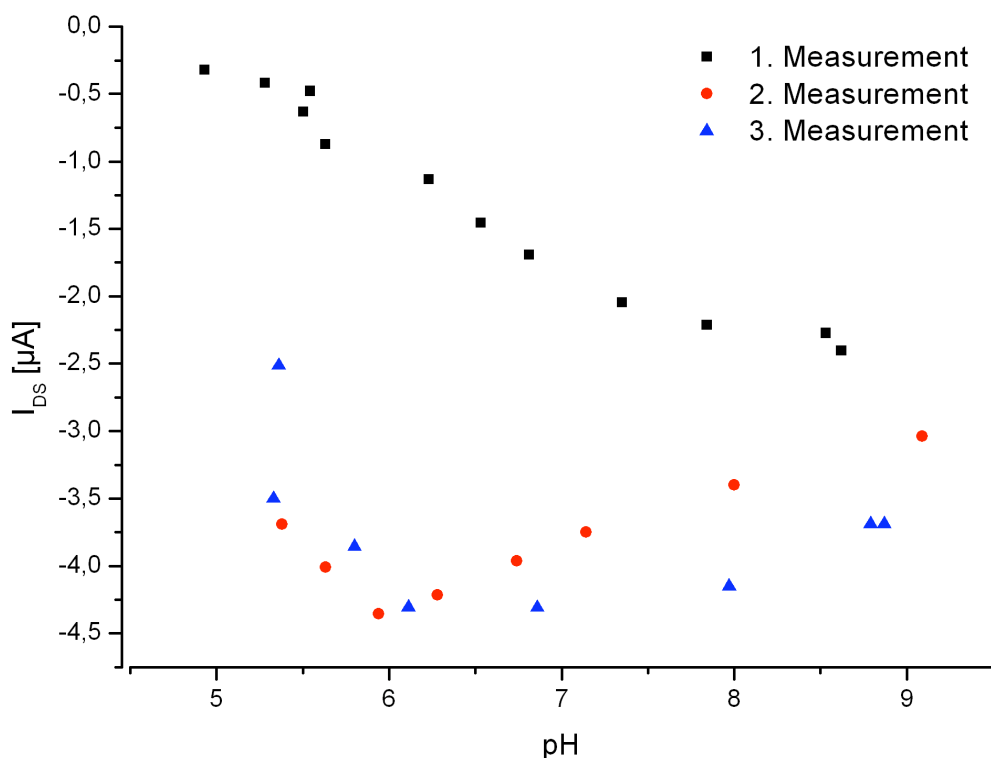


Figure 54 Comparison of I_{DS} measurements with respect to pH changes of transistors made from P3HT:PCBM 3:1 in DCB. It clearly can be seen that the first measurement shows a different behaviour than the second and third measurement.

c) pH Sensitivity of the Composition P3HT in DCB

Here, the sensitivity of transistors made from P3HT in DCB is characterised. The output measurements were performed as described above. The next graphs (Figure 55) are depicting the results for 1wt% and 2wt% P3HT in DCB.

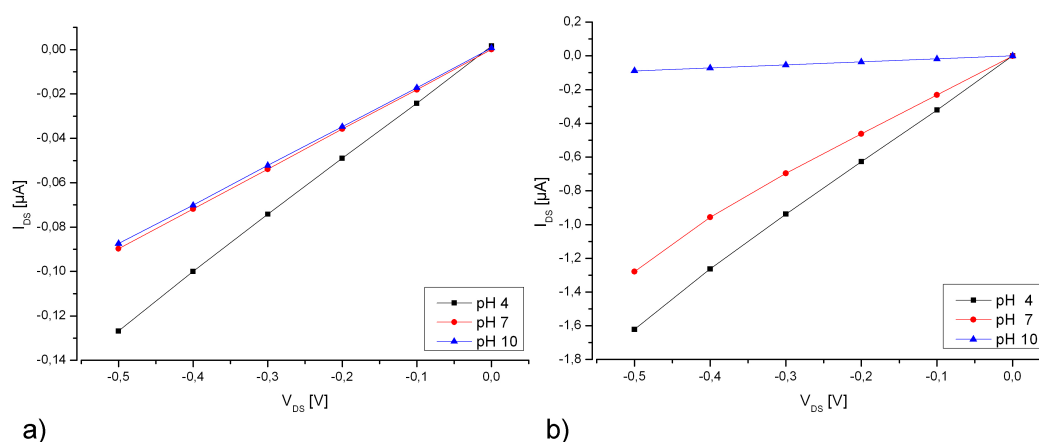


Figure 55 Characteristic of a) 1wt% and b) 2wt% P3HT in DCB transistors with respect to different pH values. V_{DS} was decreased from 0V to -0.5V in -0.1V steps, $V_G = -1V$ and $L = 50\mu m$. A non-linear pH dependency is visible.

The transistor made from 1wt% P3HT in DCB shows a very low drain-source current. Furthermore, almost no effect between pH 7 and pH 10 is detectable. 2wt% P3HT in DCB shows a non-linear behaviour. The effect between pH 7 and pH 10 is much bigger than between pH 7 and pH 4. But in general the drain-source current increases with increasing pH. For measurements with varying pH, the simultaneous usage of an additional pH electrode is necessary.

Summary

The presented results showed that the transistor behaviour differs with device composition. All transistors worked properly in a pH range from 4-10 and no optical degradation was visible after the measurements. The configuration of P3HT in $CHCl_3$ shows linear pH dependency whereas the configuration of P3HT in DCB does not. It is possible that the device made from DCB are more sensitive to oxygen doping than the devices made from $CHCl_3$ due to their different thin-film morphology. This aging process results in a changed pH dependency after different storage times which also could be

observed for the blend P3HT:PCBM in DCB. With this set-up configuration no reproducible results could be gained. Consequently, when performing measurements with devices made from DCB the pH needs to be measured simultaneously with a pH electrode.

The obtained results are very well in line with previous findings of other authors. Loi *et al* (10), Bartic *et al* (112) and Roberts *et al* (113) already proved the possibility to monitor pH with organic thin film transistors. Loi and Bartic used a conventional ISFET. Here, the gate electrode was contacted by electrolyte solution with the gate oxide. The drain-source current flows via the drain channel from the source electrode to the drain electrode and the channel resistance depends on the potential difference over the gate oxide. Therefore, the source-drain current is influenced by the potential at the interface between electrolyte and gate oxide. With more positive ions accumulating at this interface, the amount of charges in the channel will be altered. Since the used materials (pentacene and P3HT) are p-type materials, the drain source current decreases. In our case, the polymer is in direct contact with the electrolyte thus positive charges at the electrolyte/P3HT interface will increase the drain-source current. This was also reported by Roberts *et al* (15, 113) using other p-type organic semiconductors 5,5-bis-(7-dodecyl-9H-fluoren-2-yl)-2,2'-bithiophene (DDFTTF) also directly immersed in solution. Here, the source-drain current decreases with increasing pH, which is consistent with our findings. This behaviour is caused by hydronium ions diffusing into the channel region through the grain boundaries of the organic film and act as additional charge carriers.

The presented results show the possibility of detecting pH variations by usage of devices made from P3HT in CHCl_3 . For the devices made of P3HT in DCB a pH sensitivity could be observed which is non linear and which is probably altered by aging of the device. Even though, the blend P3HT:PCBM did not show reproducible results all three configurations were further characterised concerning the sensitivity to different ions.

4.3.2 Ion Sensitivity

In cell-cell communication processes, different ions like sodium or calcium play an important role. These ions are messengers that are adsorbed or released by the cells caused by e.g. external stimuli. In this process, the local ion concentration is altered. The alterations range from 10^{-3}M to 150^{-3}M for sodium and from 10^{-7}M to 10^{-5}M for calcium (51). Several studies reported the importance of calcium signalling of cells during or after exposure to ionising radiation (59, 87) (see also chapter 2.2). To explore the capability of the devices to detect these small variations in the concentration of the ions different tests were performed. To analyse the devices' sensitivity with respect to the different thin-film morphologies, aqueous solutions from ions with different valences were prepared. Sodium (monovalent) and calcium (bivalent) solutions were used due to their biological importance. Additionally, a trivalent ion, aluminium was analysed to further characterise the semiconductor/analyte interactions.

The different ion solutions with varying ion concentration were prepared from commercially available standard solutions. For the sodium solution, a NaCl standard solution with 1g/L Na^+ was used. The composition of the calcium and aluminium standard solutions are as follows: $\text{Ca}(\text{NO}_3)_2$ in 0.5M nitric acid (HNO_3) with 1g/L Ca^{2+} and $\text{Al}(\text{NO}_3)_3$ in 0.5M HNO_3 with 1g/L Al^{3+} . Nitric acid is needed to provide an acidic environment since aluminium salts are only soluble in a specific pH range. At $\text{pH} < 5$ aluminium ions (Al^{3+}) exist, starting from $\text{pH} 5$, insoluble aluminium hydroxide $\text{Al}(\text{OH})_3$ is formed (114). Also buffering of the aluminium and calcium solutions with phosphate, to prepare solutions with constant pH, was not possible due to the formation of precipitates. Working with another buffer, for example HEPES, a lot of additional ions (in this case potassium ions) are added to the solution. The concentration of this additional ion is at least 45 times higher than the concentration of the target ion, which makes a detection of the target ion impossible. Table 10 summarises the pH values of the different solutions.

Table 10 pH values of the different ion solutions.

ion concentration	NaCl	$\text{Ca}(\text{NO}_3)_2$	$\text{Al}(\text{NO}_3)_3$
$10\text{E}-5$	6.94	3.36	2.96
$10\text{E}-4$	6.31	2.38	2.33
$10\text{E}-3$	5.58	1.46	1.28

a) Ion Sensitivity of the Composition P3HT in CHCl_3

For the transistors spun from CHCl_3 the output characterisations were recorded as described in 4.3. The graphs for the gate voltage $V_G = -1\text{V}$ are shown (Figure 56).

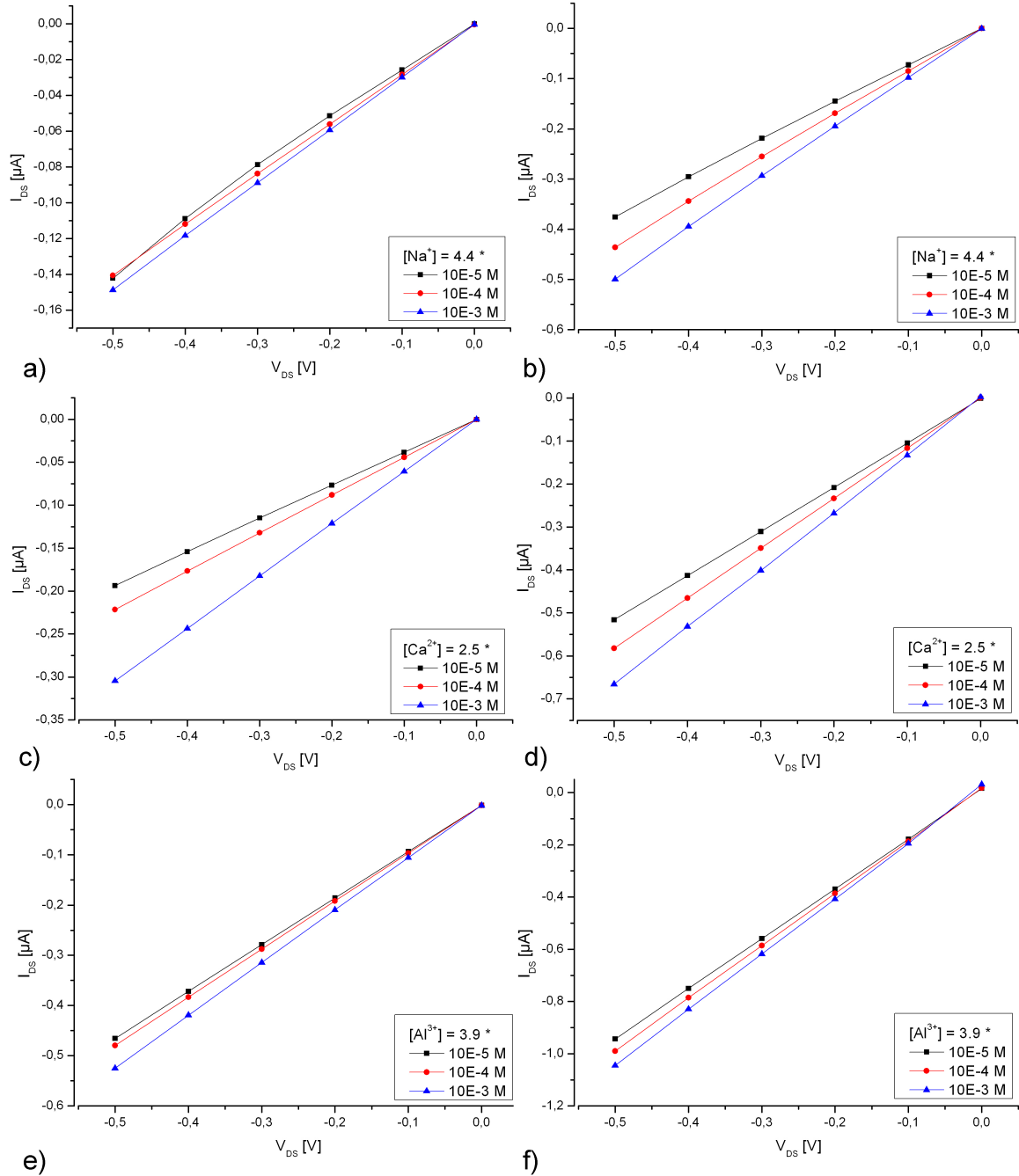


Figure 56 Characteristics of a), c) and e) 1wt% and b), d) and f) 2wt% P3HT in CHCl_3 transistors ($L = 50 \mu\text{m}$) with respect to different ion concentrations. V_{DS} was decreased from 0V to -0.5V in -0.1V steps. Measurements are shown for $V_G = -1\text{V}$.

It can be seen, that the transistors are sensitive to all ions in the ion concentration range from $2.5 \cdot 10^{-3}\text{M}$ to $2.5 \cdot 10^{-5}\text{M}$, except for sodium (1wt% in CHCl_3). The absolute currents

of the transistors made from 2wt% are approximately twice as high as the ones from 1wt% devices. Furthermore, the change $\Delta I/I$ for the different concentrations of the 1%wt transistors (for Ca^{2+} $\Delta I/I = 0.6$; for Al^{3+} $\Delta I/I = 0.12$) is higher than the ones for 2wt% (for Ca^{2+} $\Delta I/I = 0.3$; for Al^{3+} $\Delta I/I = 0.1$).

The following graphs (Figure 57) compare the different ions of one measurement. Here, the values from $V_{\text{DS}} = -0.5\text{V}$ and $V_{\text{G}} = -1\text{V}$ are plotted against the concentration. The data were linearly fitted. The next (Table 11) table summarises the slopes for the different ions.

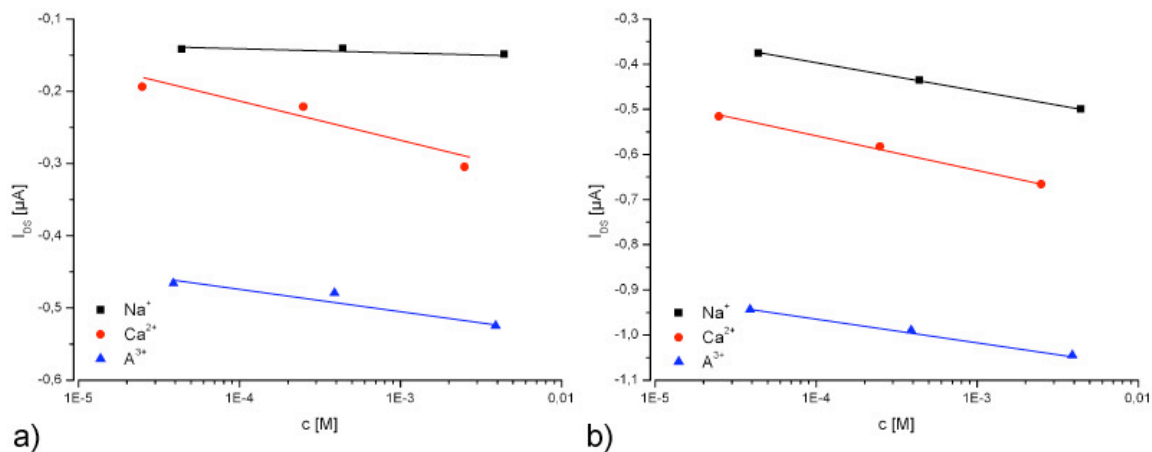


Figure 57 I_{DS} at $V_{\text{DS}} = -0.5\text{V}$ and $V_{\text{G}} = -1\text{V}$ for the different ions and concentrations for transistors of a) 1wt% P3HT in CHCl_3 and b) 2wt% in CHCl_3 .

Table 11 Slopes for different ions and transistors in $\Delta I/\Delta c$

slope	Na^+	Ca^{2+}	Al^{3+}
1wt% CHCl_3	1.48	44.8	15.5
2wt% CHCl_3	28	60.6	26.6

The slope for calcium is always the steepest, which means that the devices are highly sensitive to calcium ions. For 2wt% in CHCl_3 the slopes are almost identically. It is interesting that the slope for aluminium is lower than the slope for sodium. No trend concerning the valence of the ions can be detected.

Since ion flux measurements will be performed in real time the drain-source current was measured online with respect to the ion concentration at a fixed source-drain ($V_{\text{DS}} = -0.5\text{V}$) and gate voltage ($V_{\text{G}} = -1\text{V}$). After a conditioning time of about 1.5hrs, the first ion solution was purged through the flow chamber, then the ion solutions were changed every 15min and I_{DS} was measured simultaneously with respect to the ion concentrations (Figure 58).

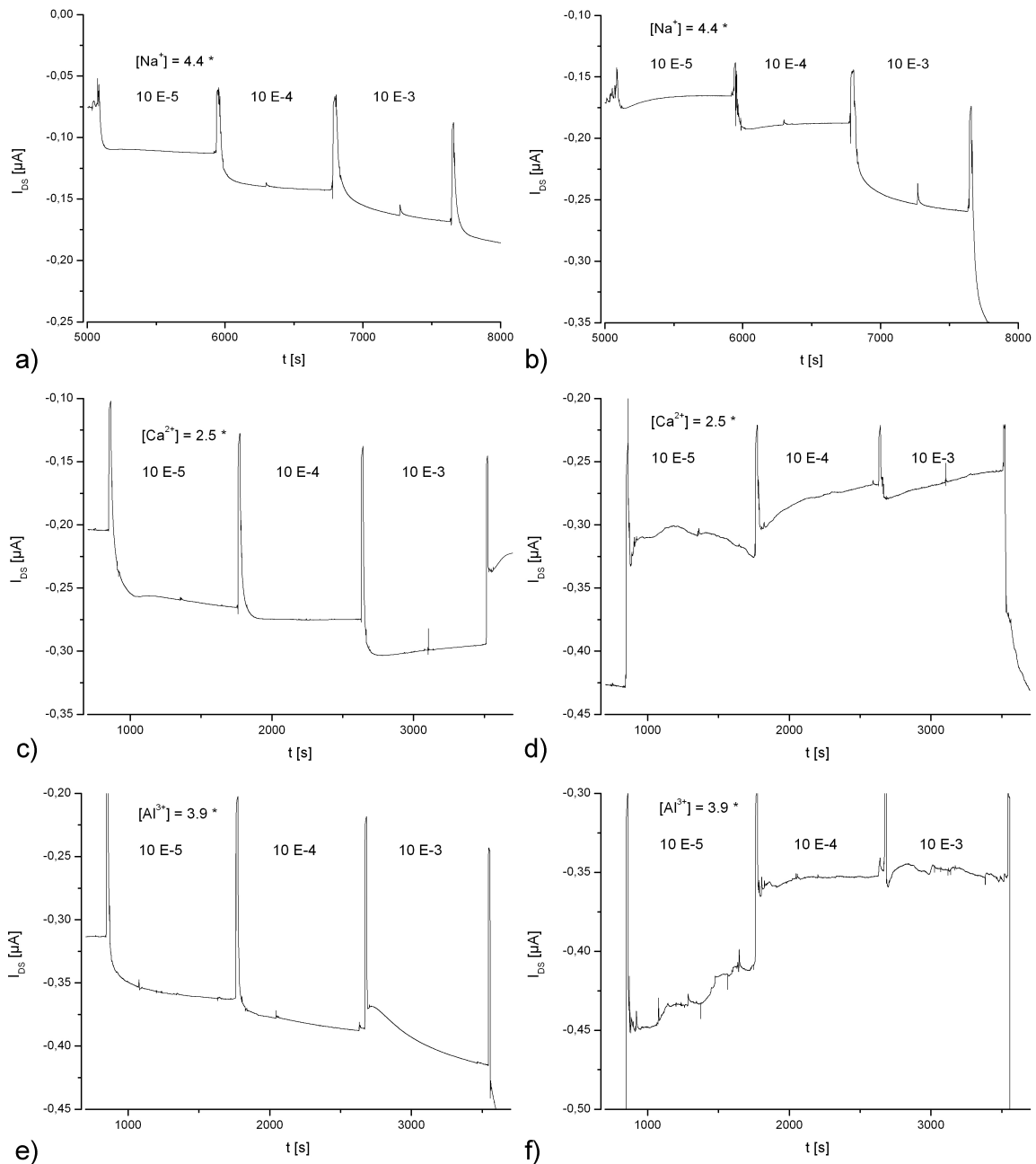


Figure 58 Drain-source current of a), c) and e) 1wt% and b), d) and f) 2wt% P3HT in CHCl_3 transistors with respect to changes of the concentration of different ions with $L = 50\mu\text{m}$, $V_{DS} = -0.5\text{V}$ and $V_G = -1\text{V}$.

Here, both transistors showed sensitivity to all sodium concentrations. The transistor 1wt% in CHCl_3 showed also a response to all other ions. For the transistor made from 2wt%, the drain-source current decreased with increasing ion concentration using the calcium and aluminium solutions. This response is oppositional to previous findings. The reason is not understood. An aging process is unlikely, since the online measurements were performed 2days after fabrication of the transistors and the output characteristics were recorded 4days after fabrication. Furthermore, no optical degradation was visible.

b) Ion Sensitivity of the Composition P3HT:PCBM 3:1 in DCB

For this transistor configuration, the output characteristics were recorded first as described in 4.3. The graphs (Figure 59) are showing the results of two measurements performed at different days.

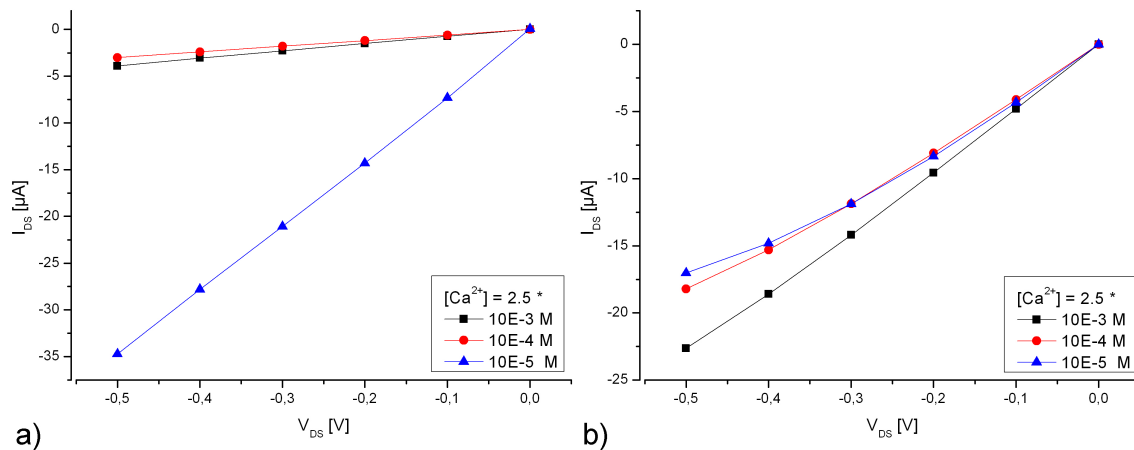


Figure 59 Characteristic of transistors made of P3HT:PCBM in DCB with $L = 20\mu\text{m}$ with respect to different calcium concentrations at $V_G = 0\text{V}$ a) first measurement and b) second measurement. The measurement is not reproducible. V_{DS} was decreased from 0V to -0.5V in 0.1V steps.

The two measurements are showing oppositional results (like during pH characterisation). In the first measurement, the current increases with increasing ion concentration, but the sensor seems to be sensitive only down to 10^{-4}M . In the second measurement, the current decreases with increasing Ca^{2+} concentration. Furthermore, there exists no differentiation between $2.5 \cdot 10^{-3}$ and $2.5 \cdot 10^{-4}\text{M}$ until a drain-source voltage of $V_{DS} = -0.3\text{V}$. For the blend it seems necessary to perform the measurements directly after fabrication, which is not possible for cell measurements since the devices need to be functionalised and the cells have to grow on the surface first. Since no reproducible measurements can be performed with the transistor this configuration is not suitable for the wanted application and was discarded.

c) Ion Sensitivity of the Composition P3HT in DCB

At first, the output characteristics of the transistors are presented (Figure 60). The measurements were performed like described in 4.3.

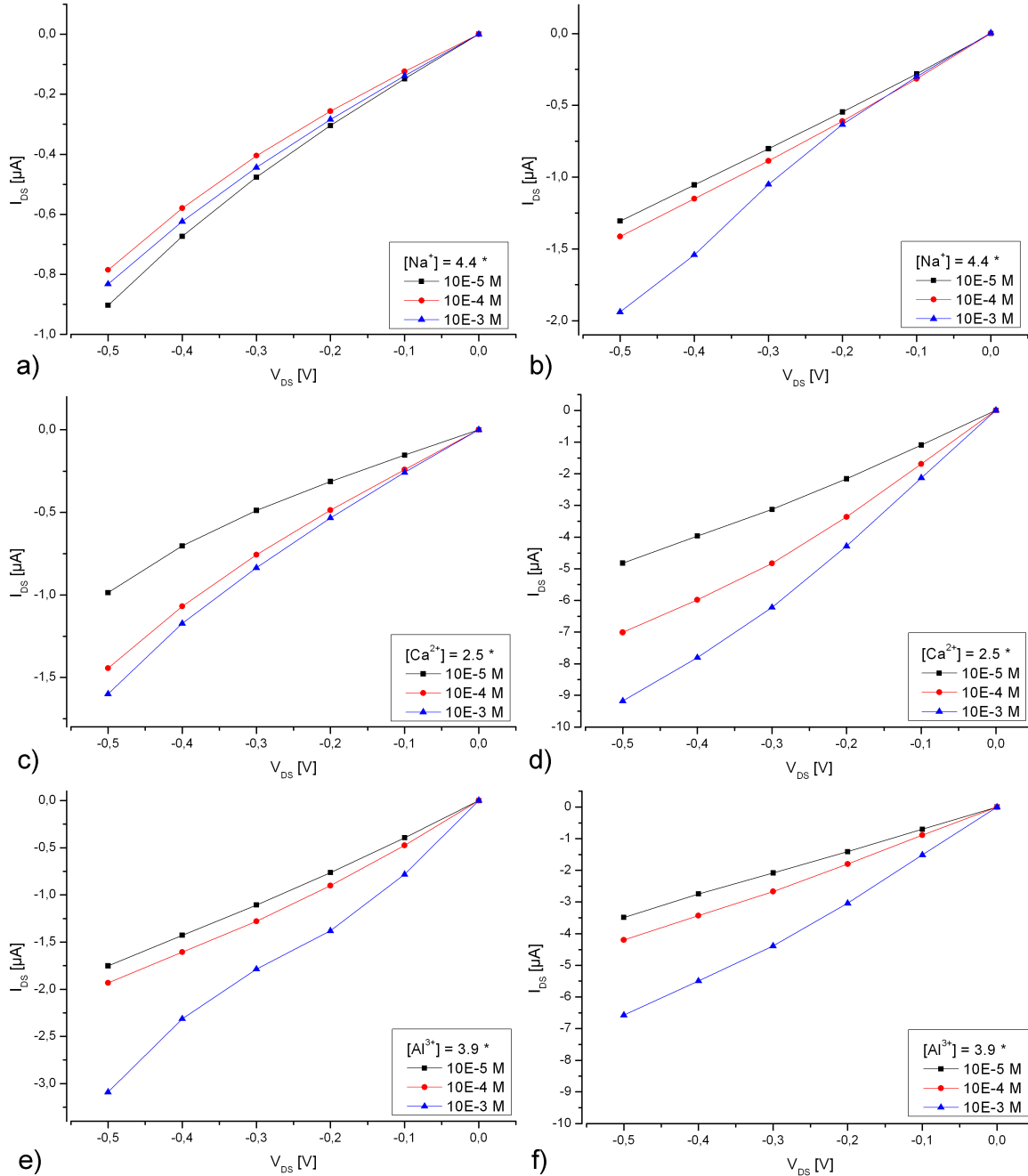


Figure 60 Characteristics of a), c) and e) 1wt% P3HT in DCB, b), d) and f) 2wt% P3HT in DCB transistors with $L = 50\mu\text{m}$ with respect to different ion concentrations. $V_G = -1\text{V}$ and V_{DS} was decreased from 0V to -0.5V in 0.1V steps.

It can be seen, that the transistors are sensitive to all ions in the range from $2.5 \cdot 10^{-3}\text{M}$ to $2.5 \cdot 10^{-5}\text{M}$, again except for sodium (1wt% in DCB). Like in the measurements with the transistors made from CHCl_3 the absolute currents of the transistors made from 2wt% is

higher than the ones made from 1wt%. Here, the current of the 2wt% devices is two to five times higher than the current of the 1wt% devices. Nevertheless, the changes $\Delta I/I$ for the different concentrations of the 1wt% transistors (for Ca^{2+} $\Delta I/I = 1.0$; for Al^{3+} $\Delta I/I = 0.9$) are higher than the ones for 2wt% (for Ca^{2+} $\Delta I/I = 0.9$; for Al^{3+} $\Delta I/I = 0.78$).

The following graphs compare the different ions of one measurement (Figure 61). Here, the values of $V_{\text{DS}} = -0.5\text{V}$ and $V_{\text{G}} = -1\text{V}$ and plotted against the concentration. The data were linearly fitted. The following table (Table 12) summarises the slopes for the different ions.

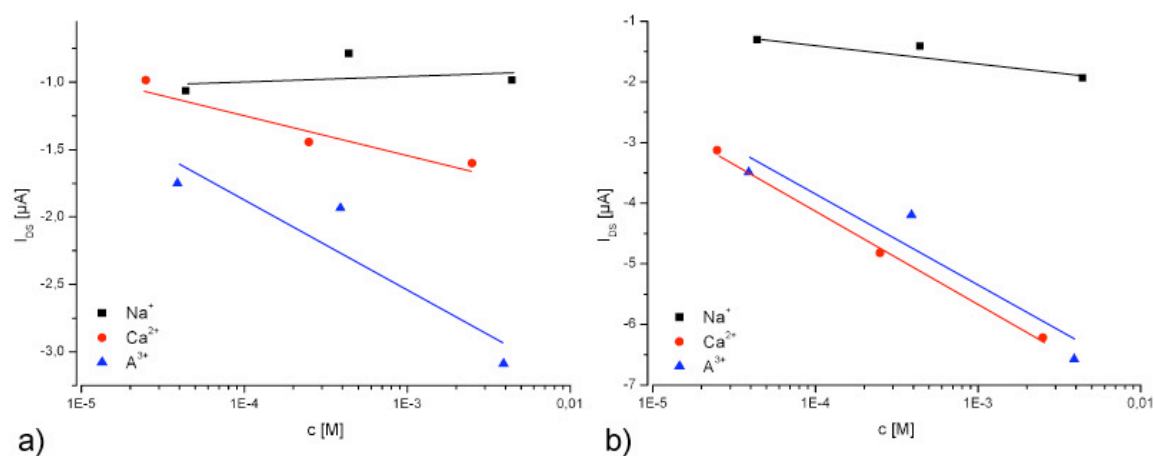


Figure 61 I_{DS} for different concentration of different ions of a) 1wt% P3HT in DCB and b) 2wt% P3HT in DCB transistor at $V_{\text{DS}} = -0.5\text{V}$ and $V_{\text{G}} = -1\text{V}$.

Table 12 Slopes for the transistors made from 1wt% and 2wt% P3HT in DCB and the different ions in $\Delta I/\Delta c$.

slope	Na^+	Ca^{2+}	Al^{3+}
1wt% DCB	-18	248	350
2wt% DCB	152	1248	809

For 1wt% in DCB, a dependency on the valence of the ion and the drain-source current modulation is visible; the slope is getting steeper with the valence of the ion. For 2wt% there is the same tendency, but between calcium and aluminium, there is almost no difference. This leads to the assumption, that the valence of the ion has an influence on the device response.

Since the output characteristics are showing promising results, online measurements were performed in a flow-chamber to see how fast the transistors react to the different ions. This is important, since we want to measure online cell-cell reactions. The next graphs (Figure 62) are showing the results for 1wt% and 2wt% P3HT in DCB with

$V_{DS} = -0.5V$ and $V_G = -1V$. The measurements were performed as described in the introduction of the chapter 4.3.

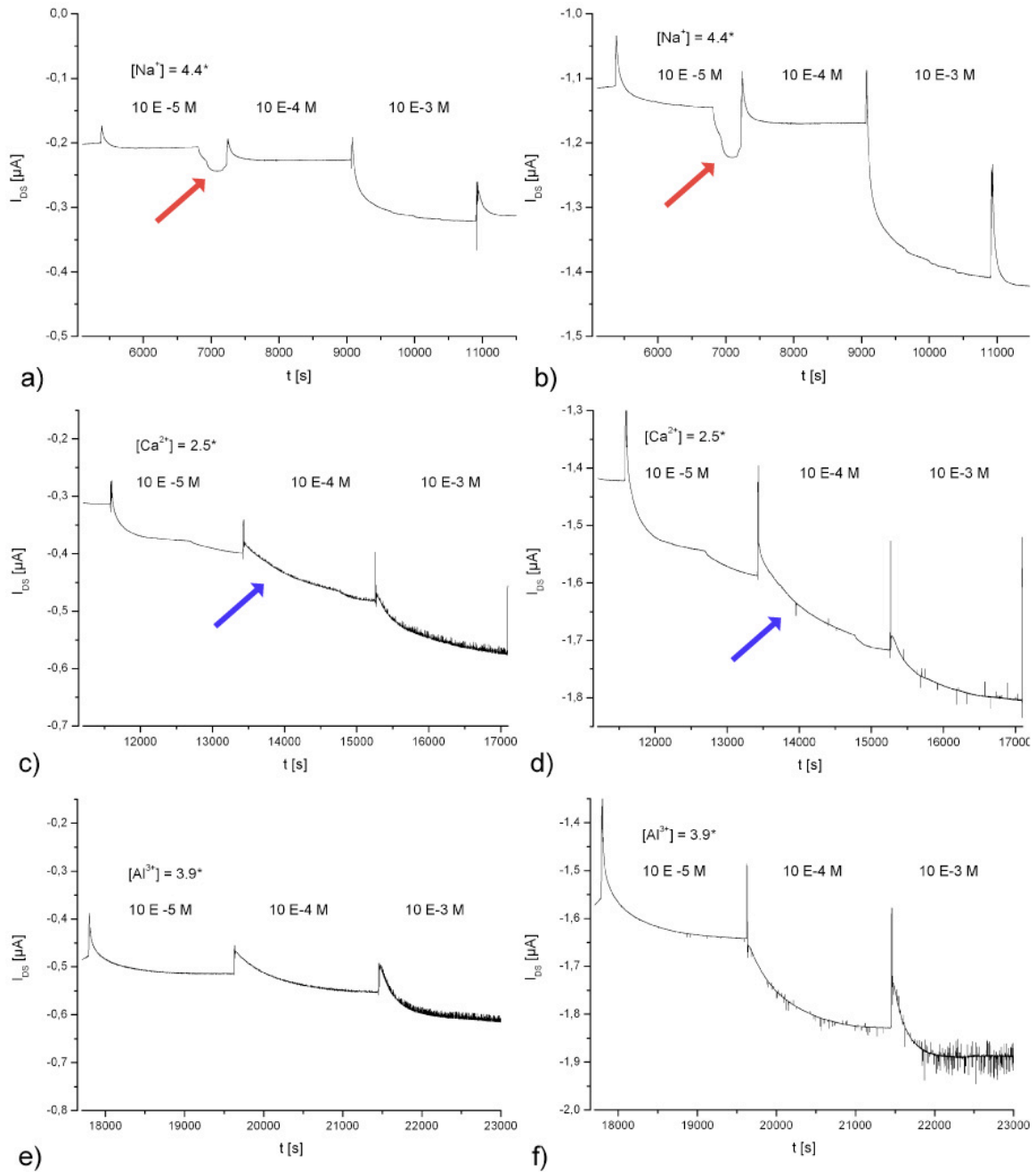


Figure 62 Online measurement of a), c) and e) 1wt% and b), d) and f) 2wt% P3HT in DCB with respect to different ions and ion concentrations. $L = 50\mu\text{m}$, $V_{DS} = -0.5V$ and $V_G = -1V$. The red and blue arrows indicate disturbance and noise from outside.

The measurements were recorded simultaneously. For sodium, a dip in the drain-source current (indicated by the red arrow) can be observed in both measurements probably resulting from disturbance from outside. The noise starting in the calcium measurement (indicated by the blue arrow) might be caused by poor connections or by disturbance

from outside. It is obvious, that the set-up is very sensitive to the surrounding conditions. For more sensible measurements, like the cell measurements it needs to be assured that the measurement is not disturbed. Nevertheless, the progression can be well discerned.

Purging the solutions through the flow chamber causes the peaks between the different concentrations. After changing the solution the drain-source current in the sodium and aluminium measurements starts to stabilise. Moreover, it seems that the drain-source current of the transistor made from 1wt% stabilises faster than the transistor made from 2wt% P3HT. The response time of the device is almost 8min for the sodium measurement. For the calcium measurement, it seems that the drain-source current did not stabilise until adding the next solution. To be able to measure cellular processes, which are in the range of some microseconds to seconds, the response time of the transistors needs to be optimised. The y-axis of the 1wt% and 2wt% graphs are scaled to the same value for a better comparability. It can be seen, that the overall current of the 2wt% measurements is higher and with it also the absolute alterations in the drain-source current. However, by calculating $\Delta I/I$, the value for the 1wt% transistors is higher indicating a higher sensitivity of the 1wt% transistors like also the output characterisations showed.

Since we are interested in cellular processes and the devices made from P3HT in DCB showed the best results in terms of stability as well as sensitivity, the ion concentrations were adapted to the concentration range important for cellular processes. For sodium the prepared solutions already matches the concentration present in a cell. For calcium, the concentration inside a cell varies from the "off" state to the "on" state from 10^{-7} M to 10^{-5} M. Outside the cell the concentration is around $2 \cdot 10^{-3}$ M. Therefore, new solutions with lower calcium concentrations (down to $2.5 \cdot 10^{-7}$ M) were prepared and the sensitivity of the devices were characterised (Figure 63).

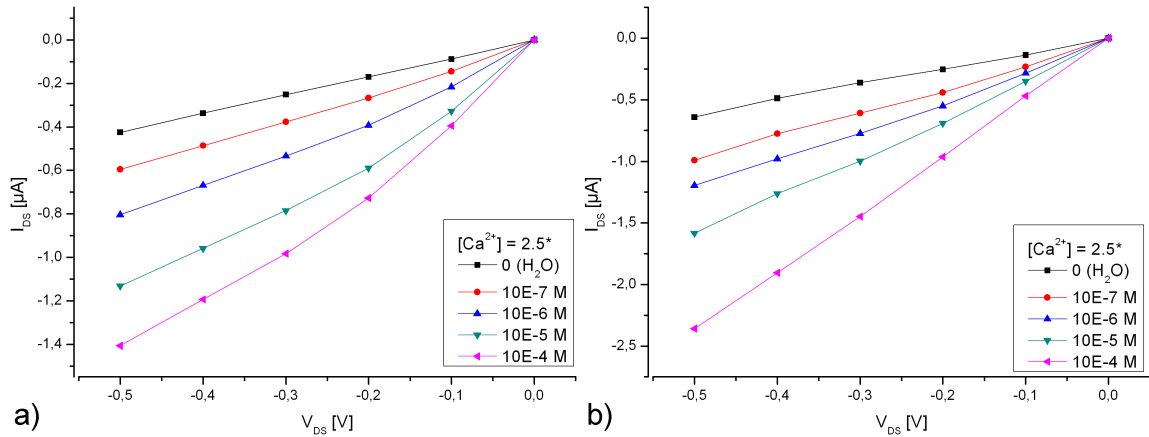


Figure 63 Characteristic of a) 1wt% and b) 2wt% in DCB transistors with $L = 50\mu\text{m}$ with respect to calcium concentrations down to the cellular level. $V_G = -1\text{V}$ and V_{DS} was decreased from 0V to -0.5V in 0.1V steps.

Here, both transistors are sensitive down to $2.5 \cdot 10^{-7}\text{M}$. Nevertheless, sensitivity down to $2.5 \cdot 10^{-7}\text{M}$ could not always be reproduced, only down to $2.5 \cdot 10^{-6}\text{M}$. Additionally this measurement was repeated at 37°C and after functionalisation of the transistor surface with fibronectin and plasma treatment. The sensitivity down to $2.5 \cdot 10^{-6}\text{M}$ was reproducible. The measurements of the transistors functionalised with fibronectin are presented in Figure 64.

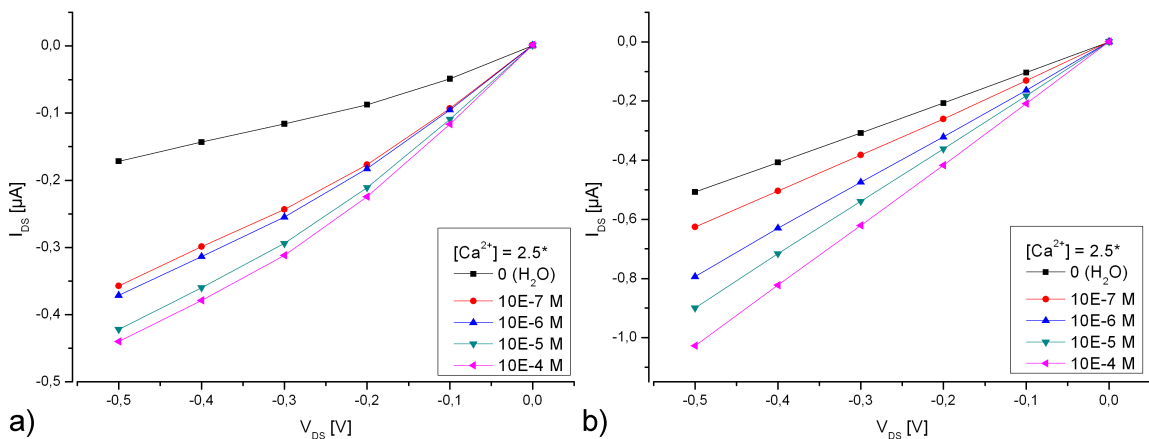


Figure 64 Characteristics the same transistors as shown in Figure 63 after functionalisation with fibronectin; a) 1wt% and b) 2wt% in DCB transistors with $L = 50\mu\text{m}$ with respect to calcium concentrations down to the cellular level. $V_G = -1\text{V}$ and V_{DS} was decreased from 0V to -0.5V in 0.1V steps. The sensitivity to the calcium concentration can still be seen.

For the measurements the same transistors as shown above were used. Comparing the measurements it is obvious that the drain-source current for both transistors is reduced. For the 1wt% transistor I_{DS} is about three times smaller after functionalisation, whereas for the 2wt% transistor I_{DS} is about two times smaller. Additionally, the drain-source current modulations were decreased for both transistors. By calculating ΔI (here:

$I_{DS}(H_2O) - I_{DS}(2.5 \cdot 10^{-7} M)$ one receive for 1wt% before functionalisation $\Delta I = 0.9 \mu A$ and after functionalisation $\Delta I = 0.3 \mu A$, which is a reduction of about 66%. For the 2wt% transistor the alteration in the modulation is even larger as for the 1wt% device. Before functionalisation $\Delta I = 1.7 \mu A$ and after functionalisation $\Delta I = 0.5 \mu A$, which is a reduction of more than 79%. Nevertheless, both transistors are still sensitive down to $2.5 \cdot 10^{-7} M$ Ca^{2+} after the functionalisation with fibronectin.

Furthermore, the online measurement could be reproduced in this concentration regime as depicted in Figure 65.

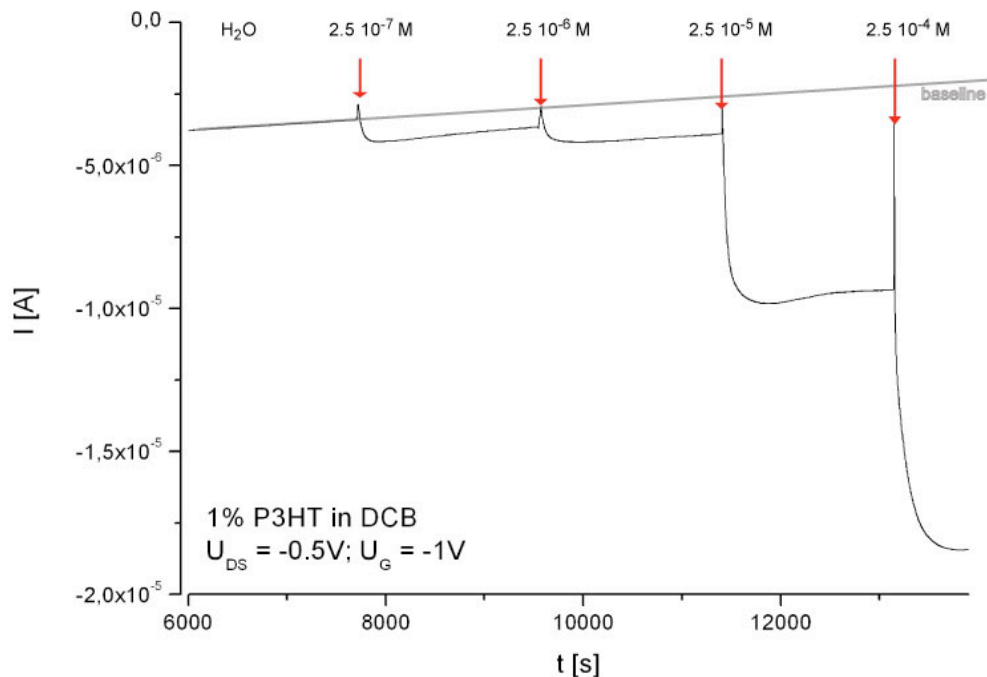


Figure 65 Online measurement of I_{DS} during variation of Ca^{2+} -concentration. The red arrows indicate the time when the solution was changed. A clear transistor response to the variation in calcium concentrations is visible.

It is obvious that the transistor is highly sensitive to the change of ion concentration. The drain-source current increases up to 600% from the initial value (see Table 13).

Table 13 Change (%) in I_{DS} during variation of the Ca^{2+} -concentration calculated from the baseline.

concentration:	$2.5 \cdot 10^{-7} M$	$2.5 \cdot 10^{-6} M$	$2.5 \cdot 10^{-5} M$	$2.5 \cdot 10^{-4} M$
change in I_{DS}	20%	43%	260%	600%

Summary and discussion

The presented results indicate that the composition of the transistor has an effect on the transistor response. The transistors made from P3HT dissolved in DCB showed sensitivity to the different ion solutions and reproducible behaviour. In contrast, no reproducible results could be gained with the blend P3HT:PCBM. For the devices made from P3HT in CHCl_3 the 1wt% transistors showed reproducible results whereas the measurements of transistors made from 2wt% were only reproducible for the output characteristics and not for the online measurements. Furthermore, the thin-film thickness affects the transistor sensitivity. For the devices with 1wt% P3HT (both DCB and CHCl_3) lower drain-source currents were detected but a higher variation in $\Delta I/I$ than for the 2wt% devices. This is consistent with already published data (39). With increasing film-thickness the interaction between the analyte and the conducting channel is reduced resulting in a smaller sensor response. It was furthermore reported by Huang *et al* (96) that with decreasing thin-film thickness, the sensor response is faster. When comparing the online measurement of the 1wt% and 2wt% DCB transistors (Figure 62) it is obvious that the drain-source current of the transistor made of 1wt% P3HT stabilises faster than the transistor made of 2wt%. This is caused by the fact that only the first few molecular layers of the organic semiconductor at the polymer/dielectric interface are important for the charge transport across the device. With a thinner organic layer the analytes binding at the polymer surface are closer to the conducting channel. The distance from surface to conducting channel is reduced and therefore the device response is faster and more prominent (96). The sensor response is further affected by the film morphology, which is specified in chapter "Sensing Principle" (4.4).

Since the transistors made from DCB showed the most promising results in terms of sensitivity and stability further measurements with calcium concentrations in the cellular regime were performed. Calcium concentrations down to $2.5 \cdot 10^{-6} \text{M}$ could reproducibly be recorded. Furthermore, online measurements of the ions were performed for both "pure" compositions. Although, the transistor response is relatively slow. It takes some minutes until the drain-source current stabilises. Calcium concentrations down to $2.5 \cdot 10^{-6} \text{M}$ could be detected online with the DCB devices.

Since biosensing, or sensing in aqueous condition with OFETs is relatively new most measurements are performed with set-up configuration where polymer is not in direct contact with the solution containing the target analyte. The sensing principle here is based on charge modulation at the dielectric as already discussed in the section pH sensitivity (chapter 4.3.1). Furthermore, for a lot of biosensor applications, the active area is functionalised with a specific recognition element to create a selective sensor

(115). One example is a study from Dabke *et al* (116). Here, a polyaniline film was incorporated with crown ethers to selectively detect potassium concentrations down to 10^{-8} M. If the cavities of the crown ether were occupied by the potassium ions a local electric field exhibits, which causes a perturbation in the polymer backbone and a change in the density of states in the band gap. This resulted in a modulation of the device conductance. With increasing potassium concentration, the modulation increases which is consistent with our findings. With the presented devices from Dabke *et al* it was possible to selectively discriminate between sodium and potassium ions. This behaviour differs from the behaviour of the sensors presented in this work. The effect of the different ions on the sensor performance differs. Nevertheless the sensor response is not selective for the different ions. Since no further functionalisation was used it might be possible to create tuneable, selective sensors with an appropriate functionalisation.

Comparing the presented results with vapour sensors where the active area is directly exposed to the vapour one can find a big difference. For example Crone *et al* (117) showed for different vapours and different p-type polymers that the drain-source current decreases while exposed to the vapour. The vapour caused electron donating or hole trapping which leads to a reduced mobility. This is in contrast to the results presented in this thesis. Here, the drain-source current increases with increasing analyte concentration. Roberts *et al* reported sensor behaviour, which is in agreement to both results (15). With OFETs made from the polymer DDFTTF as active material they observed either an increase (methylphosphonic acid) or a decrease (glucose, cysteine, trinitrobenzene) of the drain-source current with increasing analyte concentration. It was reported that the sensing mechanism involves adsorption of the analyte at grain boundaries. There, the analyte can then act either as trap or dopant, resulting in an increase or decrease of the drain-source current, depending on the nature of the chemical interaction (118). Therefore, the sensing behaviour is also dependent on the target analyte.

By comparing the detection limit of the device with already published data, one can find a higher sensitivity for the devices presented here. Lin *et al* (119) presented ion sensitive organic electrochemical transistors (OECT) based on PEDOT:PSS with detection limits down to 10^{-3} M for Na^+ , Ca^{2+} and Al^{3+} . For the devices made from 1wt% P3HT in CHCl_3 sensitivity down to 10^{-5} M was reached for all three ions and smaller detection limit is still possible. For the devices made from P3HT in DCB, sensitivity down to 10^{-6} M for Ca^{2+} and 10^{-7} M for Al^{3+} could be demonstrated in a reproducible way. Only devices with functionalisation showed higher sensitivity to specific ions like the already mentioned devices from Dabke *et al* (116).

Taking all results into account, it can be seen that sensors made from DCB suits best for application as biosensors. They are biocompatible, stable in cell culture medium and highly sensitive to the different ions, especially to Ca^{2+} . Table 14 summarises the gained results for all sensitivity test of the different compositions. Here, “+” means sensitive and reproducible, “-“ means: not sensitive, “x” measurement missing and “ \diamond ” sensitive but not reproducible.

Table 14 Properties of the different set-up configurations

sensitivity	2wt% P3HT:PCBM 3:1 in DCB	1wt% P3HT in CHCl_3	2wt% P3HT in CHCl_3	1wt% P3HT in DCB	2wt% P3HT in DCB
pH	\diamond	+	+	\diamond	\diamond
Na^+	\diamond	+	+	\diamond	\diamond
Ca^{2+}	\diamond	+	\diamond	+	+
Al^{3+}	x	+	\diamond	+	+

4.4 Sensing Principle

Up to now, the underlying mechanism for sensing in liquids is not completely understood. There are different approaches to explain the semiconductor-analyte interaction. On the one hand, it is assumed that the analyte molecules diffuse through the porous semiconductor and directly interact with the conducting channel, see Figure 66a)(15). It is also possible that the charges in the analyte form a shielding layer at the analyte-polymer interface, which leads to a modulation of the channel current (Figure 66b).

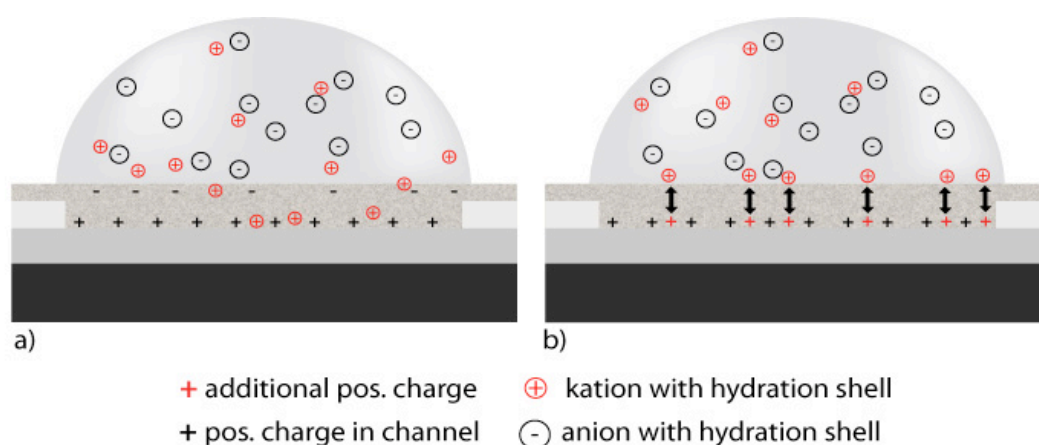


Figure 66 Interaction of ions with polymeric surface: a) diffusion of ions through grain boundaries to the conducting channel, b) formation of shielding layer. Both interactions cause additional positive charges in the conducting channel and the drain source current increases (adapted from (39)).

Nevertheless, it is known, that the chemical sensing behaviour of polycrystalline OFETs is heavily dependent on the morphological structure of the channel material and the properties of the interfaces (35, 41). The processes of analyte adsorption by the sensing film, like hydrophobic interaction or surface binding, are favoured at grain boundaries (41). Furthermore, the device geometry affects the sensing behaviour. In devices with smaller channel length, the number of grain boundaries within the channel decreases so the effect of grain boundaries on the electrical transport and chemical sensing is reduced. Hence, sensing depends on the channel length to grain size relationship (41, 96, 120, 121). Beside real-time or *in situ* measurements where a direct response to analyte exposure is measured, OFETs can be characterized previous to and directly after analyte exposure. Here, the changes in different device parameters, namely maximum and minimum currents, on-off ratio, μ and V_T are detected (39). For both ways of characterisation, the electrical response may be caused by doping of the conduction pathway, analyte induced trapping (41), partial charge transfer between the materials, local screening effects, or bulk resistive changes arising from analyte accumulation in

thin-film grain boundaries (39). The effect of doping, for example, can be observed as an increase in current and/or positive shift of threshold voltages from the addition of charge carriers at the polymer/dielectric interface (39).

To determine the effect of the film morphology and film thickness on the transistor performance, the transistors made from CHCl_3 and DCB are compared (Figure 67). AFM analysis was performed as described in 3.3.1.

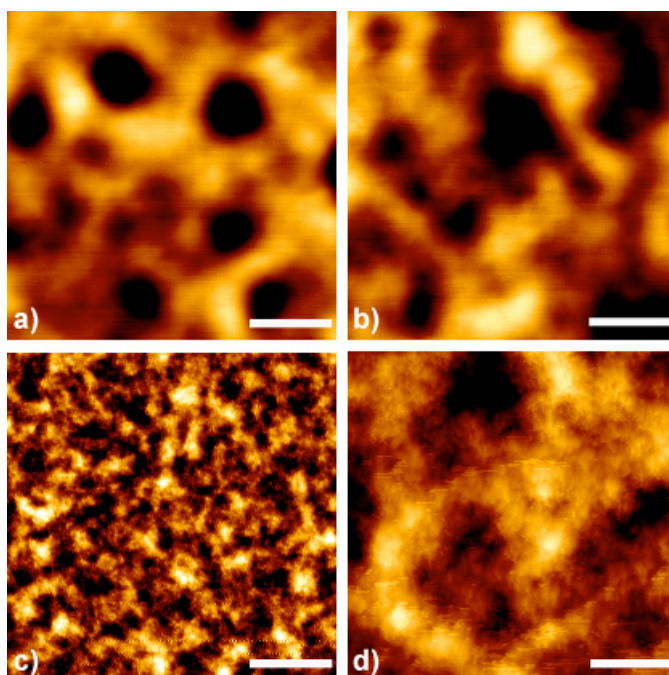


Figure 67 Topographical AFM images of the used polymer compositions: a) 1wt% P3HT in CHCl_3 , b) 2wt% P3HT in CHCl_3 , c) 1wt% P3HT in DCB and d) 2wt% P3HT in DCB. The scale bar represents 500nm.

It clearly can be seen that there is a major change in the morphology of the films depending on the different used solvents and their weight percentage. The film spun from 1wt% P3HT in DCB has the smallest grains and with it the most grain boundaries where interactions can take place (122, 123). Additionally, the shape of the grains differs. In the films spun from DCB the edges are more diffuse than in the films spun from CHCl_3 . Furthermore, films spun from CHCl_3 are thicker than those spun from DCB, whereby this might also be caused by the different parameters used for spin-coating. Table 15 summarises the thickness, RMS roughness and peak to valley roughness of the different films determined by AFM analysis. In the next table (Table 16), the relation $\Delta I/I$ is calculated for the different combinations and different ions. The data points are taken at $V_{DS} = -0.5\text{V}$ and $V_G = -1\text{V}$ at the concentrations 10^{-3}M and 10^{-5}M for every ion.

Table 15 Thickness and roughness of the different polymer layers.

	1wt% CHCl_3	2wt% CHCl_3	1wt% DCB	2wt% DCB
Thickness	150nm	300nm	50nm	100nm
RMS Roughness	3.229nm	3.258 nm	2.200nm	8.095 nm
Peak to Valley Roughness	27.69nm	25.88nm	19.53 nm	59.10 nm

Table 16 $\Delta I/I$ for the different combinations and different ions at $V_{DS} = -0.5V$ and $V_G = -1V$ at the concentrations $10^{-3}M$ and $10^{-5}M$.

	$\Delta I/I$ 1wt% CHCl_3	$\Delta I/I$ 2wt% CHCl_3	$\Delta I/I$ 1wt% DCB	$\Delta I/I$ 2wt% DCB
Ca^{2+}	0.6	0.3	1.0	0.9
Al^{2+}	0.12	0.1	0.9	0.78

It is obvious, that the changes in $\Delta I/I$ are always larger for the transistors made from 1wt% P3HT that means the transistors with the thinner polymer film. Additionally, the changes in the transistors made from DCB are major than in the transistors made from CHCl_3 . The major modulation of the drain-source current with thinner polymeric layers is in accordance to already published data (39, 96) and was already discussed in chapter 4.3.2. Furthermore, the effect of the calcium ions is always more pronounced than the effect of aluminium ions. The reason therefore is not completely understood since one could assume, that with increasing valence, the effect of the ion increases. Given that the valence is not the only difference between the ions also other factors, like ionic size and ionic mobility and the pH of the solution might affect the result which will be further analysed.

As already described above, the different ion standard solutions consists of different compounds. The ions were either dissolved in pure water or in 0.5M HNO_3 and water. For the sodium solution NaCl salt was used, whereas for calcium and aluminium calcium nitrite ($\text{Ca}(\text{NO}_3)_2$) and aluminium nitrite ($\text{Al}(\text{NO}_3)_3$) respectively. To determine the effect of the chloride and nitrite an additional solution from sodium nitrite (NaNO_3) was prepared. Furthermore, solutions of HNO_3 in water with the concentrations corresponding to the different Ca^{2+} and Al^{3+} solutions were prepared. The concentrations for the NaCl, NaNO_3 , $\text{Ca}(\text{NO}_3)_2$ and $\text{Al}(\text{NO}_3)_3$ solutions varied from $2.5 \cdot 10^{-7} M$ to $2.5 \cdot 10^{-3} M$ and for HNO_3 from $50 \cdot 10^{-7} M$ to $50 \cdot 10^{-3} M$. The next graphs are showing the measurements for the different solutions at a gate-voltage of $V_G = -1V$ (Figure 68).

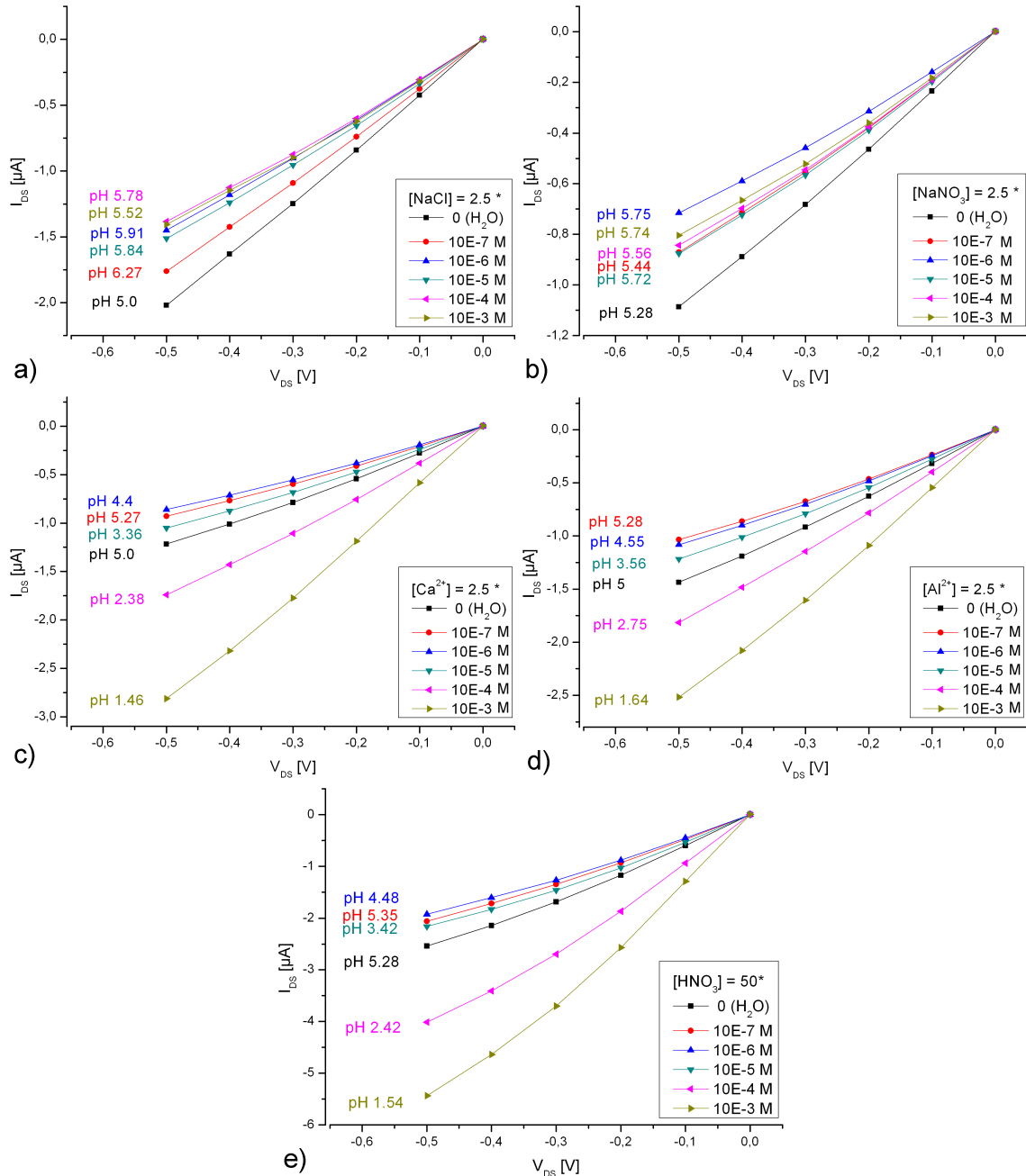


Figure 68 Characteristic of 1wt% P3HT in DCB transistors at various concentrations of ions at $V_G = -1V$. V_{DS} was decreased from 0V to -0.5V. The pH values of the different ion solutions are indicated.

Since the pH values of the different solutions vary, the values are summarised in following table (Table 17).

Table 17 pH values of the different ion solutions.

ion concentration	NaCl	NaNO ₃	Ca(NO ₃) ₂	Al(NO ₃) ₃	HNO ₃
$2.5 \cdot 10^{-7}$	6.27	5.44	5.27	5.28	5.35
$2.5 \cdot 10^{-6}$	5.91	5.75	4.4	4.55	4.48
$2.5 \cdot 10^{-5}$	5.84	5.72	3.36	3.56	3.42
$2.5 \cdot 10^{-4}$	5.78	5.56	2.38	2.57	2.42
$2.5 \cdot 10^{-3}$	5.52	5.74	1.46	1.64	1.54

The already proved ion sensitivity of the 1wt% P3HT in DCB device is confirmed. In addition the different ions unequally affect the pH of the solutions. So the effect of the ions splits up in two fractions: the presence of the ion itself and therefore a change in the pH value.

For a better comparability of the different measurements, ΔI was calculated referring to the value of 10^{-6}M for each ion. In the next graphs, ΔI was plotted against the concentration for different gate voltages. It needs to be considered that for HNO_3 the concentration is not the one indicated at the x-axis, but corresponds to the concentration of HNO_3 in the ion solutions of Na^+ , Ca^{2+} and Al^{3+} with these concentrations.

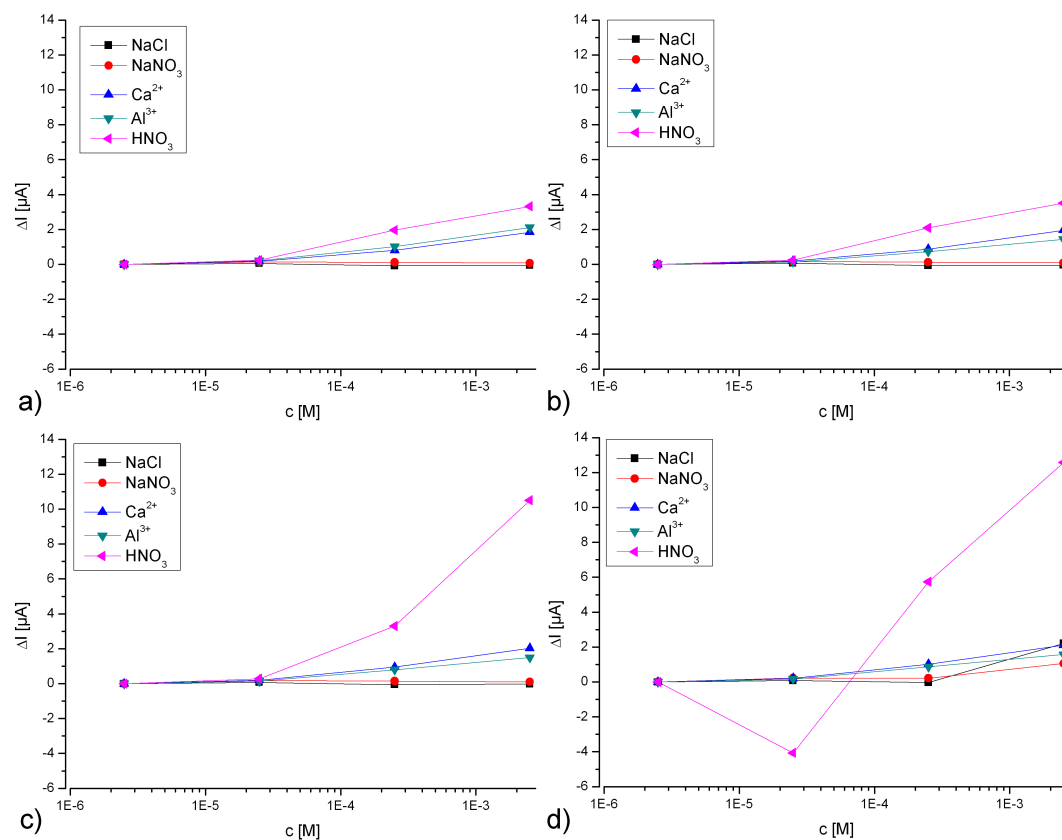


Figure 69 ΔI calculated from 10^{-6}M for different ions of 1wt% P3HT in DCB transistor with $L = 50\mu\text{m}$ in dependency of different gate voltages a) $V_G = 0\text{V}$, b) $V_G = -1\text{V}$, c) $V_G = -2\text{V}$ and d) $V_G = -3\text{V}$.

At first, the difference between NaCl and NaNO₃ is examined. Compared to the other ions, it is obvious, that the transistors are neither sensitive to NaCl, nor to NaNO₃ variations. Therefore, the negative ion $-\text{Cl}$ or $-\text{NO}_3$ does not influence the transistor behaviour, and the different used solutions made from NaCl, $\text{Ca}(\text{NO}_3)_2$ or $\text{Al}(\text{NO}_3)_3$ are comparable with each other. Moreover, it can be detected, that the HNO₃ solutions with different concentrations are having the largest effect on the transistor, followed by Ca²⁺

and Al^{3+} between which, almost no difference is visible. One theory for the sensing principle of OFETs considers the diffusion of ions within the polymer, acting as additional charges in the conducting channel (15). Based on this, one would assume, that the same amount of Ca^{2+} and Al^{3+} should have a larger effect than H^+ since Ca^{2+} and Al^{3+} are having a major charge than H^+ to influence the transistor behaviour. It was further reported, that the relative change in the transistor current depends on the applied gate bias (15). By comparing the graphs of different gate-voltage with each other, it is obvious that at higher gate-voltages, the effect of H^+ is getting larger, whereas the effect of Ca^{2+} and Al^{3+} stays almost constant. For HNO_3 , at the concentration of 10^{-3}M , the drain-source current increases from $3.5\mu\text{A}$ to $10.5\mu\text{A}$ by duplicating the gate-voltage from -1V to -2V . For Ca^{2+} the drain-source current remains relatively constant at $2\mu\text{A}$ and for Al^{3+} at $1.4\mu\text{A}$. This leads to the assumption that the sensing process is not influenced by ions that diffuses into the polymer layer.

It is assumed, that the mobility of the different ions impacts the transistor behaviour. The mobility of hydrogen ions of $36.23 \cdot 10^{-8} \text{ m}^2/\text{Vs}$ is almost six times higher than the mobility of calcium ions, which is only $6.17 \cdot 10^{-8} \text{ m}^2/\text{Vs}$ (124). Additionally, the sizes of the ions play an important role for sensing. Roberts and co-workers (15) believe that the sensing mechanism in aqueous media involves analyte diffusion to the semiconductor/dielectric interface resulting in an influence in the charge transport of the active layer by trapping and doping. To demonstrate the analyte diffusion through the semiconductor grain boundaries the influence of solutions of alcohols with increasing size on the OFET device based on the polymer DDFTTF was evaluated. As expected, they observed the greatest current modulation relative to the baseline for the smallest analyte. This means, the smaller the analyte molecule the most rapidly the molecules can diffuse through the grain boundaries. This is not confirming our results. By calculating the ion radius with the first hydration shell in the aqueous solutions it is obvious that the calcium ion has the greatest radius, followed by sodium and aluminium. Consequently, aluminium should have the greatest effect since it is the smallest ion and therefore can most easily diffuse into the polymer, but between aluminium and calcium almost no difference in the current modulation is visible. Therefore, it is possible that the ions cannot diffuse into the polymer layer due to their size.

Table 18 Ionic radii in water of the different ions from (125)

	H ₃ O ⁺	Na ⁺	Ca ²⁺	Al ³⁺
R _{ion} in H ₂ O	0.141nm	0.097nm	0.103nm	0.05nm
mean Ion-H ₂ O distance	0.2755	0.2356nm	0.2442nm	0.1887nm
calculated R _{ion} with 1 st hydration shell (R _{H₂O} =0.142nm)	0.5585	0.4746nm	0.4892nm	0.3807nm

It is interesting that the effect of H⁺ is decreased or completely absent, in the Ca²⁺ and Al³⁺ solutions. In these solutions we have the same amount of H⁺ like in the HNO₃ solutions. An explanation would be that the calcium or aluminium ions accumulate on the polymer surface since they are too large to diffuse into the polymeric layer. This layer might act as a repulsive charge for the H⁺ ions, which as a result cannot diffuse into the polymer to increase the drain-source current.

It is also thinkable that, due to their size, an accumulation of H₃O⁺ ions at the polymer/electrolyte interface occurs. This would enable an additional proton transport through the electrolyte by proton transfer between the hydronium ions at the interface, since the mobility of protons in the polymer and the solution is comparable. Such an effect would be hindered by additional ions like Ca²⁺ or Al³⁺ in the solution, because they would “occupy” the interface and proton transfer between such ions is impossible. This layer of calcium or aluminium ions again acts as a repulsive charge for the H₃O⁺ ions and the measured effect is just caused by shielding layer like depicted in Figure 66b).

For a lot of sensors, a Nernstian slope is reported (119, 126) . Here, ΔV_G is calculated and shows a logarithmic dependence on the valence of the positive ions, which decreases with increasing valence of the ion. I_{DS} is given by following equation:

$$I_{DS} = \mu C_i \frac{W}{L} (V_{DS} - V_T) \quad (4)$$

With μ field effect mobility, W channel width, L channel length, V_{DS} drain-source voltage, V_T threshold voltage and C_i capacitance. C_i , W and L are constant for every transistor. Furthermore, μ is assumed to be a material constant and a change in I_{DS} is caused by a change in $(V_{DS}-V_T)$, which fits to the Nernstian relationship. Since for the measurements presented here the drain-source current increases with increasing ion concentration it might be possible, that μ is not a material constant. μ might either change due to the positive ions that diffuse through the polymer grains to the conducting channel or by an

additional proton current through the electrolyte as described above. Both theories would enhance the modulation of μ with increasing ion concentration in the solution.

Summarising, it is assumed that:

- the transistors are sensitive on positive ions (especially H^+/H_3O^+)
- the pH has an additional influence
- the valence probably has an influence on the sensitivity (but with the additional pH effect it is not possible to separate this effect exactly)
- the thickness of the polymer film is important for sensing: the closer the ion gets to the conducting channel the more it can influence it (see also (39))
- the grain boundaries (size and amount) are important for sensing: protons can diffuse through the polymer via grain boundaries and with a higher amount of them diffusion is eased (see also (118)).

In the way, the measurements were performed it was not possible to determine which effect is caused by which factor since the system is rather complex. Different factors like ionic radii and ion mobility need to be considered. To be able to measure the effect of one type of ion, all other factors needs to be eliminated. Already, Roberts *et al* stated that the OFET response is complicated by the presence of water molecules and ions at the surface of the polymer. Furthermore, the formation of complexes must be considered that affect the local electrostatic environment at the interface (15). Aluminium salts always react acidic when dissolved (124) and buffering of the solution resulted either in the formation of precipitates or additional ions that affect the sensor performance. Thus, it is almost impossible to eliminate the additional effect of the pH. Consequently, it is necessary to adjust the set-up configuration. Functionalisation of the transistor surface with ion selective materials seems to be a promising approach. Michalska *et al* (126) showed, that the selectivity and sensitivity of ion selective electrodes can be enhanced by combining polymers with ion selective membranes.

4.5 Towards a Biosensor

The aim of the work was to develop a biosensor, which is capable to detect cell-cell communication processes. In the first part, the suitability of the OFET for application in radiation biophysics was proven. This electrical approach can further be developed combined with an optical approach, which might help to decode the measured electrical signal from the cells. Therefore, a fluorescent dye, which is sensitive to cytosolic free calcium ions inside the cells, is used.

In this chapter, the development of the optical approach is presented. For the combination of the electrical and optical methods, optimisations of the transistor set-up had to be performed. To facilitate the integration of the transistors in to microscopes, transparent electrodes and substrates are preferable. First tests with glass substrates and electrodes made from indium-tin-oxide (ITO) are presented. The second part presents an approach for online calcium flux measurements inside the cell using the calcium indicator Fluo-3. In addition, the effect of the cells on the transistors and their performance is demonstrated in the third part of this chapter.

4.5.1 Transparent Electrodes

Since electrical measurements will be combined with optical measurements of the calcium flux inside the cell, an optically transparent substrate and transparent electrodes were tested for an easy integration in to transmitted light microscopes. Normally, transparent electrodes are made from electrically conductive glass, like indium tin oxide (42, 43).

Electrodes with the same channel length of 50 μ m as the previously described Ti/Au electrodes, used for the already discussed devices, were prepared on a glass substrate. At this early stage no gate electrodes were prepared. At first, the transistor performance in tissue culture medium was tested. Therefore, a droplet of medium was placed on the active area and the drain-source current with varying drain-source voltage was measured (Figure 70). All samples showed the same effect: the drain-source current went down when exposed to tissue culture medium. However, in this set-up it takes more time until the alterations are visible. There was almost no difference in drain-source current detectable between the exposure times of 15min and 30min. All other transistors presented earlier in this work showed already after 15min a clear shift in the drain-source current. Here, only after 6hrs, a clear decrease could be observed. The

glass substrate (not silica glass) used had a different morphology than the silicon dioxide substrate of the conventional set-up. Since the morphology of the thin-film depends on the substrate it is processed on the transistor response is changed. Furthermore, a different solvent, toluene, was used for fabrication of the device, which also affects the thin-film morphology. Therefore, the interaction of the molecules with the polymer surface will be different due to the varied thin-film morphology.

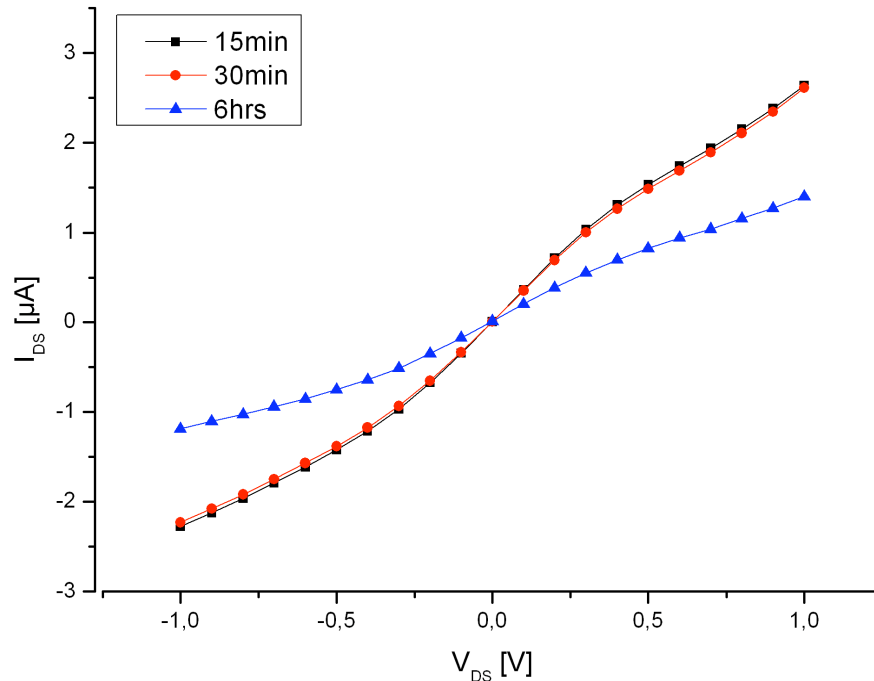


Figure 70 Characteristic of a sample with ITO contacts with $L = 50\mu\text{m}$ exposed to tissue culture medium after different measurement times with $V_G = 0\text{V}$. V_{DS} was decreased from 1V to -1V in 0.1V steps.

For stability tests in tissue culture medium, a constant drain-source voltage of $V_{DS} = -0.5\text{V}$ was applied and the drain-source current was measured while exposed to tissue culture medium. The exposure time varied from 5 to 120min. Figure 71 shows the run of I_{DS} during the online measurement of 120min. At the beginning, the drain-source current increases, indicated by the grey shaded region. Here the bias stress effect might be the more prominent effect. At around $t = 2500\text{s}$ the current decreases like seen before with all other transistor configurations. Now, probably the charge trapping effect, caused by the exposure to tissue culture medium, is the more prominent effect, which leads to a decrease in I_{DS} .

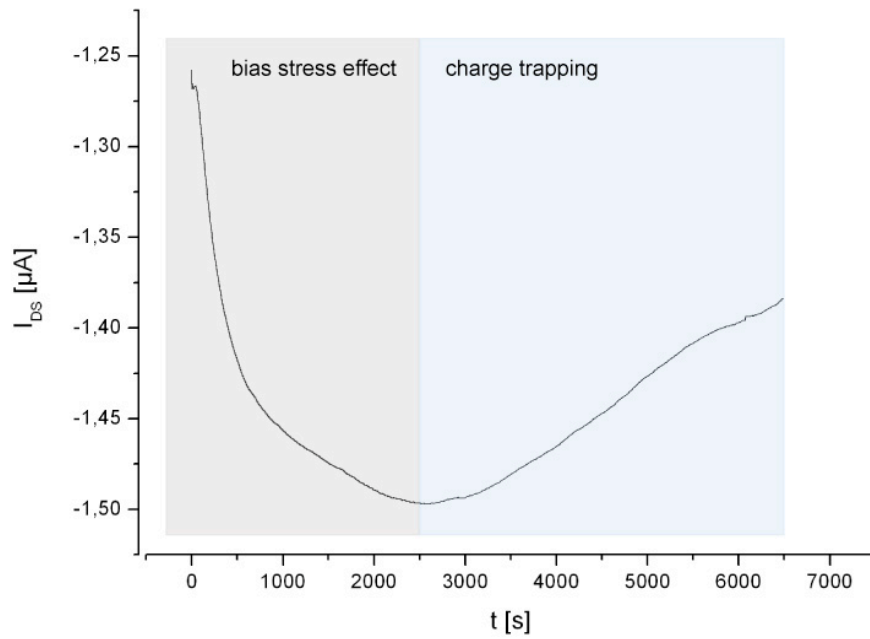


Figure 71 Drain-source current of a transistor with ITO electrodes with $L = 50\mu\text{m}$ while exposed to tissue culture medium. The applied voltage was $V_{\text{DS}} = -0.5\text{V}$. The grey and blue shaded regions indicating the more prominent effect that influences the drain-source current.

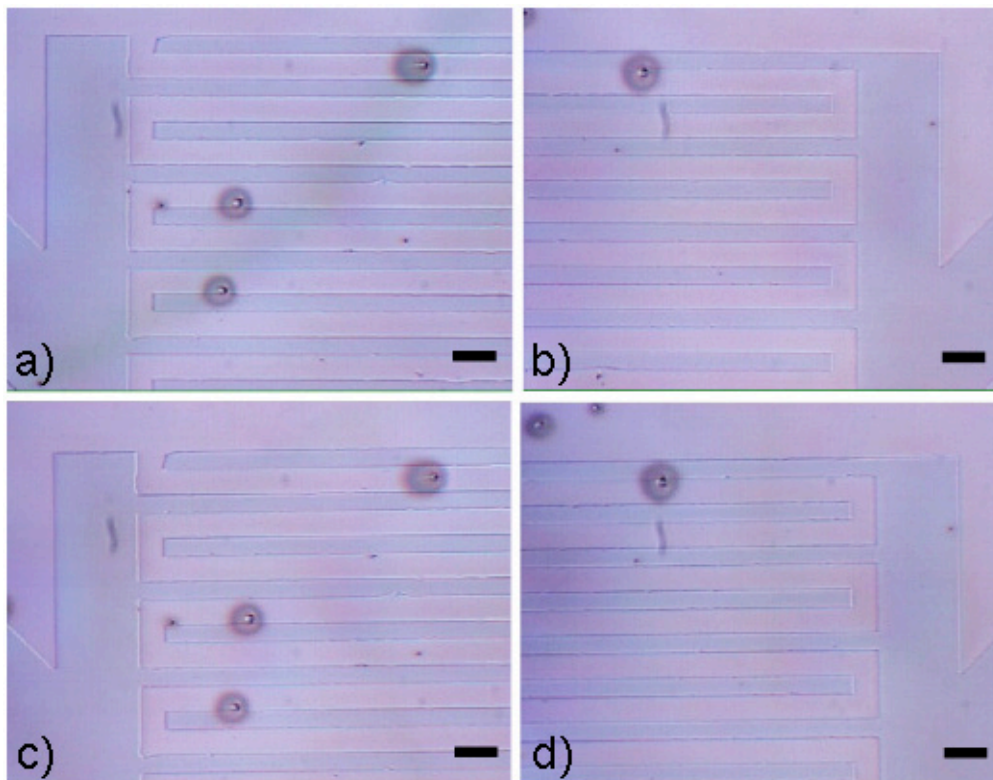


Figure 72 Glass substrate transistor with ITO contacts with $L = 50\mu\text{m}$. a) and b) are optical images of the surface before the measurement, c) and d) are images of the same spots after a measurement in tissue culture medium for 120min taken with a 10x objective. No degradation of the polymeric surface is visible. The dark spots are artefacts caused by the spin-coating process. The scale bar indicates $100\mu\text{m}$.

Figure 72 shows the transistor surface before and after the 120min measurement in tissue culture medium. Here, a) and b) are the images taken before the measurement and c) and d) at the same spots after the measurement with tissue culture medium. No degradations of the polymeric thin-film layer are visible.

Summarising these results, it could be shown that it is possible to fabricate a device with glass as substrate material instead of silicon dioxide. Furthermore, the device operates stable in tissue culture medium up to 120min without any visible degradation. Nevertheless, further characterisation concerning the device operation has to be done and a gate electrode needs to be implemented to the device.

4.5.2 Approach for the Optical Detection of Calcium Fluxes

As described above, the electrical measurements could be combined with optical measurements of the calcium flux inside the cell caused by an external stimulus. For the development of the optical approach, the widespread calcium marker Fluo-3 (82, 87) was used. Fluo-3 binds to the cytosolic free calcium inside the cell. With increasing amount of Ca^{2+} , the fluorescence intensity increases. It is a highly sensitive dye and is used for rapid measurements of calcium fluxes in cells. Because of its large fluorescence increase it provides good sensitivity. Fluo-3 has its absorption maximum at 506nm and emits at 526nm (127).

A procedure for the evaluation of the fluorescence data was developed (described in Appendix C). Furthermore, the staining protocol was optimised. The fluorescence intensity of various samples after different incubation times were compared. As a result, the incubation time could be reduced from 60min to 30min without loss of fluorescence intensity. Additionally, the bleaching effect of the dye during light exposure was determined. Therefore, the cells were loaded with Fluo-3 like described in 3.2.4. Then, the samples were placed in the microscope and illuminated. The first picture was taken directly at the beginning of the experiment. The next 20min pictures were taken every two minutes with the samples being illuminated all the time. Figure 73 shows two images of the stained cells. The left picture (a) shows the fluorescence at the beginning of the experiment, the second (b) after four minutes of illumination. It can be seen that already after 4 minutes, the fluorescence is almost not visible anymore with the bare eye.

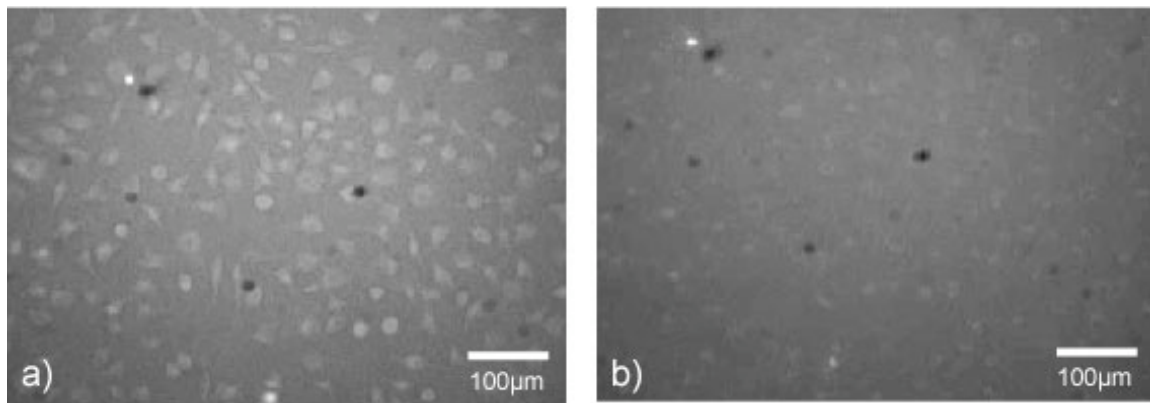


Figure 73 Fluorescence images of Fluo-3 loaded cells a) at the beginning of the experiment and b) after 4 minutes while exposed to light. The bleaching effect is clearly visible.

The following graph (Figure 74) shows the decrease of the normalised fluorescence plotted against the light exposure time. Here, at $t = 0$ the fluorescence is at its maximum and set to 1. Already after two minutes, the intensity decreases significantly to about 60% of the initial value. Therefore, the observation of calcium fluxes is only reasonable during the first few minutes.

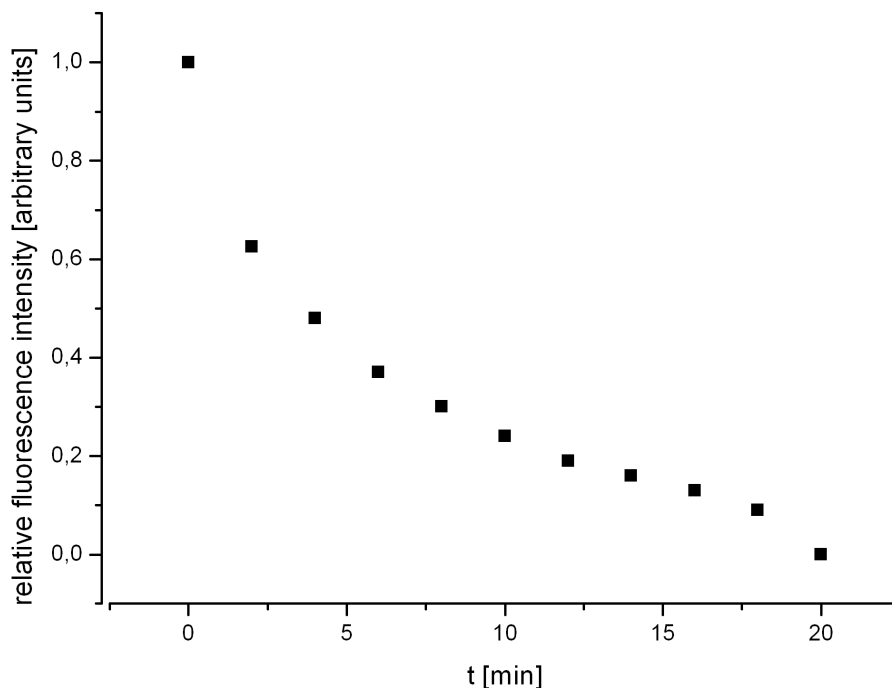


Figure 74 Decrease of the fluorescence intensity of the Fluo-3 dye due to bleaching. Values are relative to the maximum at $t = 0$. Already after two minutes, the intensity decreases significantly to about 60% of the initial value.

The bleaching effect has to be kept in mind when comparing different samples with each other. To overcome this problem, it is possible to use a combination of two fluorescent

dyes, for example Fluo-3 and Fura Red. It is reported, that the bleaching is reduced if a combination of these two dyes is used (128). Furthermore, the illumination time should be reduced with the usage of a shutter where the illumination times can be controlled and cells are only illuminated during image recording.

Since the effect of Fluo-3 on the cells themselves is not known, possible influences of the calcium indicator to the irradiation sensibility of cells were investigated. For this experiment, cells either loaded with Fluo-3 or unloaded cells were irradiated with different doses and the amount of RIFs was determined. The cells were seeded on glass slides 24hrs before irradiation. Half of the samples were loaded with the Fluo-3. Then, the cells were irradiated with doses of 100mGy, 150mGy and 200mGy and an irradiation time of 1min, 1.5min and 2min respectively. The temperature of the samples was kept at 37°C. Furthermore, sham samples were prepared, to examine the number of background RIFs. The sham sample was not irradiated, but treated like the other samples. The fixation and immunostaining was performed after a repair time of 30min like described in chapter 3.2.5. Images were recorded with a laser-scanning microscope. An example is shown in Figure 75. The green dots are the so-called RIFs while every dot represents one DSB.

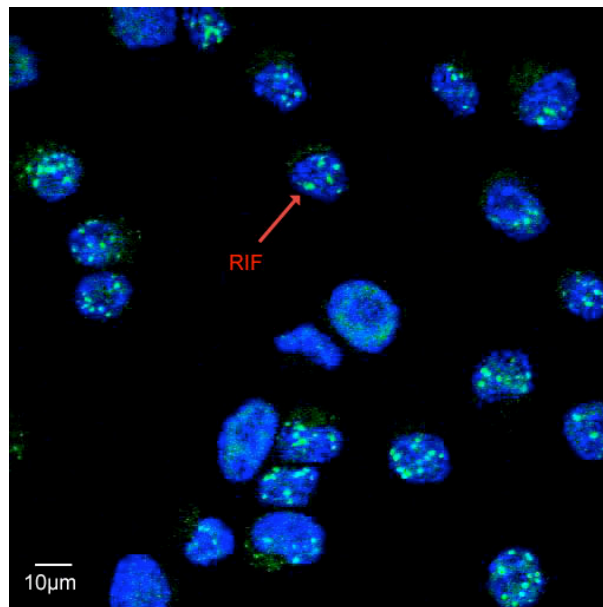


Figure 75 Confocal image taken with 63x objective of the stained cells after irradiation with 150mGy and a repair time of 30min. The green dots are the so-called radiation induced foci (RIF) and represent on DNA double strand break.

For each sample 100 cells were evaluated and the average number of RIF per cell was determined. Table 19 summarises the amount of RIF in the loaded and unloaded cells for the different doses.

Table 19 Comparison of RIF amounts in Fluo-3 loaded cells and unloaded cells.

Dose/cells	100mGy	150mGy	200mGy
with Fluo-3	5.33	13.58	18.22
w/o Fluo-3	5.72	13.49	18.53

It clearly can be seen, that the radio-sensitivity of the fibroblasts is not altered when loaded with Fluo-3. The amount of RIFs in the samples loaded with Fluo-3 show no significant discrepancy. The values are in line with internal laboratory results of experiments performed with the same parameters like dose, dose rate and repair time. Therefore, Fluo-3 can be used as Ca^{2+} marker without altering the cellular radio-sensitivity.

4.5.3 Medium Transfer Experiments

With the presented approach, online measurements could be performed. As it was technically not viable to analyse the cells directly during the irradiation, we concentrated on medium transfer experiments. For this kind of test, cells, which were not irradiated, were incubated with medium, which was collected from irradiated cells. In the medium of the irradiated cells different messengers are present that might result in a cellular response of the non-irradiated cells, the so-called bystander effect. The bystander response will be visible as a change of the fluorescence intensity of the loaded cells. For the experiment, cells were seeded on glass slides and in tissue culture flasks. The cells seeded on the glass slides were incubated with Fluo-3. The cells in the tissue culture flasks were irradiated.

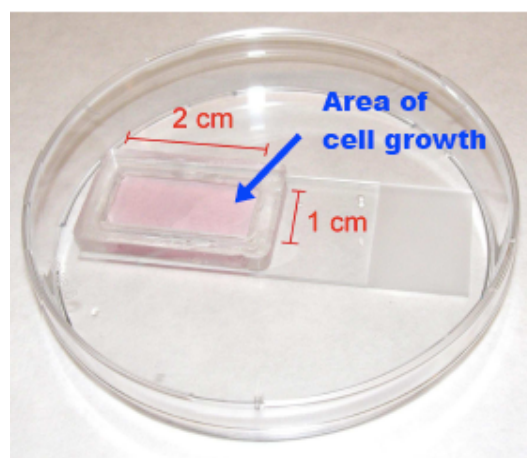


Figure 76 Image of a glass slide in Petri dish with the PDMS frame for defined cell growth. The blue arrow indicates the area of cell growth.

To be able to perform reproducible results, the amount of cells seeded either on the glass slides or in the tissue culture flasks was determined and kept constant. Furthermore, a frame made from PDMS was used to define a constant area and volume for cell growth on the glass slides (Figure 76).

The cells in the tissue flask were irradiated with 1Gy or 2Gy. The settings of the X-ray machine were 200kV and 16mA with varying duration. The tissue culture flask contained 3ml of tissue culture medium. For each experiment, a new flask was irradiated and directly after irradiation, the medium was collected and filtered through a 0.22 μ m filter to sterilise the irradiated medium and to hold back dead (that means not adherent) cells. At first a picture was taken of the cells on the glass slide, than the tissue culture medium (of the cells on the glass slide) was removed and the filtrate was added on the glass slide to avoid a dilution of the medium of the irradiated cells and to maintain a constant amount of medium on the sample. Pictures were taken every five seconds. Also a reference experiment with medium from a flask of non-irradiated cells was performed. The next graph (Figure 77) shows the fluorescence of the non-irradiated cells after adding of the medium from irradiated cells and the reference after different times. The values of Δ intensity are based on the initial intensity at $t = 0$ seconds therefore, it is possible (due to bleaching effects) that some values become negative (see reference).

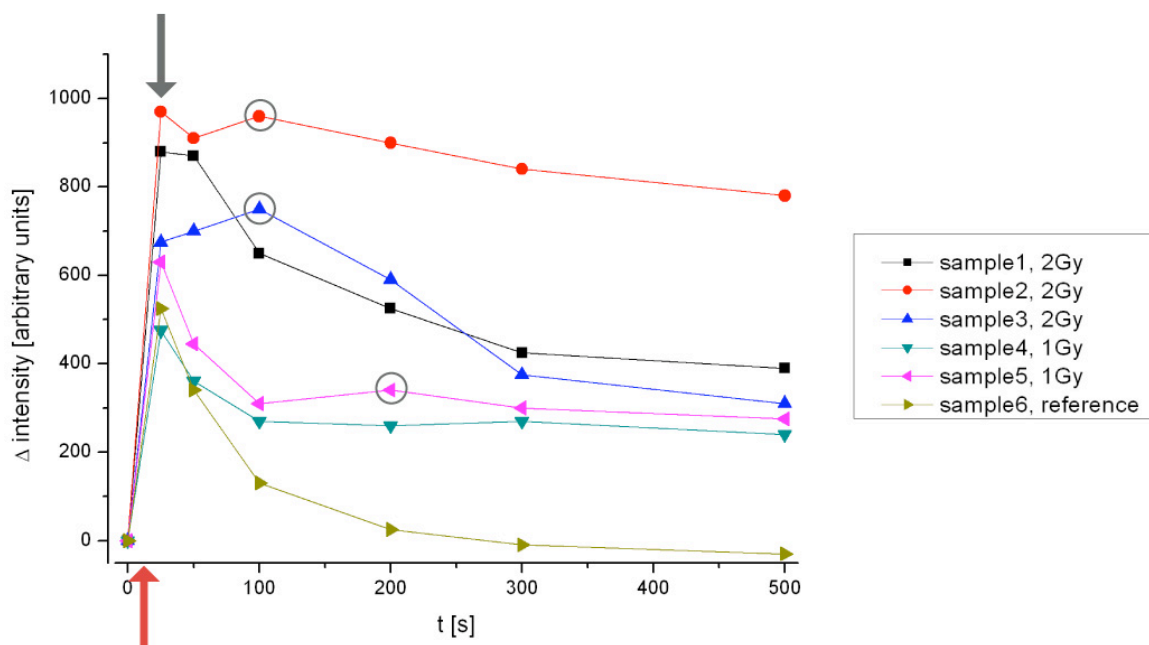


Figure 77 Change in fluorescence intensity of different samples after medium was transferred from irradiated cells to non-irradiated cells. The red arrow indicates the time the medium was added, the grey arrow indicated the peak from the glaring effect, the circles indicate the peaks maybe caused by the cells.

The red arrow indicated the time the medium was added. A clear effect can be seen. The peak which appears in all samples immediately after addition of the irradiated medium to the cells results from glare effects due to light that is scattered during the adding process itself (indicated by grey arrow). Since the height of the peak strongly varies between the different samples the light scattering process is a quite random process. This effect slowly decays with time. The fluorescence has a maximum at 100s (sample 2 and 3) or at 200s and 300s (sample 4 and 5). This effect is interpreted as cellular response to the messengers of the added medium. The bleaching of the fluorochrome probably causes the decrease of the fluorescence after about 100-200s.

The results were compared with already existing data from Mothersill *et al* (87) and Todd and Mikkelsen (59). Todd and Mikkelsen, who used HeLa cells and MCF-7 human breast tumour cells, report calcium peaks within 1.5, 2 or 3 min, which is consistent with the results presented here. In contrast to our data the fluorescence does not level off with increasing time. Mothersill *et al* worked with HVP human keratinocytes and observed a strong increase in the cytosolic free Ca^{2+} concentration 30-50s after the addition of the medium from the irradiated cells. They report also peaks of fluorescence, but at different times (100s and 200s) compared to this work. In general, the response is comparable. The different timing pattern of the peaks might be associated with the different cell lines used. Additionally, the relationship between dose and increase in fluorescence intensity was analysed, which is plotted in Figure 78.

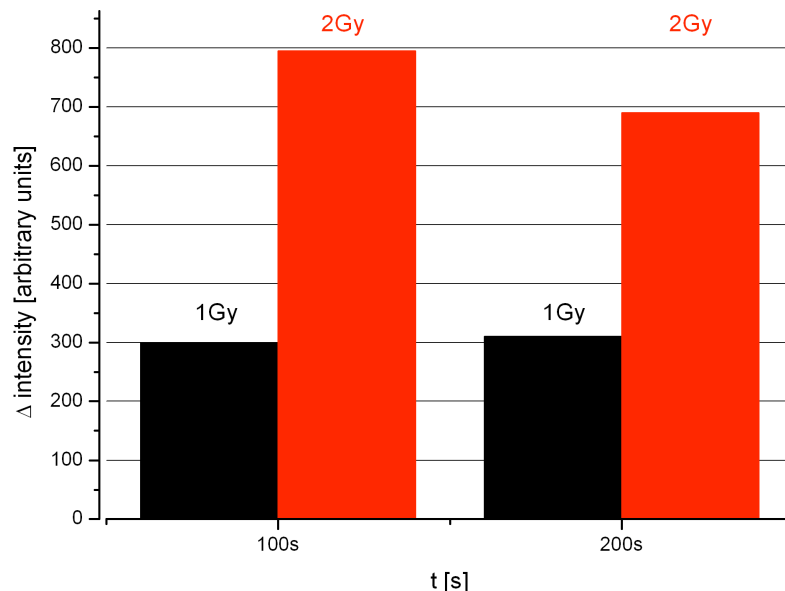


Figure 78 Comparison of the change in fluorescence intensity of different samples by addition of medium of cells irradiated with 1Gy or 2Gy after different times.

Incubating the cells with the medium of cells irradiated with 2Gy a 2 - 2.5 times higher increase in fluorescence was reached than with the 1Gy medium. The result of Todd and Mikkelsen show the same dose dependent increase of fluorescence.

Summarising, it could be shown, that it is possible to measure the so-called bystander effect with this set-up. An increase in the fluorescence intensity after adding medium from irradiated cells to non-irradiated cells was detected. Furthermore, this increase in fluorescence is dose dependent. A real-time detection of calcium fluxes within the cell is possible with fluorescence microscopy and Fluo-3 as a calcium marker. Therefore, it seems to be possible to combine this optical approach with the electrical measurements with OFET to measure cell-cell communication processes online during irradiation.

As it was written above, the amount of RIF is a measure for the damage of the cell. Therefore, the amount of RIFs created during an irradiation experiment might then be correlated with the increase in fluorescence and the change in the measured drain-source current of the transistor. This combination of online and retrospective analysis might further help to understand the cellular processes caused by low dose irradiation.

4.5.4 Effect of Cells on Sensor

Before online cell measurements can be performed, the transistors have to be functionalised. The cells need to be seeded on the transistor surface and need to grow for about 24hrs. All these steps might influence the transistor performance. Therefore, the effects of the functionalisation of the transistor and their storage in tissue culture medium must be determined. The cells, grown on the device surface, also have an effect to the transistor due to their own membrane potential.

As a first step, the sensor was characterised in tissue culture medium and after functionalisation with fibronectin. Then, the sensor was stored in tissue culture medium and was characterised again after 24hrs and 72hrs. The results are shown in Figure 79 and Figure 80. For both transistors, the drain-source current increases after functionalisation. Hence, the functionalisation with fibronectin has an impact on the transistor. Fibronectin itself is not charged, but it is diluted in a salt solution (HBSS) for the functionalisation step. Therefore, it is possible, that additional charge carriers are present in the polymeric layer, which increase the drain-source current.

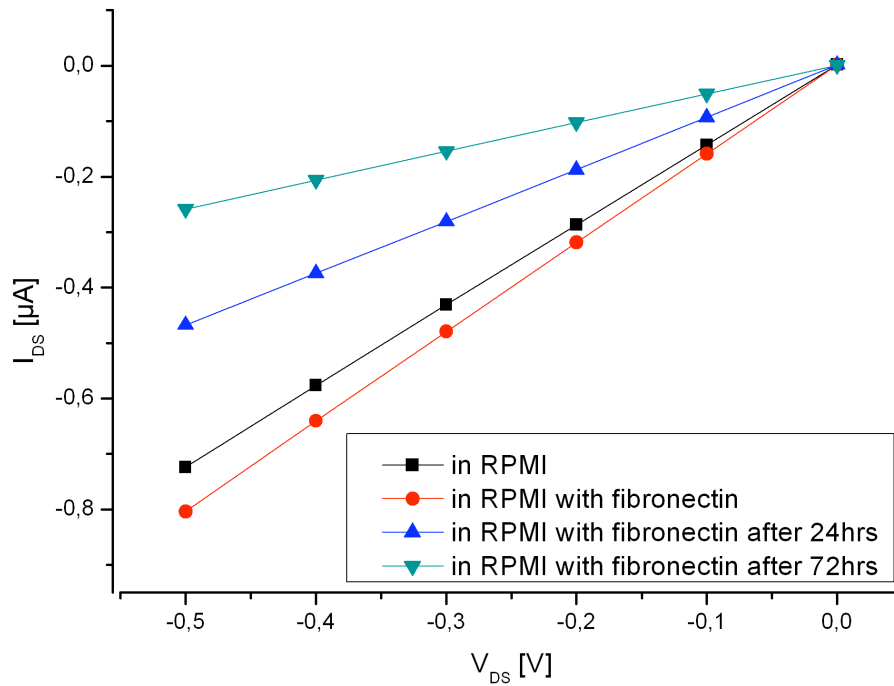


Figure 79 Effect of functionalisation and storage in tissue culture medium on the drain-source current of a transistor made of 1wt% P3HT dissolved in DCB. $V_G = -1V$ and V_{DS} was decreased from 0V to -0.5V in 0.1V steps.

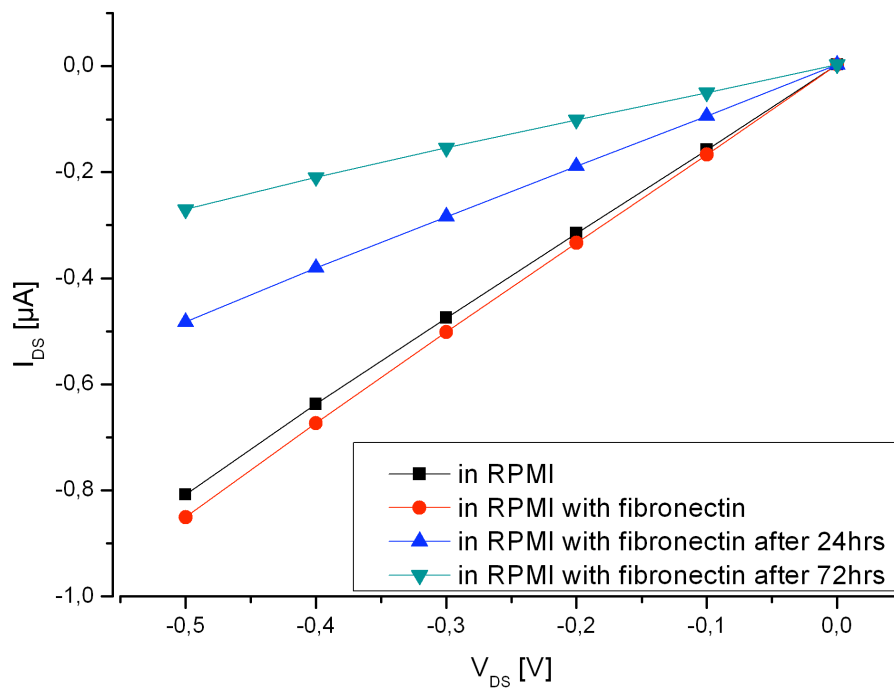


Figure 80 Effect of functionalisation and storage in tissue culture medium on the drain-source current of a transistor made of 2wt% P3HT dissolved in DCB. $V_G = -1V$ and V_{DS} was decreased from 0V to -0.5V in 0.1V steps.

With increasing storage time of the transistor in the tissue culture medium, the drain-source current decreases. This is in line with the stability test in tissue culture medium

(see chapter 4.2.2). Probably, this decrease can be attributed to charge trapping through the medium. This time dependency of the drain-source current should be kept in mind when comparing different experiments with different incubation times in tissue culture media.

As a next step the impact of the cells on the transistor was determined. It is known that most cells exhibit a membrane potential, the so-called Zeta Potential. So there is an electrostatic interaction between the cell and the adsorbent when a cell attaches to a surface, in our case, the polymeric thin-film (129). Thus, the potential between the cells and the organic layer is expected to be close to the average Zeta potential of the cells. The Zeta potential of a cell is given by (130):

$$\zeta = \frac{Q}{4\pi\epsilon\epsilon_0 Da^2} \frac{1}{\kappa} \quad (5.1)$$

with

$$\kappa = \left(\frac{e^2 n_i^0 z_i^2}{\epsilon kT} \right)^{1/2} \quad (5.2)$$

where Q is the cell surface charge, a is the cell radius, ϵ is the dielectric permittivity of the electrolyte, e is elementary charge, n_i^0 is the concentration of ions of type i in the electrolyte, z_i is the valence of z ion, k is Boltzmann constant, T is the measurement temperature and $1/\kappa$ is the double layer length. The Zeta potential of a cell is not a constant value. It is dependent on the concentration and type of ions in the electrolyte and the surface charge density of the cells. The Zeta potential of cells is normally negative and in the range of tens of millivolts (129, 130).

The Zeta potential of the used L929 mouse fibroblast, was measured with a Zetasizer ZS. For this experiment, the cells were trypsinated and filled in a special cuvette. As measurements in tissue culture medium were not possible due to degradation of the electrodes of the cuvette, the Zeta potential measurements were performed in a physiological sodium chloride solution with a pH value around 7 and a molarity of 0.154M. In preliminary tests, the maximal storage time of the cells in the physiological sodium chloride solution before they die was determined. The cells could be kept up to 30min without optical visible alterations. This is enough time to perform the Zeta Potential measurement. The measurements were replicated three times and showed a value of $\zeta = -12\text{mV}$ for the Zeta Potential of the cells. This result cannot be taken as an absolute value, since the online measurements will probably be performed in tissue culture medium and therefore the Zeta Potential of the cells will be altered due to the difference in the ionic strength of the two solutions (129).

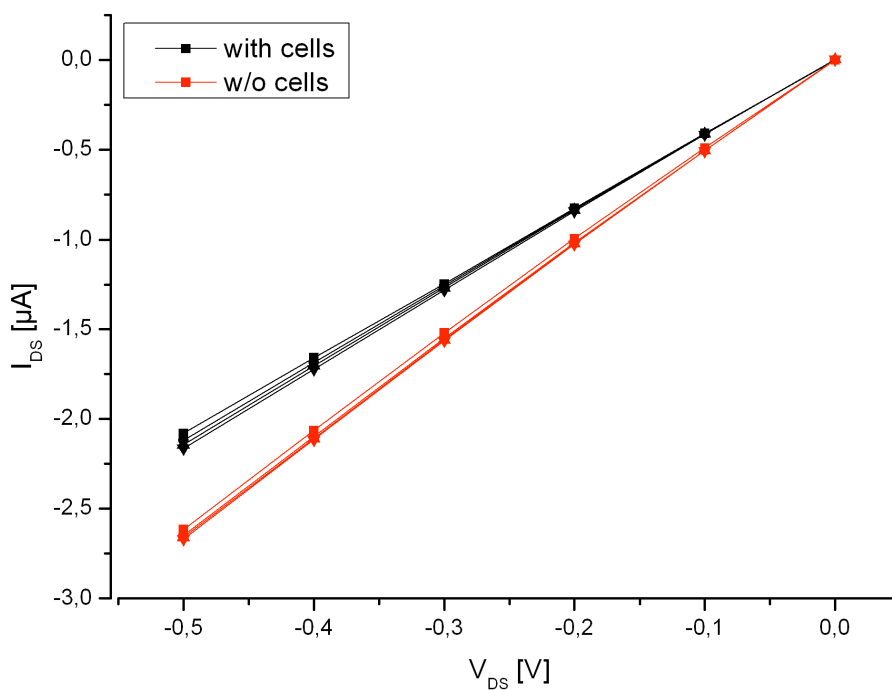


Figure 81 Characterisation of transistor for different gate voltages ($V_G = 0, -1, -2$ and $-3V$) with cells adherent grown on the transistor surface and after trypsination of the cells. The transistor was made from 1wt% P3HT in DCB. V_{DS} was decreased from 0V to $-0.5V$ in 0.1V steps.

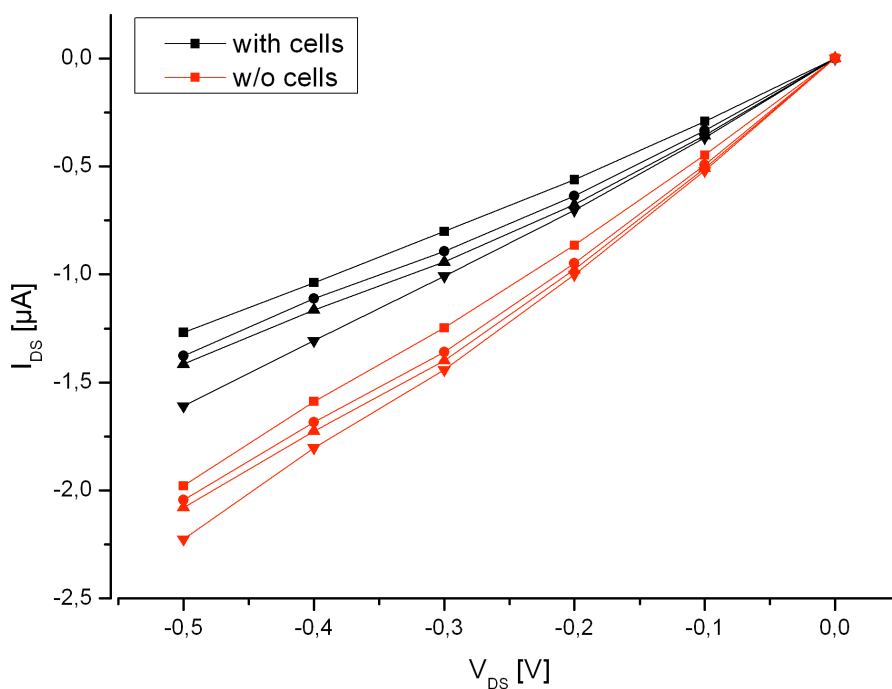


Figure 82 Characterisation for different gate voltages ($V_G = 0, -1, -2$ and $-3V$) of the transistor with cells grown adherent on the active are and after trypsination of the cells. The transistor was made from 2wt% P3HT in DCB. V_{DS} was decreased from 0V to $-0.5V$ in 0.1V steps.

Next, the influence of cell detachment on the device performance was studied. L929 mouse fibroblast were grown on the transistor surface in culture medium and the device was characterised when the cells covered more than 80% of the active area. Then, the cells were treated with trypsin solution for several minutes and simultaneously observed under a microscope. The next graphs are showing the characterisations of two different transistors (Figure 81 and Figure 82) with the cells grown on the surface and after detachment of the cells. The gate voltage was decreased from 0V to -3V in -1V steps, the drain-source voltage was decreased from 0V to -0.5V in -0.1V steps.

At first it can be seen, that the drain-source current is stable with the adherent grown cells on its surface (Figure 81 and Figure 82). Furthermore, the output characteristic of the devices shifts to higher currents after the trypsin treatment. Lin *et al* (104) used in their studies an OECT with PEDOT:PSS as active material. They determined a shift in the transfer characteristic to lower gate voltages after the detachment of the cells. The explanation of the shift is that the cells, which are attached to the polymeric surface, apply an additional negative voltage on the OECT and therefore a higher gate voltage is needed to compensate the effect of the attached cell. Here, the presented results show the output characteristic and not the transfer characteristic. Nevertheless, the result is consistent with the result from Lin *et al*. When the cells are attached to the transistor surface, the drain-source current decreases since the negative potential of the cells attract the positive charge carriers from the conducting channel as indicated in Figure 83. A higher gate voltage can compensate this effect as the positive charges contribute to the conducting channel.

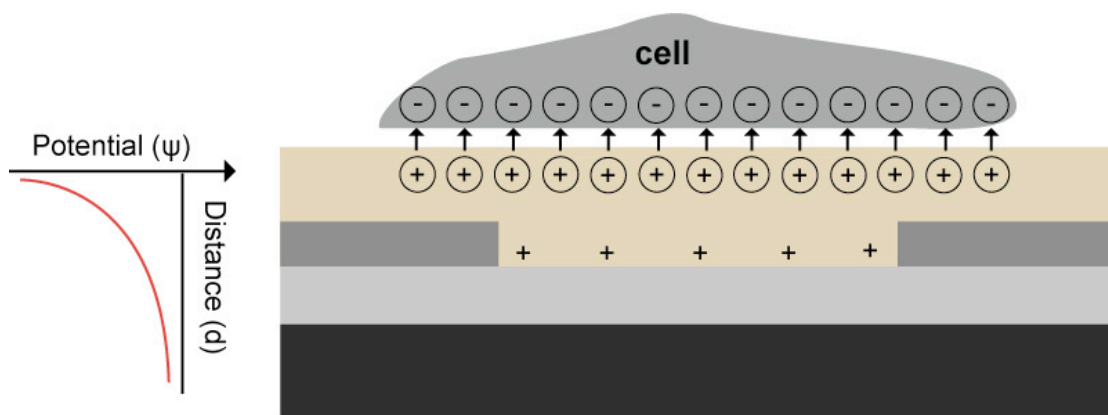


Figure 83 Schematic diagram of the electrostatic interaction between an attached cell and P3HT film. The shift in drain-source current might be caused by the negative potential of the cells, which remove the positive charge carriers from the conducting channel (adapted from (104)).

It was reported that the surface charge of a cell is related to cell biological activation (131) and is altered during and after exposure to ionising radiation (132). Therefore, the presented sensor set-up will be a useful tool to monitor cellular processes during exposure to ionising radiation. Both, cell-cell communication processes via ions or changes of the surface charge of the cells might be detected. Nevertheless, further experiments need to be performed to get statistical evidence.

5 Summary

It is of utmost interest, to use organic thin-film transistors as sensors in the field of radiation biophysics. Up to now, no sensor fulfils the special demands for this application, like biocompatibility, stability in complex tissue medium, stability under ionising radiation and ion-sensitivity in the cellular relevant regime. In this work, it was shown, that depending on the used polymer/solvent composition these demands can be fulfilled. As many factors impact the functionality of these sensors, absolute figures for sensitivity cannot be given but relative ones. The results for the different demands are briefly summarised in the following.

Biocompatibility

As the used polymer surfaces are highly hydrophobic the cells showed nearly no adhesion. Therefore a chemical or physical functionalisation was required to allow the adhesion of the cells. As chemical functionalisation, protein based coatings like fibronectin, poly-L-lysine and collagen were used. For physical functionalisation, plasma oxidation was performed. Fibronectin and plasma functionalisation showed the best results for all polymer surfaces. Further characterisation of the cells with confocal microscopy or AFM microscopy showed that the cells are not influenced by the substrate and develop their spindle like shape. The transistor current was altered by plasma or fibronectin functionalisation, but the sensitivity was not altered. Therefore, the used functionalisations, especially fibronectin and plasma can be used to enhance the cell growth on organic transistors without altering the transistor performance.

Stability in Complex Tissue Culture Medium

Since organic transistors, up to now, are mainly used as vapour sensors, it was not known how they behave in a complex tissue culture medium. The tissue culture medium consists of mono- and bivalent ions and amino acids, carbohydrates and serum proteins that are likely to interact with the electrochemical surface. Since the polymer is in direct contact with the medium, the sensors were characterised in terms of stability. For this characterisation, 3 different transistor configurations were used. P3HT dissolved in chloroform, P3HT dissolved in DCB and a blend from P3HT:PCBM dissolved in DCB. The transistor made from chloroform shows no stable operation in tissue culture medium. Already after some minutes, the polymer starts to delaminate. The transistor configurations made from DCB are both stable in tissue culture medium. The altered

behaviour of the transistors is attributed to the different morphologies of the polymeric layers caused by the different processing parameters like the solvent.

Stability under Ionising Radiation

For this characterisation, the same configurations were used. All configurations showed no degradation by ionising radiation. When the devices are irradiated in air a modulation of the drain-source current is visible. During irradiation, the drain-source current decreases. The modulations are dose dependent but in the nA regime. During irradiation in tissue culture medium, the effect is not visible anymore. The doping effect of the medium might overlay the very small variations caused by the irradiation.

pH Sensitivity

The configurations P3HT in CHCl_3 , P3HT in DCB and P3HT:PCBM in DCB could stable be operated in a pH range from pH 4 to pH 7. It was shown, that transistors made from CHCl_3 and DCB were sensitive to changes in the pH value. For all compositions the drain-source current increased with decreasing pH. Reproducible result were gained with the pure polymers, the blend of P3HT:PCBM showed no reproducible results. The reason therefore might be the aging of the transistor.

Sensitivity to Variations of Ion Concentrations

The effect of different ions, like sodium and calcium, which are important for cell-cell communication, on the transistors were tested. Additionally, aluminium ions were tested to determine the effect of mono-, bi- and trivalent ions. Moreover, the effects of morphology of the different set-up configurations on the device response were analysed. The sensitivity of the sensors depends on the type of ion used and on the sensor configuration. Measurements were performed in the concentration range from $2.5 \cdot 10^{-3} \text{M}$ to $2.5 \cdot 10^{-7} \text{M}$. 1wt% P3HT in CHCl_3 showed sensitivity for all ions down to $2.5 \cdot 10^{-5} \text{M}$. For 2wt% P3HT in CHCl_3 and for P3HT:PCBM in DCB no reproducible results were gained. The devices made from P3HT in DCB were sensitive to calcium and aluminium ion concentration down to $2.5 \cdot 10^{-7} \text{M}$.

Sensing Principle

Based on the presented results, a new sensing principle for the used transistor set-up was developed. Protons either diffuse into the polymer or stay at the surface and therefore affect the drain-source current. For the other ions tested here only the latter effect is possible. Different morphologies and different thicknesses of the polymer layers led to variations of the sensitivity of the sensors. With a thicker layer, the sensitivity is reduced, since the ions are more far away from the conducting channel. The size and amount of grains also affect the sensitivity. With more and smaller grains (1wt% P3HT in DCB) the sensitivity is the highest, since more grain boundaries are present that can interact with the solution.

The following table (Table 20) summarises the different properties of the all set-up configurations. Here, “+” means sensitive and reproducible, “-“ means: not sensitive and “◇” means not reproducible.

Table 20 Summary of different properties of all set-up configurations.

	2wt% P3HT:PCBM 3:1 in DCB	1wt% P3HT in CHCl ₃	2wt% P3HT in CHCl ₃	1wt% P3HT in DCB	2wt% P3HT in DCB
biocompatibility	+	+	+	+	+
stability in medium	+	-	-	+	+
stability in IR					
air	+	+	+	+	+
medium	+	-	-	+	+
pH	◇	+	+	◇	◇
Na ⁺	◇	+	+	◇	◇
Ca ²⁺	◇	+	◇	++	++
Al ³⁺	◇	+	◇	+	+

The device made from 1wt% P3HT in DCB suits best the demands for application in radiation biophysics. It can be operated in a stable way in tissue culture medium and under ionising radiation. It is also sensitive to different ions, especially calcium.

Towards a biosensor

An *in situ* approach for the optical detection of calcium fluxes inside the cell was developed. With this optical calcium approach it was possible to detect the bystander signal of non-irradiated cells after addition of medium of irradiated cells. In a last step, the possibility to run the devices with cells adherently grown on the sensor surface was proved and the effect of the cells on the sensors was determined.

Summarising, it was proven that OFETs can be used in the field of radiation biophysics. With varying the polymer or solvent, the transistor properties can be tailored due to a changed morphology and surface-polymer interaction. Nevertheless, further optimisation in the transistor preparation needs to be done. Sensitivity and especially selectivity need to be enhanced.

6 Outlook

It could be shown that biosensors based on organic materials with a bottom contact/bottom gate structure are good candidates for applications in radiation biology. Nevertheless, reproducibility and also selectivity have to be further optimised.

With the presented set-up reproducible measurements can be performed, but since the set-up is very sensitive to interferences by the conditions under which it is operating, the signal to noise ratio has to be optimised by a proper shielding against any disturbing factors, especially from the outside. Part of this is a sample holder with an integrated heating system to keep the temperature controlled during the measurements.

Sensitivity should be further enhanced by either reducing the size of the active area or by choosing another working point of the transistor. In this case, the measurements were performed in the linear regime due to the stability problems in liquids. Nevertheless, Torsi *et al* (133) showed, that sensitivity could be enhanced when the transistor is operated in the saturation regime. To be able to run the transistors in the saturation regime, higher driving voltages have to be applied and therefore, the stability in terms of tissue culture medium needs to be characterised again.

The sensors are sensitive to positive ions, but not selective. To achieve selectivity, two approaches could be pursued. On the one hand, sensor architectures in combination with lipid bilayers could be used (6). They are considered as simplified cell membranes and can be “functionalised” with the integration of specific ion-channels and easily adsorbed to different surfaces. This set-up would make use of the transport process across the membrane, for example an ionic current generated by the integrated ion channel. When the ion channel is triggered to open, the selective pore allows the transport of only the channel specific ion through the channel, which then can directly be read out by the sensor. On the other hand, ion selective membranes can be combined with the sensor. Michalska *et al* (126) developed so-called all-solid ion-selective electrodes. They consist of a transducer layer, which couples the ionic and electronic conductivity between the substrate and the ion-selective membrane. With these selective electrodes it was possible to detect Ca^{2+} concentrations down to $5 \cdot 10^{-9}\text{M}$ and of potassium (K^{+}) to $4.4 \cdot 10^{-7}\text{M}$. A combination of ion-selective materials with the used OFETs could lead to very selective and sensitive sensors.

Furthermore, a combination of CNTs and P3HT could enhance stability and sensitivity. Transparent and flexible pH sensors could be prepared from combinations of CNT/polypyrrolle and CNT/pani (93). Here, the CNTs worked as electrodes. The sensors showed an improved sensitivity, linearity, stability and reproducibility in a pH range from

pH 1 to pH 13 in various buffer solutions compared to pure CNT networks. Further advantages of CNT modified electrodes are their high surface area, mechanical strength, excellent electrical conductivity and good chemical stability (6).

Another problem is the so-called “bias stress effect”, which is a well-known effect in organic transistor (29, 30). This effect might influence the transistor response to the cell signals. To avoid this, pulsed measurements could be performed like often used for vapour sensors (134). Furthermore the response time, which is about some minutes, needs to be enhanced since cellular processes are in the range of microseconds.

Additionally, the effect of storage in air and in tissue culture medium needs to be determined. Since a disposable sensor device should be developed the sensor does not need to be stable for a very long storage time in tissue culture medium.

Our approach is a first step for the online cell-cell communication detection during an online irradiation experiment. After further optimisation of the set-up, a combination of optical and electrical detection of communication messengers will be possible. This will be a step forward to decode the complex cell-cell communication process. Moreover, the altered communication process of cancer cells might possibly be determined. A further step is the development of a full organic disposable device for online cell-cell communication detection.

Literature

1. BfS (2010) Ionisierende Strahlung: Risikoabschätzung und -bewertung. (Bundesamt für Strahlenschutz).
2. UNSCAR (2008) Sources and Effects of Ionizing Radiation. ed Radiation UNSCotEoA (UNSCAR, New York).
3. BfS (2010) Ionisierende Strahlung: Röntgendiagnostik. (Bundesamt für Strahlenschutz).
4. Hooker AM, *et al.* (2004) The linear no-threshold model does not hold for low-dose ionizing radiation. *Radiation research* 162(4):447-452.
5. Owens R & Malliaras G (2010) Organic Electronics at the Interface with Biology. *MRS Bulletin* 35: 449-456.
6. Grieshaber D, MacKenzie R, Voeroes J, & Reimhult E (2008) Electrochemical biosensors-Sensor principles and architectures. *Sensors* 8(3):1400-1458.
7. Thèvenot DR, Toth K, Durst RA, & Wilson GS (2001) Electrochemical biosensors: recommended definitions and classification1. *Biosensors and Bioelectronics* 16(1-2):121-131.
8. Clark Jr LC & Lyons C (1962) Electrode systems for continuous monitoring in cardiovascular surgery. *Annals of the New York Academy of Sciences* 102(1):29-45.
9. Bartic C, Campitelli A, & Borghs S (2003) Field-effect detection of chemical species with hybrid organic/inorganic transistors. *Applied Physics Letters* 82(3):475-477.
10. Loi A, Manunza I, & Bonfiglio A (2005) Flexible, organic, ion-sensitive field-effect transistor. *Applied Physics Letters* 86:103512.
11. Bartic C & Borghs G (2006) Organic thin-film transistors as transducers for (bio) analytical applications. *Analytical and bioanalytical chemistry* 384(2):354-365.
12. Jaffrezic-Renault N (2001) New trends in biosensors for organophosphorus pesticides. *Sensors* 1(2):60-74.
13. Poghossian A, *et al.* (2001) Penicillin detection by means of field-effect based sensors: EnFET, capacitive EIS sensor or LAPS? *Sensors and Actuators B: Chemical* 78(1-3):237-242.
14. Munoz J, *et al.* (1997) Photosensitive polyurethanes applied to the development of CHEMFET and ENFET devices for biomedical sensing. *Biosensors and Bioelectronics* 12(7):577-585.
15. Roberts M, *et al.* (2008) Water-stable organic transistors and their application in chemical and biological sensors. *Proceedings of the National Academy of Sciences* 105(34):12134.
16. Fromherz P (2002) Electrical interfacing of nerve cells and semiconductor chips. *ChemPhysChem* 3(3):276-284.
17. Steinhoff G, *et al.* (2005) Recording of cell action potentials with AlGaIn/GaN field-effect transistors. *Applied Physics Letters* 86:033901.
18. Lovat V, *et al.* (2005) Carbon nanotube substrates boost neuronal electrical signaling. *Nano letters* 5(6):1107-1110.
19. Torsi L, Angione MD, & Cotrone S (2009) Organic electronic biological sensing. *SPIE Newsroom*.
20. Svennersten K, Bolin MH, Jager EWH, Berggren M, & Richter-Dahlfors A (2009) Electrochemical modulation of epithelia formation using conducting polymers. *Biomaterials* 30(31):6257-6264.
21. Bonner WM (2003) Low-dose radiation: Thresholds, bystander effects, and adaptive responses. *Proceedings of the National Academy of Sciences* 100(9):4973.
22. Bachtler B (1999) Erkenntnisse über Zellkommunikation liefern Basis für Entwicklung neuer Krebsmedikamente.).

23. Diallo A, *et al.* (2009) Trimethylamine biosensor based on pentacene enzymatic organic field effect transistor. *Applied Physics Letters* 94:263302.
24. Dimitrakopoulos CD & Malenfant PRL (2002) Organic thin film transistors for large area electronics. *Advanced Materials* 14(2):99.
25. Katz HE & Huang J (2009) Thin-film organic electronic devices. *Annual Review of Materials Research* 39:71-92.
26. Svennersten K, Larsson KC, Berggren M, & Richter-Dahlfors A (2011) Organic bioelectronics in nanomedicine. *Biochimica et Biophysica Acta* 1810(3):276-285.
27. Brütting W & Riefl W (2008) Grundlagen der organischen Halbleiter. *Physik Journal* 7(5):33-38.
28. Horowitz G (1998) Organic field-effect transistors. *Advanced Materials* 10(5):365-377.
29. Zaumseil J & Sirringhaus H (2007) Electron and ambipolar transport in organic field-effect transistors. *Chem. Rev* 107(4):1296-1323.
30. Singh T & Sariciftci N (2006) Progress in plastic electronics devices. *Materials Research* 36(1):199.
31. Bao Z, Dodabalapur A, & Lovinger AJ (1996) Soluble and processable regioregular poly (3-hexylthiophene) for thin film field effect transistor applications with high mobility. *Applied Physics Letters* 69:4108.
32. Sethuraman K, Ochiai S, Kojima K, & Mizutani T (2008) Performance of poly (3-hexylthiophene) organic field-effect transistors on cross-linked poly (4-vinyl phenol) dielectric layer and solvent effects. *Applied Physics Letters* 92:183302.
33. Brütting W (2005) *Introduction to the physics of organic semiconductors* (Wiley-VCH Verlag GmbH & Co. KGaA, Weinheim).
34. Goetz S, *et al.* (2009) Organic field-effect transistors for biosensing applications. *Organic Electronics* 10(4):573-580.
35. Salleo A (2007) Charge transport in polymeric transistors. *Materials Today* 10(3):38-45.
36. Jimison LH, Toney MF, McCulloch I, Heeney M, & Salleo A (2009) Charge Transport Anisotropy Due to Grain Boundaries in Directionally Crystallized Thin Films of Regioregular Poly(3-hexylthiophene). *Advanced Materials* 21(16):1568-1572.
37. Kline RJ, McGehee MD, & Toney MF (2006) Highly oriented crystals at the buried interface in polythiophene thin-film transistors. *Nature Materials* 5(3):222-228.
38. Sirringhaus H, *et al.* (1999) Two-dimensional charge transport in self-organized, high-mobility conjugated polymers. *Nature* 401(6754):685-688.
39. Sokolov A, Roberts M, & Bao Z (2009) Fabrication of low-cost electronic biosensors. *Materials Today* 12(9):12-20.
40. Mabeck J & Malliaras G (2006) Chemical and biological sensors based on organic thin-film transistors. *Analytical and bioanalytical chemistry* 384(2):343-353.
41. Wang L, Fine D, Sharma D, Torsi L, & Dodabalapur A (2006) Nanoscale organic and polymeric field-effect transistors as chemical sensors. *Analytical and bioanalytical chemistry* 384(2):310-321.
42. Mathine D, *et al.* (2005) Indium tin oxide electrodes for cell-based biosensors. *Microtechnology in Medicine and Biology*, (IEEE), pp 180-183.
43. Choi CK, *et al.* (2008) Opto-Electric Cellular Biosensor Using Optically Transparent Indium Tin Oxide (ITO) Electrodes. *Sensors* 8(5):3257-3270.
44. Majewski L, Grell M, Ogier S, & Veres J (2003) A novel gate insulator for flexible electronics. *Organic Electronics* 4(1):27-32.
45. Dimitrakopoulos C & Malenfant P (2002) Organic thin film transistors for large area electronics. *Advanced Materials* 14(2):99-117.
46. Majewski L, Schroeder R, & Grell M (2004) Organic field-effect transistors with electroplated platinum contacts. *Applied Physics Letters* 85:3620.

47. Tate J, *et al.* (2000) Anodization and microcontact printing on electroless silver: Solution-based fabrication procedures for low-voltage electronic systems with organic active components. *Langmuir* 16(14):6054-6060.
48. Kawase T, Shimoda T, Newsome C, Sirringhaus H, & Friend RH (2003) Inkjet printing of polymer thin film transistors. *Thin Solid Films* 438:279-287.
49. Park I, *et al.* (2008) Nanoscale patterning and electronics on flexible substrate by direct nanoimprinting of metallic nanoparticles. *Adv. Mater* 20(3):489-496.
50. Feili D, *et al.* (2006) Flexible organic field effect transistors for biomedical microimplants using polyimide and parylene C as substrate and insulator layers. *Journal of micromechanics and microengineering* 16:1555.
51. Alberts B, *et al.* (2002) *Molecular Biology of the Cell* (Garland Science, New York).
52. Popp MJJ (2008) Licht im Kampf gegen Krebs und andere Volkskrankheiten. *Biophotonik* 1:32-35.
53. Sutherland EW, Robison G, & Butcher RW (1968) Some aspects of the biological role of adenosine 3', 5'-monophosphate (cyclic AMP). *Circulation* 37(2):279-306.
54. Berridge MJ, Bootman MD, & Roderick HL (2003) Calcium signalling: dynamics, homeostasis and remodelling. *Nature Reviews Molecular Cell Biology* 4(7):517-529.
55. Bootman MD, *et al.* (2001) Calcium signalling - an overview. *Seminars in Cell & Developmental Biology*, (Elsevier), pp 3-10.
56. Berridge MJ, Lipp P, & Bootman MD (2000) The versatility and universality of calcium signalling. *Nature Reviews Molecular Cell Biology* 1(1):11-21.
57. Berridge MJ (1997) Elementary and global aspects of calcium signalling. *The Journal of Physiology* 499(2):291.
58. Roderick HL & Cook SJ (2008) Ca²⁺ signalling checkpoints in cancer: remodelling Ca²⁺ for cancer cell proliferation and survival. *Nature Reviews Cancer* 8(5):361-375.
59. Todd DG & Mikkelsen RB (1994) Ionizing radiation induces a transient increase in cytosolic free [Ca²⁺] in human epithelial tumor cells. *Cancer research* 54(19):5224.
60. Rink PDH (Physikalische Grundlagen der Strahlenwirkung. (Uni Bonn).
61. Köhnlein W (2001) *Die Wirkung niedriger Strahlendosen* (Springer).
62. Lengfelder E & Forst D (1988) *Strahlenwirkung-Strahlenrisiko: Ergebnisse, Bewertung und Folgerungen nach einem kerntechnischen Unfall aus Ärztlicher Sicht* (Hugendubel).
63. Turner JE (2007) *Atoms, radiation, and radiation protection* (Vch Pub).
64. Friedberg EC (2003) DNA damage and repair. *Nature* 421(6921):436-440.
65. Rothkamm K, Kruger I, Thompson LH, & Lobrich M (2003) Pathways of DNA double-strand break repair during the mammalian cell cycle. *Molecular and cellular biology* 23(16):5706.
66. Rothkamm K & Löbrich M (2003) Evidence for a lack of DNA double-strand break repair in human cells exposed to very low X-ray doses. *Proceedings of the National Academy of Sciences of the United States of America* 100(9):5057.
67. van Veelen LR, *et al.* (2005) Analysis of ionizing radiation-induced foci of DNA damage repair proteins. *Mutation Research/Fundamental and Molecular Mechanisms of Mutagenesis* 574(1-2):22-33.
68. Barcellos-Hoff MH, Park C, & Wright EG (2005) Radiation and the microenvironment-tumorigenesis and therapy. *Nature Reviews Cancer* 5(11):867-875.
69. Stevenson AFG (2001) Strahlenbiologisches Gutachten. in *Onkogene Effektivität niedriger Strahlendosen*, ed Köhnlein W (Institut für Toxikologie der Christian-Albrechts-Universität zu Kiel, Kiel).

70. Brenner DJ, *et al.* (2003) Cancer risks attributable to low doses of ionizing radiation: assessing what we really know. *Proceedings of the National Academy of Sciences of the United States of America* 100(24):13761.
71. White R, *et al.* (1993) Bone sarcoma characteristics and distribution in beagles fed strontium-90. *Radiation Research* 136(2):178-189.
72. BfS (2010) Ionisierende Strahlung: Hormesis. (Bundesamt für Strahlenschutz).
73. Preston DL, Shimizu Y, Pierce DA, Suyama A, & Mabuchi K (2003) Studies of mortality of atomic bomb survivors. Report 13: Solid cancer and noncancer disease mortality: 1950-1997. *Radiation research* 160(4):381-407.
74. Cornforth MN, Bailey SM, & Goodwin EH (2009) Dose responses for chromosome aberrations produced in noncycling primary human fibroblasts by alpha particles, and by gamma rays delivered at sublimiting low dose rates.
75. Nagasawa H & Little JB (1992) Induction of sister chromatid exchanges by extremely low doses of alpha-particles. *Cancer research* 52(22):6394.
76. Prise K (1998) Studies of bystander effects in human fibroblasts using a charged particle microbeam. *International Journal of Radiation Biology* 74(6):793-798.
77. Prise KM, Folkard M, & Michael BD (2003) Bystander responses induced by low LET radiation. *Oncogene* 22(45):7043-7049.
78. UNSCAR (2006) Effects of Ionising Radiation New York).
79. Morgan WF & Sowa MB (2007) Non-targeted bystander effects induced by ionizing radiation. *Mutation Research/Fundamental and Molecular Mechanisms of Mutagenesis* 616(1-2):159-164.
80. Mothersill C & Seymour CB (2004) Radiation-induced bystander effects--implications for cancer. *Nature reviews. Cancer* 4(2):158.
81. Mothersill C & Seymour C (2001) Radiation-induced bystander effects: past history and future directions. *Radiation research* 155(6):759-767.
82. Lyng FM, Seymour C, & Mothersill C (2002) Initiation of apoptosis in cells exposed to medium from the progeny of irradiated cells: a possible mechanism for bystander-induced genomic instability? *Radiation research* 157(4):365-370.
83. Belyakov P, Trott, Michael (1999) Delayed lethality, apoptosis and micronucleus formation in human fibroblasts irradiated with X-rays or alpha-particles. *International Journal of Radiation Biology* 75(8):985-993.
84. Suzuki M, Zhou H, Geard CR, & Hei TK (2004) Effect of medium on chromatin damage in bystander mammalian cells. *Radiation research* 162(3):264-269.
85. Morgan WF (2003) Non-targeted and delayed effects of exposure to ionizing radiation: I. Radiation-induced genomic instability and bystander effects in vitro. *Radiation research* 159(5):567-580.
86. Watson GE, Lorimore SA, Macdonald DA, & Wright EG (2000) Chromosomal instability in unirradiated cells induced in vivo by a bystander effect of ionizing radiation. *Cancer research* 60(20):5608.
87. Lyng F, Seymour C, & Mothersill C (2000) Production of a signal by irradiated cells which leads to a response in unirradiated cells characteristic of initiation of apoptosis. *British journal of cancer* 83(9):1223.
88. Lyng FM, Howe OL, & McClean B (2011) Reactive oxygen species-induced release of signalling factors in irradiated cells triggers membrane signalling and calcium influx in bystander cells. *International Journal of Radiation Biology* 87(7):683-695.
89. Shao C, Lyng FM, Folkard M, & Prise KM (2006) Calcium fluxes modulate the radiation-induced bystander responses in targeted glioma and fibroblast cells. *Radiation research* 166(3):479-487.
90. Optik L ((Labor Optik).
91. Schmitz S (2009) *Der Experimentator: Zellkultur* (Spektrum, Akad. Verl.).
92. Plattner H & Hentschel J (1997) *Taschenlehrbuch Zellbiologie* (Thieme).
93. Ferrer Anglada N, Kaempgen M, & Roth S (2006) Transparent and flexible carbon nanotube/polypyrrole and carbon nanotube/polyaniline pH sensors. *physica status solidi (b)* 243(13):3519-3523.

94. Kline R & McGehee M (2006) Morphology and charge transport in conjugated polymers. *Journal of Macromolecular Science-Part C-Polymer Reviews* 46(1):27-46.
95. Surin M, *et al.* (2006) Relationship between the microscopic morphology and the charge transport properties in poly (3-hexylthiophene) field-effect transistors. *Journal of Applied Physics* 100:033712.
96. Huang J, Sun J, & Katz HE (2008) Monolayer Dimensional 5, 5 Bis (4 hexylphenyl) 2, 2 bithiophene Transistors and Chemically Responsive Heterostructures. *Advanced Materials* 20(13):2567-2572.
97. Chua LL, *et al.* (2005) General observation of n-type field-effect behaviour in organic semiconductors. *Nature* 434(7030):194-199.
98. Al-Ibrahim M & Roth H (2005) Flexible large area polymer solar cells based on poly (3-hexylthiophene)/fullerene. *Solar energy materials and solar cells* 85(1):13-20.
99. Mas-Torrent M, *et al.* (2005) Single-crystal organic field-effect transistors based on dibenzo-tetrathiafulvalene. *Applied Physics Letters* 86(1):012110-012110-012113.
100. Allen LT, *et al.* (2003) Interaction of soft condensed materials with living cells: phenotype/transcriptome correlations for the hydrophobic effect. *Proceedings of the National Academy of Sciences of the United States of America* 100(11):6331.
101. Duffy DC, McDonald JC, Schueller OJA, & Whitesides GM (1998) Rapid prototyping of microfluidic systems in poly (dimethylsiloxane). *Analytical chemistry* 70(23):4974-4984.
102. Williams Y, *et al.* (2008) Comparison of three cell fixation methods for high content analysis assays utilizing quantum dots. *Journal of Microscopy* 232(1):91-98.
103. Scarpa G, Idzko AL, Götz S, & Thalhammer S (2010) Biocompatibility Studies of Functionalized Regioregular Poly (3-hexylthiophene) Layers for Sensing Applications. *Macromolecular bioscience* 10(4):378-383.
104. Lin P, Yan F, Yu J, Chan HLW, & Yang M (2010) The Application of Organic Electrochemical Transistors in Cell Based Biosensors. *Advanced Materials* 22(33):3655-3660.
105. Ji T, Rai P, Jung S, & Varadan VK (2008) In vitro evaluation of flexible pH and potassium ion-sensitive organic field effect transistor sensors. *Applied Physics Letters* 92(23):233304-233304-233303.
106. Someya T, Dodabalapur A, Gelperin A, Katz HE, & Bao Z (2002) Integration and response of organic electronics with aqueous microfluidics. *Langmuir* 18(13):5299-5302.
107. Scarpa G, Idzko AL, Yadav A, & Thalhammer S (2010) Organic ISFET based on poly (3-hexylthiophene). *Sensors* 10(3):2262-2273.
108. Raval HN, Tiwari SP, Navan RR, & Rao VR (2009) Determining ionizing radiation using sensors based on organic semiconducting material. *Applied Physics Letters* 94(12):123304-123304-123303.
109. Binda M, *et al.* (2009) Squaraine-based organic photodetector coupled to a scintillating crystal for X-ray sensing applications. (IEEE), pp 1970-1973.
110. Kingsley JW, Pearson AJ, Harris L, Weston SJ, & Lidzey DG (2009) Detecting 6 MV X-rays using an organic photovoltaic device. *Organic Electronics* 10(6):1170-1173.
111. Lee K, Nair PR, Scott A, Alam MA, & Janes DB (2009) Device considerations for development of conductance-based biosensors. *Journal of Applied Physics* 105(10):102046-102046-102013.
112. Bartic C, Palan B, Campitelli A, & Borghs G (2002) Monitoring pH with organic-based field-effect transistors. *Sensors and Actuators B: Chemical* 83(1-3):115-122.
113. Roberts ME, Mannsfeld SCB, Stoltenberg RM, & Bao Z (2009) Flexible, plastic transistor-based chemical sensors. *Organic Electronics* 10(3):377-383.

114. Mortimer CE & Müller U (2003) *Chemie: Das Basiswissen der Chemie* (G. Thieme).
115. Schöning MJ & Poghossian A (2002) Recent advances in biologically sensitive field-effect transistors (BioFETs). *Analyst-Cambridge* 127(9):1137-1151.
116. Dabke R, Singh G, Dhanabalan A, Lal R, & Contractor A (1997) An ion-activated molecular electronic device. *Analytical chemistry* 69(4):724-727.
117. Crone B, *et al.* (2001) Electronic sensing of vapors with organic transistors. *Applied Physics Letters* 78:2229.
118. Locklin J & Bao Z (2006) Effect of morphology on organic thin film transistor sensors. *Analytical and bioanalytical chemistry* 384(2):336-342.
119. Lin P, Yan F, & Chan HLW (2010) Ion-Sensitive Properties of Organic Electrochemical Transistors. *ACS Applied Materials & Interfaces* 2(6):1637-1641.
120. Becerril HA, Roberts ME, Liu Z, Locklin J, & Bao Z (2008) High Performance Organic Thin Film Transistors through Solution Sheared Deposition of Small Molecule Organic Semiconductors. *Advanced Materials* 20(13):2588-2594.
121. Tanese MC, Fine D, Dodabalapur A, & Torsi L (2005) Interface and gate bias dependence responses of sensing organic thin-film transistors. *Biosensors and Bioelectronics* 21(5):782-788.
122. Torsi L & Dodabalapur A (2005) Organic thin-film transistors as plastic analytical sensors. *Analytical chemistry* 77(19):380-387.
123. Torsi L, *et al.* (2002) Correlation between oligothiophene thin film transistor morphology and vapor responses. *The Journal of Physical Chemistry B* 106(48):12563-12568.
124. Atkins PW & Ludwig R (2001) *Kurzlehrbuch Physikalische Chemie* (Wiley-VCH).
125. Marcus Y (1988) Ionic radii in aqueous solutions. *Chemical Reviews* 88(8):1475-1498.
126. Michalska A & Maksymiuk K (2004) All-plastic, disposable, low detection limit ion-selective electrodes. *Analytica chimica acta* 523(1):97-105.
127. Invitrogen.
128. Lipp P & Niggli E (1993) Ratiometric confocal Ca²⁺-measurements with visible wavelength indicators in isolated cardiac myocytes. *Cell Calcium* 14(5):359-372.
129. Lin DQ, Zhong LN, & Yao SJ (2006) Zeta potential as a diagnostic tool to evaluate the biomass electrostatic adhesion during ion exchange expanded bed application. *Biotechnology and bioengineering* 95(1):185-191.
130. Zhang Y, *et al.* (2009) A Surface Charge Study on Cellular Uptake Behavior of F3 Peptide Conjugated Iron Oxide Nanoparticles. *Small* 5(17):1990-1996.
131. Veronesi B, Haar C, Lee L, & Oortgiesen M (2002) The surface charge of visible particulate matter predicts biological activation in human bronchial epithelial cells. *Toxicology and applied pharmacology* 178(3):144-154.
132. Somosy Z, Kubasova T, Ecsedi G, & Köteles G (1986) Radiation-induced changes of negative charge on the cell surface of primary human fibroblasts. *International Journal of Radiation Biology* 49(6):969-978.
133. Torsi L, *et al.* (2008) A sensitivity-enhanced field-effect chiral sensor. *Nature Materials* 7(5):412-417.
134. Chang JB (2006) Functionalized polythiophene thin-film transistors for low-cost gas sensor arrays. PhD (University of California, Berkeley).

Appendix

A) List of Abbreviations

53BP1	tumour suppressor p53 binding protein 1
Å	Angstrom
Ag	silver
Al	aluminium
Al(NO ₂) ₃	aluminium nitrite
Al(OH ₃)	aluminium hydroxide
Al ₂ O	aluminium oxide
Al ³⁺	aluminium ion
AlCl ₃	aluminium chloride
Au	gold
BC	bottom contact
BG	bottom gate
BS	biosensor
BSA	bovine serum albumin
C _i	capacitance per unit area
Ca	calcium
Ca(NO ₂) ₂	calcium nitrite
Ca ²⁺	calcium ion
CaCl ₂	calcium chloride
cAMP	cyclic adenosine monophosphate
CHCl ₃	chloroform
ChemFET	chemical sensitive field-effect transistor
cm	centimetre
CO ₂	carbon dioxide
Cr	chrome
CT	computer tomography
D	dose
DB-TTF	dibenzotetrathiafulvalen
DCB	dichlorobenzene
DDFTTF	5,5-bis-(7-dodecyl-9H-fluoren-2-ly)-2,2'-bithiophene

DNA	deoxyribonucleic acid
DSB	double strand break
e^-	electron
e_{aq}	electron with hydration shell
EnFET	enzyme-immobilised field-effect transistor
ER	endoplasmic reticulum
FBS	fetal bovine serum
FET	field effect transistor
γ H2AX	phosphorylated histone H2AX
GaN	gallium nitride
GOx	glucose oxidase
Gy	Gray
h	hour
H	equivalent dose
H ₂ O ₂	hydrogen peroxide
HBSS	hanks based salt solution
HH	head-head
HNO ₃	nitric acid
HOMO	highest occupied molecular orbital
HR	homologous recombination
HT	head-tail
Hz	Hertz
I _{DS}	drain-source current
IP ₃	inositol triphosphate
IR	ionising radiation
IS	ionisierende Strahlung
I _{sat}	saturation current
ISFET	ion-sensitive field-effect transistor
ITO	indium-tin-oxide
J	Joule
K	potassium
keV	kilo electron volt
kg	kilograms

L929	mouse fibroblast cell line
LET	linear energy transfer
LNT model	linear no-threshold model
LUMO	lowest unoccupied molecular orbital
M	molar
MeV	mega electron volt
min	minutes
mM	milimolar
mSv	milisievert
mv	milivolt
M_w	molecular weight
n	negative charge
N	Newton
Na	sodium
Na^+	sodium ion
NaCl	sodium chloride
nm	nanometre
O_2	oxygen
OECT	organic electro-chemical transistor
OFET	organic field-effect transistor
OH^-	hydrogen oxide
OH^\cdot	hydroxyl radical
p	positive charge
P3HT	poly(3-hexylthiophene)
PBS	phosphate buffered saline
PCBM	phenyl-C61-butric acid methyl ester
PEDOT:PSS	poly(3,4-ethylenedioxythiophene): poly(styrenesulfonate)
Pen	penicillin
PMMA	poly(methy metacrylate)
Pt	platinum
Q	quality factor
R	receptor
Rad52	repair protein

RBE	relative biological effectiveness
RIF	radiation induced foci
RNA	ribonucleic acid
rpm	rounds per minute
rr-P3HT	regioregular P3HT
RT	room temperature
s	second
Si ⁺	doped silicon
Si ₂ N ₄	silicon nitride
SiO ₂	silicon dioxide
SSB	single strand break
Sv	Sievert
TC	top contact
tol	toluene
TT	tail-tail
TU	Technical University
UV	ultraviolet
V _{DS}	drain-source voltage
V _G	gate voltage
V _{TH}	threshold voltage
W	Watt
w/o	without
wt%	weight percent
μ	mobility
μl	microliter
μm	micrometer
μM	micromolar

B) List of Materials

Tissue culture

L929 mouse fibroblast	
RPMI 1640 medium	Biochrom AG, 12247 Berlin, Germany
10% FBS Superior	Biochrom AG, 12247 Berlin, Germany Sigma Aldrich Biochemie, 21147 Hamburg, Germany
Penicillin/Streptomycin	Biochrom AG, 12247 Berlin, Germany
70% Ethanol Sorte 642	Kottkamp Alkoholvertrieb, 26123 Oldenburg, Germany
PBS – DULBECCO	Biochrom AG, 12247 Berlin, Germany
Trypsin (1:250) 0,25% (w/v) in PBS	Biochrom AG, 12247 Berlin, Germany
Tissue culture flask	Greiner bio-one GmbH, 72636 Frickenhausen, Germany
Seriological pipettes 10ml	Greiner Bio-One GmbH, 72636 Frickenhausen, Germany
Seriological pipettes 5ml	Greiner Bio-One GmbH, 72636 Frickenhausen, Germany
Seriological pipettes 2.5ml	Greiner Bio-One GmbH, 72636 Frickenhausen, Germany
Falcon tubes 15ml	Omnilab GmbH & Co. KG, 28359 Bremen, Germany
Petri dish 10cm	Greiner Bio-One GmbH, 72636 Frickenhausen, Germany
Coverslip 18 x 18 mm	Menzel-Gläser 38116 Braunschweig, Germany

Biocompatibility

Fibronectin, 0,1% Solution from Bovine Plasma	Sigma-Aldrich Biochemie, 21147 Hamburg, Germany
Collagen A L7220	Biochrom AG, 12247 Berlin, Germany
Poly-L-lysine $M_w > 3000$ 0.1mg/ml	Biochrom AG, 12247 Berlin, Germany
Microscope Slide	Carl Roth GmbH + Co. KG,

	76185 Karlsruhe, Germany
	Paul Marienfeld GmbH & Co.KG, 97922 Lauda-Köngishofen, Germany
Fixogum Rubber Cement	Marabuwerke, 71732 Tamm, Germany
Plasma-Processor 500-E	Technics GMBH Europa
<u>Antibodys and dyes</u>	
Trypban Blue	Biochorm AG, 12247 Berlin, Germany
Fluo-3, AM, cell permeant, special packing	Invitrogen GmbH, 76313 Karlsruhe, Germany
Anti-53BP1 (Rabbit Polyclonal) Golden,	ABR-Affinity BioReagents CO 80403, U.S.
Alexa Flour 488 goat anit-rabbit IgG (H+L)	Invitrogen GmbH, 76131 Karlsruhe, Germany
Hoechst 33342 trihydrochloride	Invitrogen GmbH, 76131 Karlsruhe, Germany
Vybrant DiO	Invitrogen GmbH, 76131 Karlsruhe, Germany
Rhodamine Phalloidin	Invitrogen GmbH, 76131 Karlsruhe, Germany
Vectashield H-1000	Vector Laboratories, Inc Burlingame, CA 94010, U.S.
Hank's balanced salt solution (HBSS) GIBCO 1X	Invitrogen GmbH, 76131 Karlsruhe, Germany
Triton X-100	Merck KGaA, 64293 Darmstadt, Germany
Albumin from bovine serum (BSA),	Sigma-Aldrich Biochemie 21147 Hamburg, Germany
Paraformaldehyde P6148 reagent grade/crystalline	Sigma-Aldrich Biochemie 21147 Hamburg, Germany
Calbiochem Glutaraldehyde 25% aqueous solution	EMD Chemicals, Inc. Gibbstown, NJ 08027, U.S.
Sylgard 184 silicone elastomer kit (PDMS)	Dow Corning GmbH, 65201 Wiesbaden, Germany

Sterile syringe filter (0,22µm CM membrane) Merck KGaA,
76601 Bruchsal, Germany

Equipment for characterisation in liquids

Salts (NaCl, CaCl₂, AlCl₃) Merck KGaA,
76601 Bruchsal, Germany

Standard solutions Merck KGaA,
Na 19791; K 19784; Cl 19897; Ca 19778, Al 19770; 76601 Bruchsal, Germany

pH standard solutions 10.01, 7.01, 4.01 Hanna instruments GmbH
77694 Kehl am Rhein, Germany

Simplicity Millipore Corporate,
Billerica, MA 01821, U.S.

Equipment for irradiation experiments

X-ray machine Stabilipan TR300f Siemens AG,
80333 München, Germany

Dose area product meter Diamentor M4 PTW,
79115 Freiburg, Germany

GWWP004 hotplate Günter Witt GmbH,
78315Radolfzell, Germany

Microscopes and cameras

Light optical microscope Axiovert 40 C Carl Zeiss AG
73447 Oberkochen, Germany

Light optical microscope Axio Observer. Z1 Carl Zeiss AG
73447 Oberkochen, Germany

in combination with Pixelink
Frewire camera PL-A662 Ottawa, ON K1G 6C2, Canada

Sony Camera Exwave SSC-DC58AP Sony AG,
Tokyo 108-0075, Japan

Laser scanning microscope LSM 510 Carl Zeiss AG
73447 Oberkochen, Germany

Fluo 3 Filterset Basic AHF analysetechnik AG
72074 Tübingen, Germany

Atomic Force Microscopy

JPK Nanowizard JPK Instruments,
12435 Berlin, Germany

Fire wire Camera DFK 31 AF03 The Imaging Source Europe
GmbH,

	28215 Bremen, Germany
Zeiss Axiovert S100	Carl Zeiss AG 73447 Oberkochen, Germany

μMash tips (NSC 35/ AIBs; NSC 36/AIBS; CSC 37/AIBS; CSC38 /no AI)	MicroMash, 2618 Tallinn, Estonia
--	-------------------------------------

Zeta Potential Measurements

Zetasizer ZS+	Malvern Instruments GmbH, 71083 Herrenberg, Germany
---------------	--

Folded Capillary Cell DTS1060	Malvern Instruments GmbH, 71083 Herrenberg, Germany
-------------------------------	--

Electric and Electronic Devices and experimental Set-Up

Keithley Semiconductor Characterization System 4200-SCS	Keithley Instruments Inc. Cleveland, Ohio 44139, U.S.
Triple Power Supply HM 7042-5	Hameg Instruments GmbH 63533 Mainhausen, Germany
Model 2400 Series SourceMeter	Keithley Instruments Inc. Cleveland, Ohio 44139, U.S.
Model 2000 Series Multimeter	Keithley Instruments Inc. Cleveland, Ohio 44139, U.S.
Model 2700 Series Multimeter/Switch System	Keithley Instruments Inc. Cleveland, Ohio 44139, U.S.
GBIP Interface Board KPCI-488LP IEEE-488.2	Keithley Instruments Inc. Cleveland, Ohio 44139, U.S.
Silicone rubber Scrintec RTV 1K 901	Carl Roth GmbH + Co. KG 76231 Karlsruhe, Germany
Silver glue Doduco	Doduco GmbH + Co. 75181 Pforzheim, Germany
Silicone temperature sensor KTY 11-6	Infineon Technologies AG 85579 Neubiberg, Germany
Coaxial cable RG-174	Reichelt Elektronik 26452 Sande, Germany
Gold connectors SMB EB2-L174	Reichelt Elektronik 26452 Sande, Germany
Gold connector plugs SMB ST-C174	Reichelt Elektronik 26452 Sande, Germany
Gold cable couplings SMB KU-KU	Reichelt Elektronik 26452 Sande, Germany
BNC-Buchse	Conrad Electronic, 92240 Hirschau, Germany

BNC-Stecker	Conrad Electronic, 92240 Hirschau, Germany
BNC Buchsen Adapter	Conrad Electronic, 92240 Hirschau, Germany
<u>Transistors</u>	
Wafer Uni BW	Universität der Bundeswehr München, 85577 Neubieberg, Germany
Wafer hochdotiert	Si-Mat, 86916 Kaufering, Germany
Photolack MAN1420	Microresist, 12555 Berlin, Germany
Gold (99.999 %)	Alfa Aesar Ward Hill, MA 01835 USA
Titan (99.99%)	Alfa Aesar Ward Hill, MA 01835 USA
Chrome (99.995%)	Alfa Aesar Ward Hill, MA 01835 USA
P3HT	Rieke Metals NE 68521, U.S
	Merck KGaA, 76601 Bruchsal, Germany
PCBM	
DB- TTF	Sigma-Aldrich Biochemie 21147 Hamburg, Germany
Glove box MBRaun MB 200MOD	M Braun, 65748 Garching, Germany
in combination with Spin coater delta 6RC	
UNIVEX 350G evaporation chamber	Leybod Optics GmbH, 63755 Alzenau, Germany
<u>Software</u>	
LabView 8.2 Express	National Instruments Dtl. 81369 München, Germany
Keithley Communicator	Keithley Instruments Inc. Cleveland, Ohio 44139, U.S.
JPK data analysis software	JPK Instruments, 12435 Berlin, Germany
Imgage J	Free software (Open Source) Http://imagej.nih.gov/ij

Adobe Illustrator CS3	Adobe Systems Incorporated San Jose, Ca 95110, U.S.
Adobe Photoshop CS3	Adobe Systems Incorporated San Jose, Ca 95110, U.S.
Origin 7.5	OriginLab Corporation Northampton, MA01060, U.S.
Microsoft Office Power Point:mac 2008	Microsoft, Redmond, WA-98052-6399, U.S.
Microsoft Office Word:mac 2008	Microsoft, Redmond, WA-98052-6399, U.S.

C) Lab-intern protocol: Method for fluorescence evaluation

To be able to get comparable results, a procedure for the data evaluation has been elaborated. Here, the required steps are explained. All details and the protocol for data proceeding with the image processing software ImageJ are presented.

Figure 1 shows the cells loaded with Fluo-3. It can be seen, that the illumination is not uniform. Therefore, only the cells, which are located in the centre of the image, indicated with the circle, will be evaluated for data processing. It is important, that the circle is always at the same place when analysing different images of one sample to ensure that the same cells were analysed. This can be guaranteed by defining the circle coordinates with the ImageJ software. Therefore, the image is opened with ImageJ.

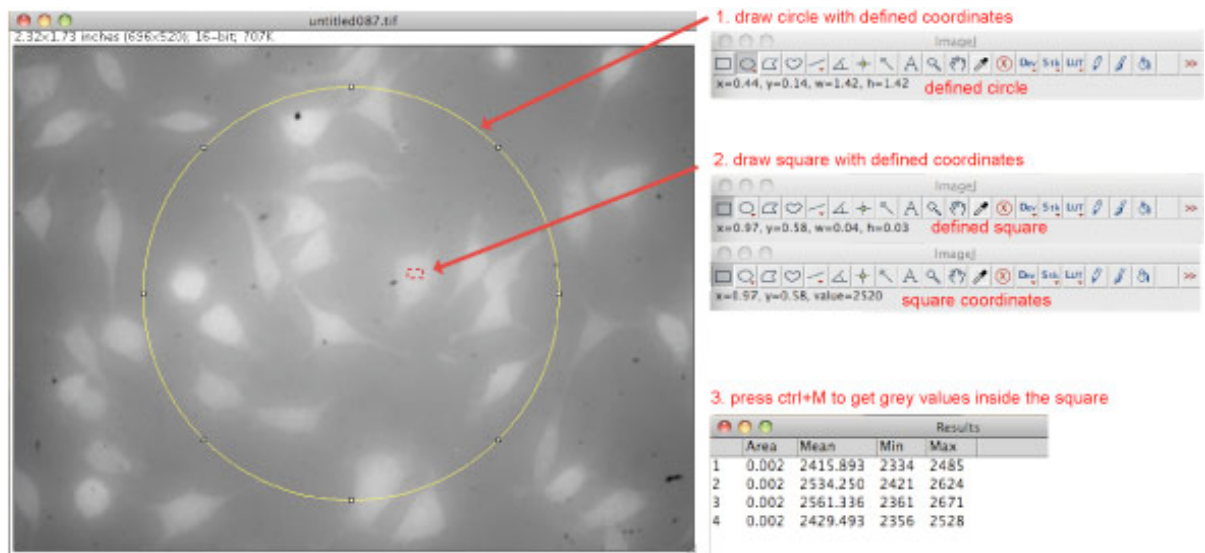


Figure 84 Different steps for evaluation of the cell's grey values

With the "elliptical" tool a circle with defined area and coordinates is drawn. The x and y coordinates and further the width and height of the circle, are given in the tool bar of the program. These data should be recorded to ensure the reproducible selection of the evaluation area. After that, the coordinates of all analysed cells are recorded. These coordinates have to be used for all pictures of one sample. To determine the gray value of every sample a square is defined. It should be placed in the centre of each cell and also here the coordinates need also to be saved to put the square always at the same place of every cell of every image of one sample. The registered coordinates exactly define the coordinates of the square. To get the gray value of the selected area, open the "analyse" menu and select "measure". A new window with different values opens.

The area of the square and the mean, minimum and maximal grey values are given. Repeat this until all gray values of the cells are recorded. After that, the data can be saved as excel file. This procedure is repeated for all recorded images of the sample.

We have to consider, that for every sample the microscope automatically adjusts the image brightness. To be able to compare the images no absolute values are used. Therefore, the first image, at $t = 0\text{sec.}$, is set to zero and the gray value of this image is subtracted from all other images. This has to be done for every cell on every image. For plotting the data, the x-axis is used for time and the y-axis for the variation in fluorescence intensity.

D) Curriculum Vitae

Persönliche Angaben

Anna-Lena Idzko
geboren am 03.07.1983 in São Paulo, Brasilien

Wissenschaftliche Ausbildung

seit 05/2008	Dissertation am Helmholtz Zentrum München Thema: "Organic Field-Effect Transistors for Application in Radiation Biophysics"
10/2002 - 03/2008	Studium Diplom Physik mit Schwerpunkt Biophysik an der Universität Augsburg
09/1993 - 06/2002	Gymnasium Maria Stern, Augsburg, Abitur 2002
09/1989 – 07/1993	Grundschule Bobingen/Siedlung
Auslandsaufenthalt	Unicamp, Campinas, Brasilien, über ein DAAD Stipendium vom 06.04. - 12.05.2010

Veröffentlichungen

- G. Scarpa, A.L. Idzko, E. Martin, S. Thalhammer (2010): Towards cheap disposable sensing devices for biological assays. IEEE Transactions on Nanotechnology 9(5): 527-532
- G. Scarpa, A.L. Idzko, S. Götz, S. Thalhammer (2010): No more biocompatibility problems - Advantages and applications of low-operating voltage organic thin-film transistors. IEEE Nanotechnology Magazine, September: 15-19
- G. Scarpa, A.L. Idzko, S. Götz, S. Thalhammer (2010): Biocompatibility studies of functionalized regioregular poly(3-hexylthiophene) layers for sensing applications. Macromolecular Bioscience 10(4): 378–383
- G. Scarpa, A.L. Idzko, A. Yadav, S. Thalhammer (2010): Organic ISFET based on poly(3-hexylthiophene). Sensors 10: 2262-2273
- G. Scarpa, A.L. Idzko, S. Götz, S. Thalhammer (2010): Biocompatibility studies of solution-processable organic thin-film transistors for sensing applications. Proceedings IEEE Nanomedicine, in press
- B. Wunderlich, C. Leirer, A.L. Idzko, U.F. Keyser, A. Wixforth, V.M. Myles, T. Heimbürg, M. Schneider (2009): Phase-state dependent current fluctuations in pure lipid membranes; Biophys. J. 11:4592-4597.

